ACTIVATED SINTERING IN THORIA-YTTRIA SOLID ELECTROLYTES

by

George P. Halbfinger

A dissertation submitted to the Graduate Faculty in Engineering in partial fulfillment of the requirements for the degree of Doctor of Philosophy, The City University of New York

1971

This manuscript has been read and accepted for the Graduate Faculty in Engineering in satisfaction of the dissertation requirement for the degree of Doctor of Philosophy.

December 1, 1971
date

Morris Kolodney
Chairman of Examining Committee

Dec 1, 1971
date

Jacques E. Benveniste
Executive Officer

Professor Robert A. Graff
Professor Jack Morrow
Professor Henry S. Myers
Professor Morris Kolodney
Chairman

Supervisory Committee

The City University of New York

ABSTRACT

A method of production of thoria-yttria solid electrolyte material at about 1500°C, which is more than 500°C below the temperature normally needed, was studied and developed. The method is based on the activated sintering of the unalloyed powders using additions of 0.8 weight percent of either NiO or ZnO. A number of other oxides and halides were tested and found less efficacious.

The sintering kinetics were studied by cathetometer measurements at temperature. An effort has been made to explore the mechanism of sintering principally by using existing theories of sintering rates and scanning electron microscopy. However, the standard theory is based on a model of one component, monosized spheres, whereas this investigation deals with thoria in plate form and with three components of different particle size. Consequently, the application of standard theory is qualitative at best. Analysis of the Kuczynski log-log and Johnson differential equation indicates that sintering occurs in three distinct regions:

1) an initial very rapid shrinkage rate
2) a slower shrinkage region where volume diffusion is probably occurring
3) a final slow densification region where inclusions probably slow down pore annihilation so that a temperature dependent end point appears to be reached at short times

These regions resemble sintering in the presence of a liquid phase. A search for an eutectic in the system disclosed none below at least 1650°C whereas a significant sintering occurs in the vicinity of 1300°C. Nor was evidence of a liquid found by scanning electron microscopy. Furthermore, the activation energy appears to lie between 70 and 100 kcal/mole which is high for diffusion in a liquid phase.

A number of solid state mechanisms are proposed as alternatives to the liquid phase theory.

Acknowledgements

I wish to express my deep appreciation to the following people:

Professor Morris Kolodney, my mentor, without whose steadfast guidance I would probably still be searching up some dark alleys, and without whose help this work would have been impossible;

The National Aeronautics and Space Administration (Grant #33-013-017), the CUNY Research Foundation, and the Chemical Engineering Department at The City College for keeping me solvent for 4½ long years;

My colleagues on this project under whom I learned so much, Drs. Fred Schwettman, Stanley Levine, and Leon Schwartz, and the entire professorial staff;

My committee members, Professors R.A. Graff, J. Morrow, H.S. Myers and H. Heideklang, who unstintingly aided my efforts and helped review my thesis;

"The gang" that got me to school early and home late so that I could do all my work, and kept me stimulated: Leon Levine, Larry Ruth and most of all Leon Paretsky, without whose "just two hours more" I never would have found 26 hours a day;

To the stout hearts of the chemical engineering shop, without whose helpful remarks such as "you can't do it that way" it would never have been done.

To Edith Diamond, a good friend, a great typist, and a beautiful person, for typing up this thesis and putting up with my handwriting.

And last, but not least, to MOM.

List of Sections

List of Tables

List of Figures

LIST OF ENGLISH SYMBOLS

Symbol	Meaning	Units
A	Area of diffusion flux travels through	cm^2
a_i	Activity of a chemical species at site i	$mole/cm^3$
C_i	Concentration at site i corresponding to the activity	$mole/cm^3$
$\mathscr{D}$	Diffusivity based on concentration	cm^2/sec
D_v	Volume diffusivity	$\frac{cm^5}{sec(gm\ mole)}$
E	Electromotive force of an electro-chemical cell	volts
ΔE	Surface driving pressure	$ergs/cm^3$
$\mathscr{F}$	Faraday's constant	
ΔG	Free energy of mixing	cal/mole
K	Arbitrary constant	
k	Boltzman's constant	
L(t)	Length of a compact at time t	cm
L_o	Initial length of compact	cm
Lc(t)	Observed length of compact	cm
δL	Length error to Johnson-Cutler equation	cm
ΔL	(Lo-L) or shrinkage	cm
m	Sintering index, exponent to the Kuczynski equation	
m_j	Exponent to the Johnson differential equation	
n_p	Number of particles in a compact	
n	Exponent of the particle radius in the Kuczynski equation	
PW	Weight of a dry pellet	gm

P_{O_2}	Oxygen partial pressure	atm
Q	Activation energy of a process	cal/gm mole
R	Gas constant	
r	Radius of a particle	cm
S	Weight of pycnometer with pellet and immersion fluid	gm
T	Absolute temperature	^{o}K
t	Time	sec
t_{ion}	Anionic transference number	
δt	Time error of the Johnson-Cutler curve	sec
μ	Incremental exponent of the Kingery liquid phase relationship	
$\overline{V}$	Molar volume	cm^3/gm mole
dV/dt	Volume rate of flow	cm^3/sec
ΔV	Volume shrinkage	cm^3
V_o	Initial volume	cm^3
w	Width of pellet	cm
WP	Weight of wet pellet	gm
x	The interparticle neck radius	cm
X_i	Mole fraction of a solid	
y	The length of sphere overlap from center-to-center approach	cm
z	Arbitrary distance	cm

ABBREVIATIONS USED

$TY\text{-}Th_{.85}Y_{.15}O_{1.925}$ - mixture of ThO_2+15 mole % $YO_{1.5}$

$TYN\text{-}Th_{.829}Y_{.146}Ni_{.025}O_{1.902}$ - mixture of ThO_2+14.6 mole% $YO_{1.5}$ +2.5 mole% NiO

$TN\text{-}Th_{.972}N_{.028}O_{1.972}$ - mixture of ThO_2 + 2.77 mole% NiO

$TYZ\text{-}Th_{.829}Y_{.146}Zn_{.025}O_{1.902}$ - ThO_2 + 14.6 mole% $YO_{1.5}$ + 2.5 mole% ZnO

LIST OF GREEK SYMBOLS

		Units
α	"Break point" or time when two linear extrapolations meet	min.
α_x	Coefficient of linear expansion	cm/cm
α_j	Coefficient of the Johnson differential equation	
β	Arbitrary constant	
β_j	Coefficient of the Johnson differential equation	
γ	Solid-vapor surface energy	
δ	Thickness of boundary between grains (solid or liquid)	
ϵ	Fractional included volume [1-fractional porosity]	
η	Apparent viscosity at infinite shear	
θ	Angle of tilt of an observed pellet	
μ	Chemical potential	
μ_o	Chemical potential on a planar surface	
$\overline{\rho}$	Relative density	
ρ_i	Radius of curvature on orthogonal planes at site i	
ρ	Density	
τ_c	Critical shear stress for a Bingham solid	
ϕ	Fractional shrinkage, $\Delta L/L_o$	
Ω	Atomic volume	

1. Background

1.1 Electrolytes

The last decade has seen the widespread application of anion-conducting solid electrolytes, especially those involving oxygen transfer. They have been used for such diverse purposes as the electrolyte in galvanic cells for the determination of thermodynamic and kinetic data (achieving much higher accuracies than conventional methods can obtain); as the electrolyte for fuel cells; and as the electrolyte for anion sensing meters in gases, liquids and solids.

The most common solid electrolytes for high temperature use are based on zirconia, ZrO_2, or thoria, ThO_2. These are doped with aliovalent solid oxides such as calcia, CaO, or yttria, Y_2O_3. These cations replace the Zr^{+4} or Th^{+4} in the host lattice, forming a solid solution. Since its valence is lower, oxygen ion defects are created (as shown for an ideal lattice in figure 1.1).

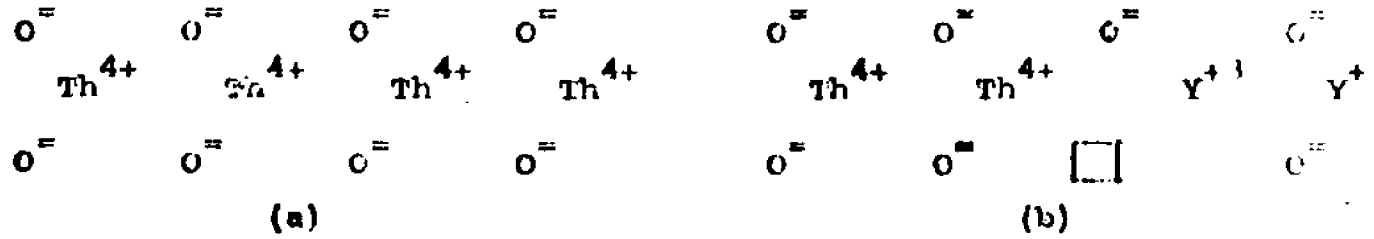

□ Indicates vacancy

a) Perfect ThO_2 Lattice

b) ThO_2 doped with Y_2O_3

Figure 1.1 Defect Structure of ThO_2 - Y_2O_3

The product has a much higher conductivity and has been found to conduct almost completely by oxygen ion transport in certain domains of oxygen partial pressure. Outside of this region, electronic conduction occurs and reversibility is impaired. Then, instead of the EMF across the electrolyte being given by:

$$E = \frac{RT}{4\mathcal{F}} \ln \frac{(P_{O2})_2}{(P_{O2})_1} \qquad (1)$$

it becomes (R2):

$$E = -\frac{1}{2\mathcal{F}} \int_{(\mu_{O_2})_1}^{(\mu_{O_2})_2} t_{ion}\, d\mu$$

where (μ_{O_2}) indicates oxygen activity because the oxygen ion transport number (t_{ion}) must be known as a function of oxygen activity. This latter expression is not easy to evaluate.

Our laboratory has used electrolytes of this kind with electrodes that are physically hard, brittle and difficult to fabricate in dense form (e.g. tantalum silicide-oxides (R1) and tantalum-oxide mixtures). The nature of the electrode makes it impossible to create a perfect seal between the electrode and the electrolyte. As a result there is seepage of ambient atmosphere to one or both surfaces of the solid oxide electrolyte when employing the technique of stacking the pellets in an open cell. The consequence is erroneous values of the EMF, since the cell is an oxygen concentration cell. A typical example is shown in figure 1.2 using a thoria-yttria electrolyte and Fe, FeO versus Ta, Ta_2O_5

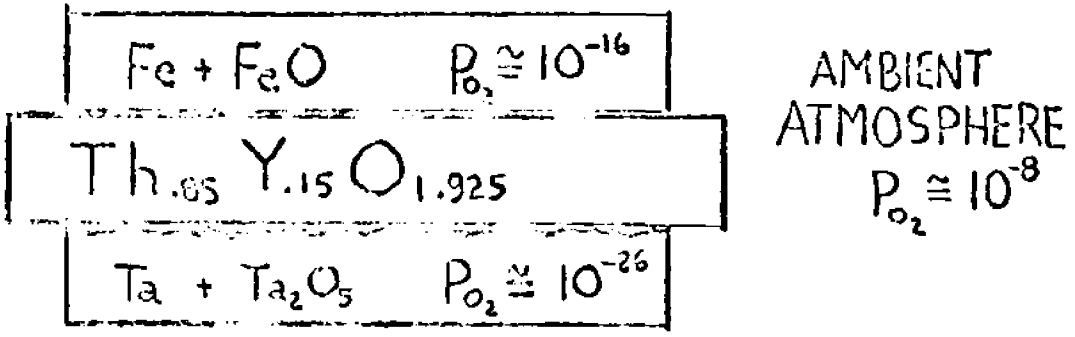

Figure 1.2 - Open Cell Stacked Pellet Technique

electrodes. The calculated interface oxygen partial pressures (R3) are given for 1200°K, as a typical ambient temperature. The cell is of the form:

$$Pt/Fe, FeO//Th_{.85}Y_{.15}O_{1.925}//Ta_2O_5, Ta/Pt$$

Using the typical numbers given in this example and equation 1, not only could leakage cause a lowering of the electromotive force, but it might produce a reversal of polarity.

To remedy this problem, a method of electrode encapsulation, i.e., a reference electrode totally encased in electrolyte material, was proposed. With this approach, the two environments are totally separated from one another and the chance of leakage greatly reduced. In addition, the need for a sinterable, deformable, flat surface is eliminated and powders may be used as electrodes.

A simple oxygen probe of this type would be valuable in a variety of applications. It would be desirable to make the electrolyte out of thoria-yttria because this material is usable at very low oxygen partial pressures. Since its melting point is extremely high, the electrolyte is fabricated by the solid state sintering of pressed powders. However, an obstacle to this approach is the high sintering temperature of thoria-yttria (TY) (>2000°C) which precludes the use of platinum or similar oxidation-resistant metal connectors with high melting points. It also makes difficult the choice of a suitable electrode metal-metal oxide mixture. For this reason, the major effort of this research was directed at reducing the sintering temperature to about 1500°C

where platinum or its alloys may be used and a variety of electrodes are available. This reduction may be achieved by adding less than 1% of sintering aids which activate the sintering process. In order to understand this process, the general theory of sintering will first be highlighted and a description of activated sintering will follow.

1.2. Introduction to Sintering Theory

In order to form a solid shape from powders, the components are first mixed and then usually pressed in a die or other device to the desired shape. The "green" pressed compact, whose density is very low, is then fired at an elevated temperature to achieve strength and to approach theoretical density. This sintering process may be regarded phenomenologically as nothing more than the migration of matter among the array of pressed particles by various mechanisms to form a bonded and more stable matrix. It is convenient to describe material transport in terms of a driving force, a resistance, and a path. Mechanisms of transport that are generally considered include bulk diffusion, plastic flow, surface diffusion, and vaporization - condensation. These will be described in more detail.

When two particles begin to sinter, a neck is formed between them (see figure 1.3). When the mechanism is either vaporization-condensation or surface diffusion, a rearrangement of shape is observed. However, there is no center-to-center approach and therefore no observed shrinkage, but enlargement of the neck may make it easier

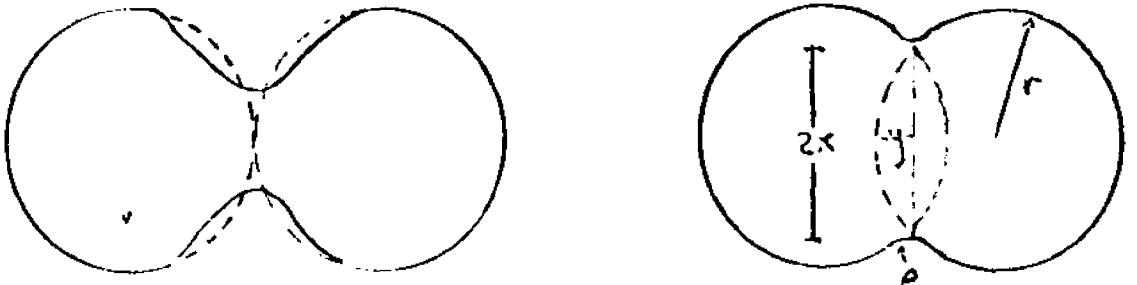

a) no shrinkage b) shrinkage

Figure 1.3 - Neck Formation in Sintering

for the other two mechanisms to occur. Both of these, volume diffusion and plastic flow, yield an overall shrinkage of the mass because the included mass (shaded area, figure 1.3) takes up the volume of the voids. In sinterable materials, any one or combination of these mechanisms may take place, either together or in stages. If neck growth is measured, then the sintering mechanism may be identified, since neck growth occurs in each. If shrinkage is measured, then only the effect of plastic flow or bulk diffusion will be observed, or the sum of both.

A major driving force for the sintering process is the decrease of free energy which accompanies the reduction of internal surface area of the compact when pores are eliminated. To understand the magnitude of this driving force (R4) consider a compact of unit volume consisting of n_p individual equisized spheres of radius r and fractional voidage $(1-\epsilon)$. The total internal surface area is $4\pi r^2 n_p$, while the number of particles per unit volume is $\epsilon/\frac{4}{3}\pi r^3$). Therefore, the surface area of these particles per unit volume is $3\epsilon/r$. It should be noted that this is for spherical particles, so larger areas would be found if the particles are rough or irregularly shaped. Therefore, use of $3\epsilon/r$ as the surface area is a minimum estimate. The energy associated with the internal surface area is this area multiplied by the solid-vapor surface energy (γ). Inserting representative numbers yields

$$\Delta E = \frac{3\epsilon\gamma}{r} = 2 \times 10^7 \text{ ergs/cm}^3 = 0.5 \frac{\text{cal.}}{\text{cm}^3} \qquad (3)$$

This is small, but if smaller particles were present, larger values may be obtained.

1.3 Volume Diffusion Mechanisms - Kuczynski Model (R40, R44)

For volume diffusion to occur, there must be a driving force for the diffusing species. Evidence favors the transport of lattice vacancies from near a pore to an adjacent grain boundary, which acts as a vacancy sink. Burke (R5) observed this experimentally by examining coarse-grained alumina with pores inside the grains. He found that upon annealing, the pores which were closest to the grain boundaries were preferentially annihilated. Since shrinkage had occurred, the only mechanisms possible were volume diffusion and plastic flow. However, if plastic flow had occurred, pores should have disappeared equally throughout the grains. Therefore, he concluded that the operative mechanism was bulk diffusion.

The gradient in vacancies (driving force) is due to the shape of the pore. This can be shown from the Kelvin equation

$$\mu - \mu_o = RT \ln\left(\frac{a}{a_o}\right) = \bar{V}\gamma\left(\frac{1}{\rho_1} + \frac{1}{\rho_2}\right) \qquad (4)$$

where μ = chemical potential on curved surface

μ_o = chemical potential on flat surface

$\bar{V}$ = molar volume

γ = surface free energy

a, a_o = activities corresponding to μ and μ_o

ρ = radius of curvature on orthogonal planes

For a spherical pore, $\rho_1=\rho_2$ and both are negative (the chemical potential is lower at a pore surface). Therefore, after rearranging and substituting concentration C for the activity

$$\frac{\mu-\mu_0}{RT} = \ln\left(\frac{C-C_0}{C_0}+1\right) = \frac{\bar{V}\gamma}{RT}\frac{2}{\rho_{1,2}} \qquad (5)$$

expanding the middle term in equation (5) for small values of $\Delta C/C_0$ yields:

$$\Delta C = C - C_0 = \frac{2\gamma\bar{V}C_0}{\rho_{1,2}RT} \qquad (6)$$

Therefore, due to a lower chemical potential at the pore surface than at the grain boundary, there is an overall material transport from the boundaries to the pores.

Though sintering of compacts is the interaction among adjacent particles throughout a large array, it can be accurately treated mathematically as the interaction between a set (usually a pair) of particles. The assumption of isotropic behavior then predicts the overall behavior.

The governing equation for volume diffusion is Fick's law

$$\frac{dV}{dt} = -D_V A \frac{dc}{dz} \qquad (7)$$

That is, that the volume flow of material to the pore (or vacancy flow away from the pore) is equal to the driving force (concentration gradient) times the reciprocal of the resistance. From here on, assumptions must be made with respect to geometry and path. Different authors have derived different expressions

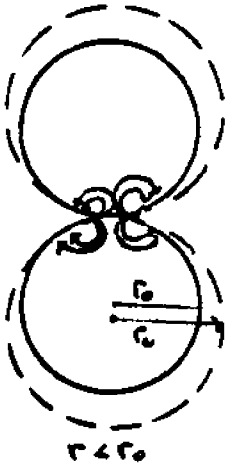

(a) NECK TO PARTICLE SURFACE

(b) NECK TO GRAIN BOUNDARY

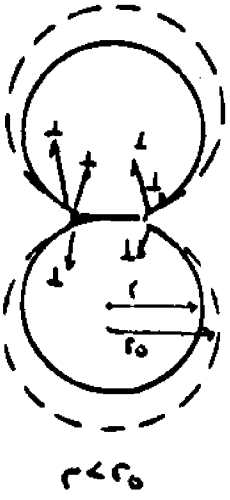

(c) NECK TO DISLOCATIONS

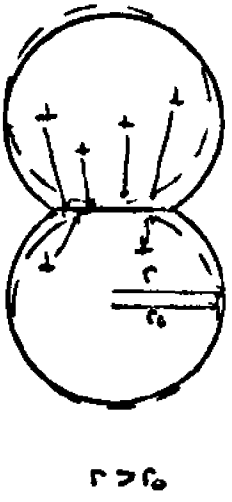

(d) DISLOCATIONS TO GRAIN BOUNDARY

Figure 1.4 - Vacancy Diffusion Paths

relating the fractional shrinkage $\Delta L/Lo$, temperature T, particle radius r and time t to one another. The following is a typical derivation of an operating equation assuming that the vacancies diffuse from the curved neck to the midpoint of the grain boundary (vacancy sink) (R6). There are at least three other possible sources and sinks, as shown in figure 1.4. They are neck to particle surface, dislocations to grain boundary, and dislocations to particle surfaces. Mathematically, dislocations and pores behave similarly to vacancy sources.

Assuming that the overlapping shperical surfaces can be represented by the equations (see figure 1.3)

then:

$$\text{Volume} = \pi x^2 y = 16\pi r^3 \left(\Delta L/L_o\right)^2$$

$$\text{Area} = 2\pi y x = 4\pi r^2 \left(\Delta L/L_o\right)^{3/2}$$

$$\rho = y = r\left(\Delta L/L_o\right)$$

$$\Delta C = \frac{2\gamma \bar{V} C_o}{RT}\frac{1}{\rho} = \frac{2\gamma \bar{V} C_o}{RTr}\frac{1}{\left(\Delta L/L_o\right)}$$

$$D = C_o D_v$$

then substitution into equation 7 yields (see Appendix A):

$$\left(\frac{\Delta L}{L_o}\right) = \left(\frac{2\delta\gamma\bar{V}}{RTr^3}t\right)^{1/2} \qquad (13)$$

There are many other models, but all workers have started with Fick's law and ended with an equation of the form:

$$\left(\frac{\Delta L}{L_o}\right) = \left(\frac{K\delta\gamma\bar{V}}{RTr^n}t\right)^m \qquad (14)$$

with values of K of order one, m between .3 and .5 and n between 2 and 4, but usually 3. These variations are caused by the assumptions made concerning the geometry of the joined spheres. The most critical assumption is the value of the radius of curvature of the neck between particles. Values range from $\rho_i = (\Delta L/L_0)r$ to $(\Delta L/L_0)^{4/5} 2.9r$. Even values of x range from $2.0\, r(\Delta L/L_0)^{1/2}$ to $1.74\, r(\Delta L/L_0)^{.46}$. It should be carefully noted that this is for spherical, monosized particles with only one mechanism assumed operative.

If a liquid has formed, either by the melting of one component or by the formation of a eutectic, it may coat the spheres. Then mass transfer will occur only along the low energy liquid boundary of thickness δ (R9). Sintering is then accomplished through a three stage process (R8). First there is a rearrangement of particles by viscous flow in the liquid phase, decreasing friction. If greater than about 35 volume % liquid is present, total densification is possible by this process alone. This can be followed by a second stage. When the solid is soluble in the liquid, material is transported by dissolution and diffusion in the melt until it reprecipitates. The driving force for transport is due to pressure gradients and high solubility in the contact zones. This process results in shrinkage, but at a slower rate than the first stage. The last stage is coalescence, due to normal bulk diffusion type mechanisms. This is the case when wetting isn't complete.

The rearrangement process occurs as a result of particles sliding on each other in order to minimize the pore surface. The driving force for this is the capillary pressure

of the liquid phase. Subsequently, necks are formed and then broken by dissolution into the liquid. This leads to rearrangement again with the resulting structure capable of achieving high density. For spherical particles, this cannot lead to complete densification. The initial rearrangement behaves like a viscous-flow process, with subsequent rearrangement comparable to a Bingham-type flow. For this stage of sintering, the shrinkage obeys the relationship

$$\frac{\Delta L}{L_0} = \frac{1}{3}\frac{\Delta V}{V_0} \sim t^{1+u} \tag{15}$$

where u is small. Mathematically, Fick's law and the modified Kelvin equation yields (see Appendix B):

$$\left(\frac{\Delta L}{L_0}\right) = \left(\frac{6\delta D \gamma \bar{V}}{RT r^4} \cdot t\right)^{1/3} \tag{16}$$

This equation should hold for all cases of grain boundary diffusion.

There are many other approaches, a brief summary of which is given in table 1.1. Even assumptions of different shapes don't greatly alter the overall behavior (refer to Appendix C for derivation of sintering between tetrakaidecahedrons).

Table 1.1 Constants for the Diffusion Equation (14)

Diff. path	Between	k	m	n	Author
Bulk Diff.	spheres	3	.46	3	Johnson & Cutler (R7)
Grain Boundary (dissol-reprecip)	spheres	-	.33	3	Kingery (R8)
Rearrangement	spheres	-	1+x	1	Kingery (R8)
Bulk Diff.	spheres	2	.50	3	Coble (R6)
Bulk Diff.	spheres	14.1	.40	3	Johnson & Cutler (R7)
Bulk Diff.	parabolic	6.3	.46	2	Johnson & Cutler (R7)
Bulk Diff.	prismatic		.20		Kingery (R8)
Grain Boundary	prismatic		.33		
Grain Boundary	parabolic	-	.31	3	Johnson & Cutler (R7)
Volume	spheres	-	.80	3	Kingery & Berg (R9)
Bulk Diff.	tetrakai-decahedrons	14	.50	3	Coble (R43)

It will be observed that the sintering mechanism may in principle be deduced from the value of the sintering index, m. This has been widely used by many workers (R6, R7, R8, R9, R43, etc.). However, doubt has been cast on this procedure by Rockland (R11). Mechanisms may also be determined by a differential equation (R9, R10) due to Johnson

$$\frac{L}{L_0} = 1 - \alpha_j (K\alpha\vartheta)\left(\frac{dL}{dt}\right)^{-m_j} \qquad (17a)$$

$$\left(\frac{\Delta L}{L_o}\right)^{-(1+m_j)} = \beta_j (K\Theta)^{-m_j} t \qquad (17b)$$

where Θ is diffusivity, Φ is ($\Delta L/Lo$), and the constants α_j, β_j, m_j & K are given in table 1.2. These equations predict end points independent of temperature as expected by atomic

Table 1.2 Constants for the Johnson Equations (17a & b)

	α_j	β_j	m_j	t
Volume diffusion	2.56	.80	.97	$\gamma\Omega/ktr^3$
Grain boundary diff.	.84	3.64	.48	$\gamma\Omega\delta/ktr^4$

where γ = surface tension, Ω = atomic volume, r = particle radius, δ = grain boundary width, k = Boltzman constant, T = absolute temperature

considerations, that is, that the compact, given enough time, will sinter to theoretical density.

1.4 Use of Kinetic Equations

Measurements of rates of sintering as a function of temperature have great practical value in establishing sintering conditions. In addition, rate measurements have theoretical value because once kinetic data are obtained, an accurate log ΔL vs. log t plot at constant temperature will yield values for m in the Kuczynski-type model. Inspection of table 1.1 discloses that a mechanism may be deduced if this constant has been established. However, as pointed out by Rockland (R11)

and others, there are many inherent doubts about this procedure. Detailed analysis of the mathematics alone shows that the method is very insensitive to changes in m so that only approximate m's and possible mechanisms may be hypothesized. If the particles are not perfect spheres, or any regular monosized shape, the value of the sintering index (m) may well be erroneous. In addition, initial rearrangement (stress release mechanisms, etc.) will yield an initial shrinkage not dependent on the Kuczynski model. These erroneous initial shrinkages invalidate the plotting method because only one mechanism was assumed for this method.

If a single mechanism holds over only a limited region of the kinetic curve, a more accurate value of the sintering index may be obtained by using the value of L_o as the length at the start of this region while t is set at zero for this value of L_o. This would mean the substitution of $(L-L_R)$ and $(t-t_R)$ for ΔL and t respectively in equation (14), where L_R = length at the beginning of the region and t_R = time at the beginning of the region. This is very similar to the correction factor for initial incubation time in the furnace as first proposed by Johnson and Cutler (R7). This will be discussed below.

Other initial errors are caused by linear expansion, finite times for the specimens to reach furnace temperature, and fragility of the compact. Another important source of error involves the methods of support and measurement. These will be described in detail later.

These errors lead to nonlinearities. However, Lay and Carter (R12) found that the first two of these could be accurately predicted from the coefficient of linear expansion and thermal conductivity. Johnson and Cutler (R7) put an incubation time and length, similar to the L_R and t_R described above, into the equation. They found that a plot of length instead of shrinkage was more insensitive to errors and would yield values for the incubation times and lengths.

The Johnson dynamic equation (17) is more sensitive in obtaining values for the sintering index, but relies on the slope of the kinetic shrinkage curve. This is good when using a dilatometer, but suffers from errors when using other methods. This method also fails when irregular shapes are used or more than one mechanism occurs.

For complex, non-spherical powder systems, such as are involved in this research, even an accurate knowledge of the sintering index will allow only for a broad interpretation of the sintering mechanism. Exact mechanisms may not be deduced with any assurance although frequently some mechanisms may be ruled out as unlikely.

1.5 Pores and Discontinuous Grain Growth

Since pores are the source of vacancies which in turn establish the driving force for sintering, a closer look at their structure, formation, and properties is desirable.

A particulate compact has voids which are filled with the surrounding atmosphere. Upon heating, necks form,

completely enclosing the void. This region is called a pore. Surface tension causes the pores to become spherical to minimize surface area, then drive it to disappear (see figure 1.5).

If pores exist, they annihilate themselves more quickly if there are many smaller ones. This can readily be shown for the case of pores on a grain boundary (R46). The smaller pores, spaced closer together than larger pores for equal voidage (green density) would have a shorter diffusion distance between pores and also between the pores and the vacancy sink. In addition, the internal surface area would be larger and therefore more of an internal driving force exists. Evidence shows that grain boundary diffusion may be controlling in many cases.

Discontinuous grain growth (R47) is deleterious to the final stage of densification, where pores are supposedly annihilated. It manifests itself as a large variation of grain size. It may be produced when growth of most grains is inhibited by inclusions in the matrix, while some with more sides have sufficient energy to grow. Grains with many sides have very small radii of curvature at the sides. Hence the driving force for growth is larger. These grains will grow so that large grains become larger while small ones remain the

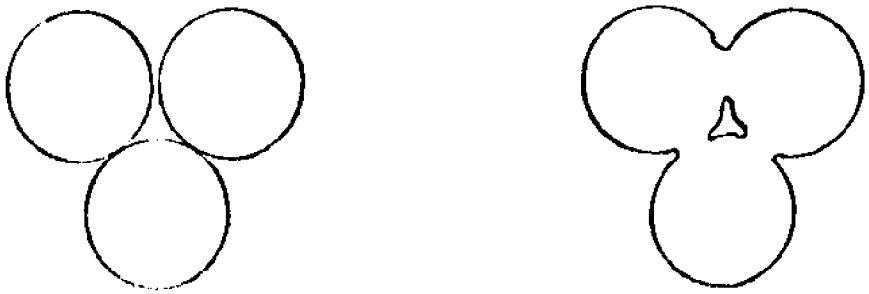

a) particles

b) neck growth

c) pore rounding

Figure 1.5 - Pore Formation

same size.

In the sintering compact, pores act as inclusions. In the early stage, there are many pores and grain growth is totally inhibited. After a while, the smaller pores will disappear and pores located near grain boundaries will also disappear. If this happens more readily in some grains, these grains will grow, sweeping their boundaries past pores that they reach, until after sufficient time, only large grains and included pores exist. These trapped pores are not likely to escape because of the large spacings between the pores (the vacancy source) and grain boundaries (the vacancy sinks). The result is a permanent residual porosity and the sintered mass will not attain theoretical density.

1.6 Plastic Flow Mechanisms

Plastic flow mechanisms have been used to describe the sintering behavior in crystalline solids (R45, R28). Material transport by plastic flow is caused by the hydrostatic forces between particles. There are two models used to describe sintering by plastic flow, the Clark-White and Mackenzie-Shuttleworth models.

The Clark-White model mathematically treats the connected pore stage (early stage) of sintering. In it, viscous forces of either a Newtonian fluid or Bingham solid (one in which a finite critical shear stress is necessary to make it flow) cause a liquid lens to form between two spherical particles. Crystalline oxides or halides can behave like Bingham solids. The resulting differential equation is not integrable

in closed form, but agrees well with kinetic data for CaF_2 and NaF.

The Mackenzie-Shuttleworth model mathematically treats the closed pore stage of sintering. The driving force here is the surface tension in the pores of the material. Viscous or Bingham flows may again be assumed. In addition, since the pressure that causes pore closure is equivalent mathematically to an external load, this model may be used to predict hot-pressing characteristics. This mechanism also shows good agreement with the later stages of sintering of CaF_2 and NaF (R28). The mathematics yields a differential equation which does not lend itself to a closed form. A general closed form of the equation is (R45)

$$\frac{\sqrt{2}\,\gamma}{\tau_c\, r}\ \ln\left[1+\frac{\sqrt{2}\,\gamma}{\tau_c\, r}(1-\rho)\right]_{\rho_0}^{\bar{\rho}} = \frac{3}{2}\frac{\gamma}{r\eta}t \qquad (18)$$

where $\bar{\rho}$ is the relative density, τc the critical shear stress of a Bingham solid, η is the apparent viscosity of the solid at infinite shear and everything else is as given previously. This has a generally exponential shape of length with respect to time.

A consequence of assuming a Bingham solid is that a temperature dependent end-point density is obtained, since the critical yield shear is generally diffusion controlled and related exponentially to the temperature

$$\tau_c = Ke^{-Q/RT} \qquad (19)$$

and appears in the densification equation.

1.7 Activated Sintering

When the rate of sintering or final density is greatly altered by small changes in composition or operating conditions, "activated sintering" is said to occur.

One such perturbation is a change of atmosphere. In general, atmospheres are either inert of reactive, but each category has many subcategories. Inert gases by definition do not react with the material in use. This does not mean that they have no effect. If the inert atmosphere has a pressure greater than the equilibrium pressure of the pores ($2\gamma/r$), then pore annihilation and full density will not be obtained. If an inert atmosphere has a lower pressure, then an added driving force will exist for pore elimination. In both cases the solubility of the pore and furnace atmospheres in the ceramic in question will determine the rate. If the solubility is appreciable, then gaseous diffusion will not play a major role in sintering.

The question of reactive gases is different for ceramics than for metals. Oxides generally will sinter in oxidizing atmospheres if interstitial oxygen can form. This aids sintering by making available for transfer a mobile oxygen anion of low diffusional activation energy. It has also been found that transfer induced when the dissociation pressure and atmospheric partial pressures are comparable is enhanced in compounds of variable valence (R13). In metals, reactive atmospheres can cause oxide or halide formation on the surface.

Arenberg et al. (R14) noted that firing of thoria in vacuum slightly aids the sintering. This will be discussed in greater detail later, Cases involving metals are more frequent, with oxide formation yielding increased sintering in copper (R15) and iron (R16), while carbon monoxide was found by Jones (R17) to aid the sintering of silver despite its hindering flow deformation.

Large changes in sinterability of ceramics can be caused by small additions of different compounds. These additives can go into solid solution and alter the defect structure of the material, as previously described for thoria-yttria. This increases the diffusivity and assists densification. Additives may also segregate at grain boundaries, providing a low energy short circuit mechanism for diffusion. Similarly, if they are at the surface of the particle, they may enhance surface diffusion or evaporation-recondensation leading to accelerated neck formation and aiding the spheroidization of voids. If the material is a liquid, or forms a eutectic, then an extremely low resistance diffusion path is formed. In addition, wet surfaces allow for slip between particles. This rearrangement causes massive shrinkage of non-monosized irregular particles (R39, R43, R8). If liquid is present, Burke (R19) suggests that an idiomorphic microstructure might be noted instead of the regular polygonal one.

Arenberg et al. (R14) studied the effect of additives on thoria. They found that 1% additions of CaF_2, Bi_2O_3, V_2O_5 and others oxides and halides aid densification.

Hyatt et al. (R20) and Spacil and Tedmon (R21) noted that 1% additions of Fe_2O_3, CoO, Fe_3O_4, or NiO to ZrO_2 greatly increased its sintering rate while maintaining complete anionic conduction (R21). The nature of this activation was not investigated.

We have found that as little as 0.4 wt % NiO or ZnO added to $Th_{.85}Y_{.15}O_{1.925}$ (TY) greatly increased the sinterability of TY, decreasing its sintering temperature by more than 600°C. The mechanisms involved will be discussed later.

Turning to additives to metals, Brophy et al. (R24) investigated sintering of tungsten coated with very small amounts of nickel. They found that sintering occurred at temperatures as low as 1100°C as compared with a normal sintering temperature of 1700°C. They attributed this to surface diffusion of tungsten on the nickel layer. This leads to the formation of necks and allows bulk diffusion to occur. Stablein and Kuczynski (R22) studied the sintering of gold-nickel wires and noted that the Kirkendall effect played a major role, with the nickel wires getting larger and the gold becoming smaller.

Inhomogeneities or the existence of multicomponent systems may cause another form of activated sintering. As with liquid phases, segregation of impurities to the particle surface or grain boundary can cause low energy mass transfer, or completely change the mechanism of transport. Furthermore, the inhomogeneity itself can become a large driving force for

sintering. The free energy of mixing for a multicomponent system is

$$\Delta G = RT \sum_{i=1}^{n} x_i \ln(x_i) \qquad (26)$$

For a two phase system of 99 and 1% at 1500°K, this is 170 cal/mole, at least one order of magnitude higher than that for internal surface area.

Inhomogeneities can also induce stresses by the Kirkendall effect (R22, R23). This stress is caused by a difference in diffusivities of the two components leading to the more mobile species diffusing into the less mobile. The more mobile one is left in tension while the other is in compression. Pores are formed in the tension region. These induced stresses, just like stresses induced by grinding or ball milling (R18, R70), may cause material transport by plastic flow.

In general, Shaler (R18) proposed five forms of "activation":

1) Increase of surface or grain boundary, yielding a larger driving force for sintering.
2) Alteration of configuration which causes a larger area over which transport can occur
3) Increase in surface free energies, increasing the driving force
4) Lower energy mechanism for mass transport that leads to pore rounding (decreased resistance)
5) Lower energy mechanism for flow which leads to densification (decreased resistance)

He also noted that the mechanisms rarely acted individually, and were therefore difficult to identify experimentally.

1.8 Sintering of Thoria, Thoria-Yttria and Similar Materials-Effect of Additives

While the general subject of sintering is of interest, specific importance in this research is attached to the sintering of ThO_2, ZrO_2, Y_2O_3 and related materials such as dopants or additives. A brief description has been given in the previous section. The thoria-yttria mixtures are of special interest because they are our selected reference materials.

Thoria, ThO_2, has the highest melting point of all the oxides - about 3300°C, and so its sintering temperature is also extremely high. Slip-cast articles are normally fired at about 2000°C, but studies have shown that maximum strength is achieved only by sintering at about 2500°C (R63). However, the latter temperature is too high for commercial manufacture and is also too high for the usual laboratory furnaces which are limited to about 2200°C (R56, R57). The addition of yttria, Y_2O_3, not only creates a solid electrolyte, but also reduces the sintering temperature to approximately 2000°C (1900-2200) (R58, 59, 60, 61).

Much work has been done at Oak Ridge on the fabrication of fully dense thoria, either pure or doped, for use in nuclear reactors. Johnson and Curtis (R61) as early as 1954 noted that additions of CaO or SrO to thoria in a

heterogeneous mixture increased the sintering rate, while pre-alloying resulted in less rapid sintering. They used sintering temperatures of 1700°-1800°C and obtained solid solutions. Much more extensive work has been done more recently at Oak Ridge by Morgan (R29, R30, R38) on both thoria and thoria-calcia. Most of his experiments were run non-isothermally. Using thoria and thoria with less than 3% calcia added, he found that there was no effect of the rate of heating on the density at high heating rates (see figure 1.6). However, at lower heating rates, an increase in density was noted. Probably in an attempt to discover the activation energy of the sintering process, Morgan used incremental techniques involving either time or temperature. Some of his results are shown in Table 1.3. The treatments used involved the heating

Table 1.3 Incremental Heating Effects - Morgan

Temp.	Hting rate	Time held	Subsequent treatment	ρ_{Thoria}	$\rho_{Thoria-calci}$
1450	2 °/sec	10 (min)	-	7.36	8.74
1450	"	10+7/6	-	7.38	8.75
1450	"	10	heated to 1600 in 7/6 min.	7.57	8.94
1100	"	10	-	-	5.14
1100	"	10+7/6	-	-	5.15
1100	"	10	heat to 1250 in 7/6 min.	-	5.47

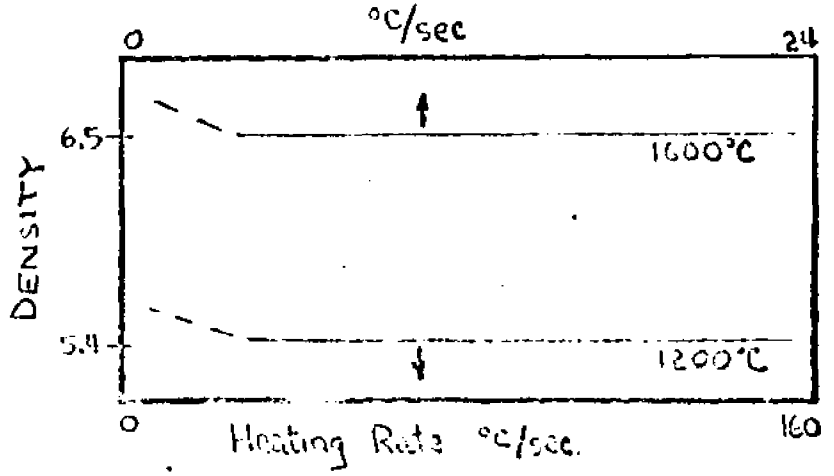

Figure 1.6 - Effect of Heating Rate on Density of Thoria - Morgan

of a sample at 2 °/sec to a given temperature and then either heating it an incremental length of time at the same temperature or to a higher temperature (150°C higher) for the same incremental length of time. The results should have been amenable to analysis by normal diffusion-type equations, but they were not. The density shows a disproportionate increase with change in either temperature or time, since between 1450 and 1600°C, the change in Th^{+4} diffusivity (the rate controlling ion) is twofold. In addition, heating for 11% longer time (7/6 minutes) yielded very little change in density. Morgan also found that the density end point was dependent only on temperature. These anomalies were found to be unexplainable by a single mechanism.

To explain this odd behavior, further work was done on ThO_2, ThO_2-CaO, ZrO_2 and ZrO_2-CaO. The data of Figure 1.7, indicating a temperature-dependent end point, was observed. Morgan also noted a maximum and minimum in the densification rates as the temperature was increased at a uniform rate. He proposed an explanation of these phenomena by a sintering mechanism of dislocation slip (R38). In this mechanism, increasing the temperature makes it easier for dislocation to move.

In order to find the source of the dislocations, Morgan heated his samples to 2450°C and cooled them at 7 °/sec. He found no dislocation and so concluded that the dislocations were produced by the sintering process itself. (This hypothesis has been proposed by Easterling (R62) and

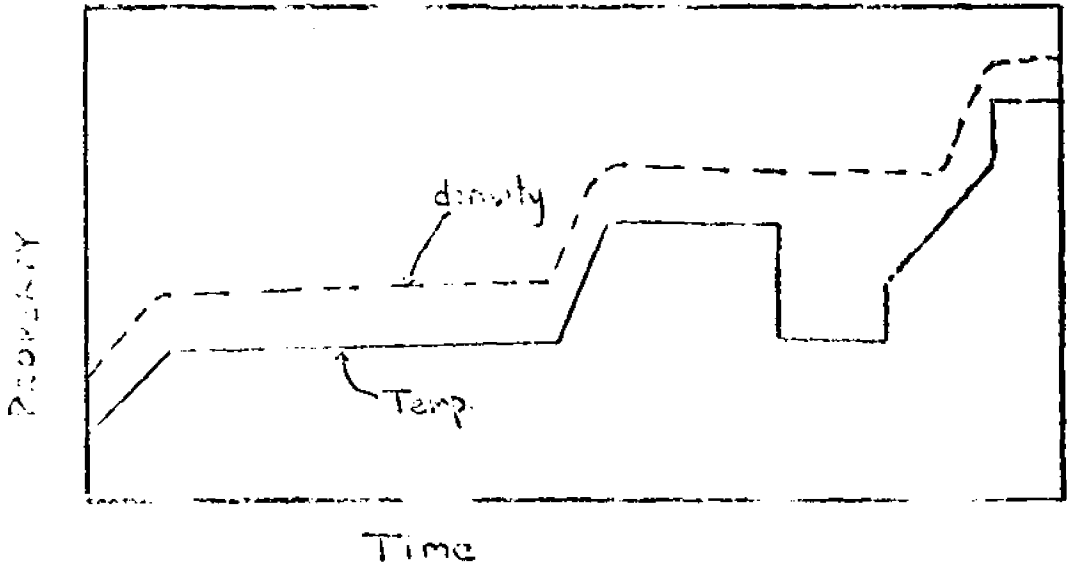

Figure 1.7 - Temperature-Density Interactions- Morgan

Easterling and Tholen (31) too, for metals).

Morgan also used the Dorn method to find the activation energy of sintering in ThO_2 compacts (R52). (The Dorn method measures the rate at one temperature and then abruptly changes the temperature and determines a new rate. The activation energy is calculated from the two rates.) He noted that the activation energy was higher for a positive increment in temperature than for a negative one. His explanation was that dislocations could move more readily on heating, while they were fixed on cooling. Hence, different mechanisms controlled in the two cases. During cooling, sintering was diffusion-controlled.

Thoria-calcia was also investigated by Jorgensen and Schmidt (R53) at General Electric. They studied final stage sintering and found that pure thoria exhibits discontinuous grain growth (see Section 1.5). However, additions of 2% calcia help to maintain uniform grain size, thereby allowing theoretical density to be approached. They explained this phenomenon by noting that two percent calcia is in excess of its solubility in thoria. It therefore precipitated at the grain boundary, reducing the grain boundary mobility. At 2000°C, in ThO_2-2 mole % CaO, grain growth stopped after 30 minutes. The grain size obeyed Zener's equation, a relationship based on the assumption of a random distribution of inclusions. The result was verified by microscopic examination.

Jorgensen and Anderson (R54) investigated the final stage sintering of Y_2O_3 and Y_2O_3-10%ThO_2. Yttria has a crystal structure quite similar to ThO_2. They found that in Y_2O_3-10 mole % ThO_2, thoria segregated at the grain boundary, causing a decrease in the mobility of the grain boundaries. Segregation of ThO_2 was deduced by microhardness profiles on the specimen. The thoria solubility limits were not exceeded, and no second phase was present, but the segregation of the thoria stopped discontinuous grain growth by limiting grain boundary migration. This resulted in a high diffusion flux of vacancies by keeping the pores and grain boundaries close together.

The methods previously discussed involved doping of the host thoria lattice to improve the mobility of anion vacancies (see Section 1.2), or to hinder mobility by forming inclusions which inhibit discontinuous grain growth (see Section 1.7). Additives may also be used for purposes other than doping. Small amounts of additives can cause a change in the sintering mechanisms as previously explained (Section 1.7). Arenberg et al. (R14) and Mitoff (R50, R51) investigated various sintering activators.

Arenberg found that thoria was activated both by firing in vacuum and by using additives such as CaF_2, Bi_2O_3 or V_2O_5. He gave no reasons for either effect, though probable causes seem obvious. Vacuum firing of pure thoria at high temperatures produces an increase of oxygen vacancies. This may cause an increased mobility of the anion to aid

sintering.although the process is controlled by the slower-moving Th^{4+} ion. In the case of the additives, although an analogy based on solid solution formation was used, materials which he found beneficial were liquid at the sintering temperature (1500°C). It may be that the additive acts as a lubricant and causes rearrangement as described in Section 1.4.

Mitoff (R50) investigated the sintering of stabilized zirconia and doped thoria. He found that additions of less than 10.5% iron oxide (either Fe_3O_4, FeO or Fe_2O_3) greatly aided the electrolyte's sintering behavior while more caused the appearance of a second phase. In subsequent work (R51), he coated the electrolyte with iron chloride from solution and followed by oxidizing it to FeO. Densification then occurred below 1400°C. Since no actual kinetic or microscopic investigation was carried out, the explanation of the activation is not known. It seems likely that the surface of the particles were covered initially and that surface diffusion was enhanced, thereby aiding sintering. Another possible explanation is that $FeCl_2$ became a liquid and coalesced into the lens region of the interparticle contact points. The chloride there oxidized to FeO which formed a stable neck to allow diffusional passage between particles by either stress or dopant action. The General Electric ceramics group inclines to the belief that a liquid phase is formed (R64).

Spacil and Tedmon (R21), as previously cited, investigated the use of additives in the sintering of zirconia-

base materials. They studied the effect of additives on zirconia-yttria solid electrolytes. Additions of 1% Fe_3O_4 or cobalt oxide were found to greatly improve the sintering behavior of the electrolyte, producing impervious tubes at temperatures as low as 1225°C. This electrolyte was found to maintain essentially anionic conduction down to an oxygen partial pressure of 10^{-20} atm. The electrolyte with Fe_3O_4 additives was found to increasingly conduct electronically with time when used with carbonaceous fuel gases. A similar behavior was not observed with cobalt oxide. This behavior was attributed to a carbon-iron interaction. The cathode of the cell was either a porous nickel-20% yttria stabilized zirconia (YSZ) or a cobalt-20% YSZ cermet. The ceramic was added as a sintering inhibitor for the basic metal, since the electrochemical cells being investigated utilized gaseous reactants.

Hyatt et al. (R20) investigated the use of additives on the sintering of zirconia for use in the ceramic industry. They tried many transition metal oxides and found that Fe_2O_3 was by far the best additive, 4% additions yielding greater than 95% theoretical density at 1500°C after firing for one hour. A comparable degree of sintering was not attained with "pure" Zirconia (99.5%) (ZrO_2 + HfO_2) at 1700°C under the same conditions. They also studied the effect of percent additive on the final density and found in general, an increase in sinterability with Fe_2O_3 additions to 1.0 wt % at all temperatures, with no marked additional improvement with up to 4% additive.

Allison and Murray (R28) investigated the sintering

of CaF_2 both with and without external loads. They applied the Clark-White and Shuttleworth-Mackenzie models to its sintering behavior. They found very good agreement between their experimental results and both models for a Bingham solid. This indicates that polycrystalline CaF_2 sinters by mechanisms that are plastic flow in nature.

1.9 Stresses

Stresses caused by grinding, compacting, Kirkendall effects, or applied loads cause creep and densification during sintering. This is especially true under non-isothermal conditions (R69), since the rate-controlling step for dislocations, solid solution, deformation or sliding is generally bulk diffusion (R25). This can easily be seen by an example. Naberro-Herring creep occurs only in polycrystalline materials. It is due to a difference in potential within a crystalline grain under external forces and causes material to "flow" from surfaces of the grain under compression to those under tensile stresses (R26, R27). This is a form of viscous flow (strain and stress proportional). For this to occur, material must diffuse within the grain, since the stresses only result in creating a driving force. In this way, necks are widened and mass transfer occurs due to stresses. In general, stresses in compacts result in some mass transport mechanism to relieve them. The consequence is rearrangement of particles and densification.

Allison and Murray (R28) noted that CaF_2, though crystalline, behaved as if it sintered by viscous flow.

Morgan and Yust (R29) and Morgan, McHargue and Yust (R30) studied thoria and thoria-calcia. They found that while being heated, their compacts sintered following a behavior that could only be described as plastic flow. They also noted that the final density was dependent upon temperature (a temperature-dependent end point). This was attributed to a rapid heating rate which limited diffusion control of the densification process. Easterling and Thölen (R31) noted that dislocations have little effect in the sintering of unstressed metals, but that large stresses and potentials were induced in the neck region between two sintering spheres. Due to interaction of stresses and diffusion, it is usually difficult to isolate these effects experimentally. The extent of the role that Nabarro-Herring creep, dislocation climb and Kirkendall stresses play in sintering are therefore hard to pinpoint.

In its early stages, our work showed that it was possible to obtain a reduction of about 600°C in the sintering temperature of thoria-yttria. Although the primary purpose was to achieve satisfactory sintering of the ceramic electrolyte, the cause of the 600°C reduction in the sintering temperature by the addition of small amounts of additives to an already heavily doped oxide mixture appeared of great interest. In addition, the nature of the resulting product, particularly the extent of solid solution is significant. Although the practical aim of producing a working electrolyte was uppermost, the mechanism and rate of sintering in this kind of system is of great interest and was studied in detail.

1.10 Properties of the Basic Materials

Very little work has been done on the properties of mixed oxides, though there is much data on the individual compounds (see Table 1.4).

Table 1.4 Properties of Oxides (R32, 33)

	ThO_2	Y_2O_3	NiO	ZnO	ZrO_2
mol. wt.	264.12	224.84	74.69	81.38	123.22
m.p. (^oC)	~3300	2410	1990	1975	~2700
ρx-ray	9.82	-	-	5.66	5.75
ρ pycnometer	10.0	4.84	6.8 or 7.45	5.61	5.58
Reactivity (in air)	2700	hydrates $\leq$ 200	$\rightarrow Ni_2O_3$ 400	boils 1950	2400
Structure	cubic fluorite	Tl_2O_3 type [C type rare earth]	cubic NaCl	hexag-onal	monoclinic to 1050 tetragonal >1050 fluorite cubic-stabilized
Thermal diff. $\left(\frac{cm^2}{sec}\right)$	.04	.03	.01	.023	.005
Coeff. of lin. exp. 25-1000°C	9.44	-	-	6.77	7.59
($^oC^{-1}$) x10^6 25-1500°C	10.17	-	-	-	11.0

Subbaro et al. (R34) studied the ThO_2-Y_2O_3 system, noting that at 1400°C, 20% $YO_{1.5}$ dissolves in ThO_2 to form a solid solution (see Figure 1.8). In addition, they studied the lattic parameters of the thoria-yttria system (Figure 1.9) and from this derived a relationship between density and percent Y_2O_3 in solution (Figure 1.10). They deduced that the solution forms with anion vacancies as mentioned earlier. The vacancies are formed in the host fluorite lattice of thoria (see Figure 1.1), which is the basic structure of the anion conducting electrolytes. This structure consists of 8 anions surrounded by 14 cations arranged in a face centered cubic type of cell (see Figure 1.11). No phase diagram was found for the system ThO_2-NiO or ThO_2-Y_2O_3-NiO, except for the observation by Pettit and Felten (R35) that ThO_2-NiO heated to 1400°C for 16 hours caused no interaction. A great deal of work has been done on conductivities in mixed oxide systems, especially thoria-yttria. For work on this, a good review article, such as that by Etsell and Flengas (R36) is recommended.

Nickelous oxide (NiO) dissolves oxygen at elevated temperatures to become a metal defect compound. These defects greatly increase the diffusivity of the material by forming a low energy diffusion path. This can easily be shown (R49). Oxygen is chemisorbed on the surface by the equation

$$\tfrac{1}{2}O_2 \rightleftharpoons O^{-(s)} + \boxed{+}$$

gaseous oxygen — surface chemisorbed oxygen — electron hole

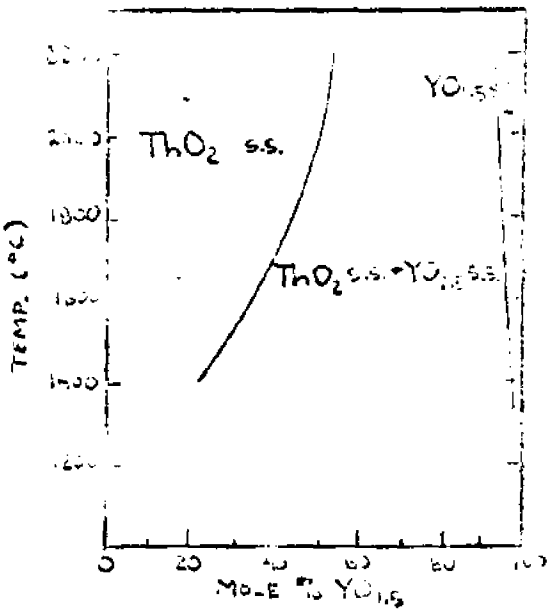

Figure 1.8
Subsolidus Phase Diagram-
ThO_2-$YO_{1.5}$

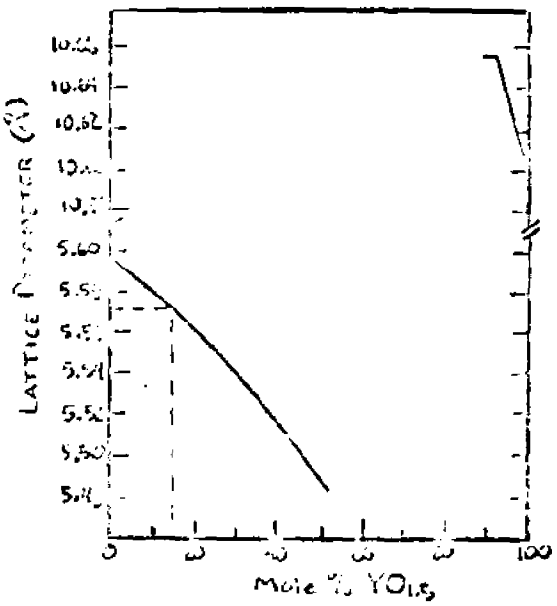

Figure 1.9
Lattice Parameters,
ThO_2-$YO_{1.5}$ solid solutions

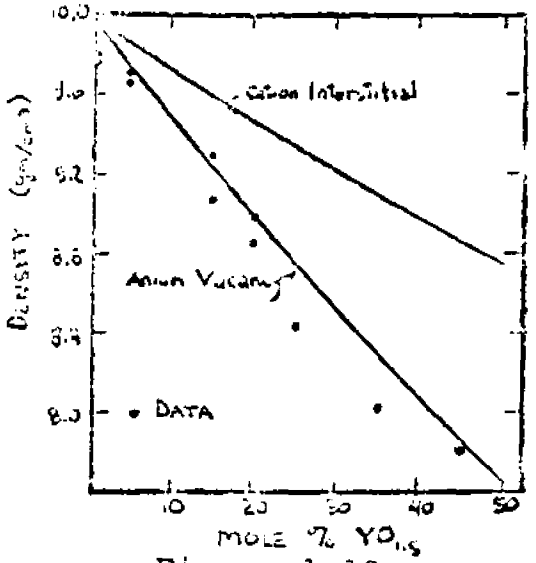

Figure 1.10
Densities of Thoria-Yttria
solid solutions

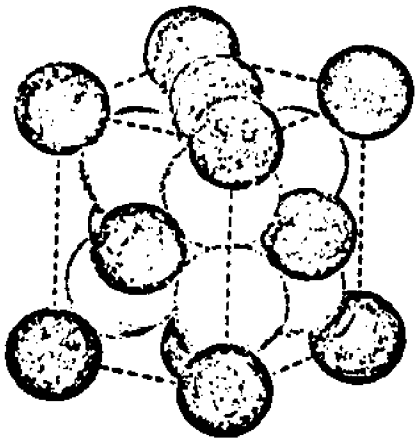

Figure 1.11 - Fluorite Structure

At sufficiently high temperatures, the absorbed oxygen reacts with the nickel ions to form nickel ion vacancies

$$O^{-(e)} \rightleftharpoons NiO + Ni\square^{''} + \boxplus$$

chemisorbed oxygen — nickel oxide — nickel ion defect — electron hole

for the overall reaction

$$\tfrac{1}{2}O_2 \rightleftharpoons NiO + Ni\square'' + 2\oplus$$

From this and the law of mass action we get that

$$[Ni\square''][\oplus]^2 = KPo_2^{1/2} \qquad (21)$$

If both the nickel vacancies and electron holes are proportional to the diffusivities,

$$[\mathcal{D}] = KPo_2^{1/6} \qquad (22)$$

a dependence of the diffusivity on the oxygen partial pressure to the one sixth power.

For nickel oxide, vaporization is unlikely in air since it has an oxygen partial pressure calculated from its free energy of 2×10^{-5} atmospheres at $1800^{\circ}K$ (R3).

In contrast to NiO, zinc oxide (ZnO) gives off oxygen on heating to form a metal excess compound (R49). This too can cause a low energy diffusion path. Zinc oxide dissociates to form an interstitial monocharged zinc ion with an electron in the lattice.

$$ZnO^{o} \rightleftharpoons Zn\overset{\bullet}{O}_i + \ominus + \tfrac{1}{2}O_2$$

Zinc Oxide — positive charged zinc interstitial — excess electron — oxygen gas

Again by the law of mass action we obtain:

$$[Zn_i^{\cdot}][\ominus] = KP_{O_2}^{-1/2} \qquad (23)$$

If both the zinc interstitials and excess electrons are proportional to the diffusivity we get:

$$[\mathcal{D}] = KPo_2^{-\frac{1}{4}} \qquad (24)$$

a dependence of the diffusivity on the oxygen pressure opposite to that of nickel oxide. At low oxygen partial pressures, zinc oxide has a high diffusivity and nickel oxide a low one.

In addition, zinc oxide vaporizes very readily above 1450°C (R48) (see Figure 1.12). These vapors contain no ZnO, but Zn and O_2. This can readily lead to mass transport by a vaporization-recondensation mechanism.

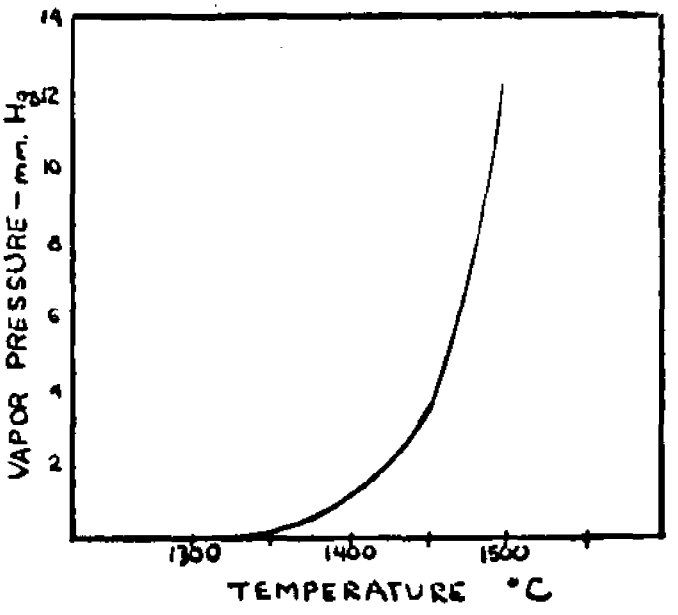

Figure 1.12 - Zinc Oxide Dissociation Pressure

2. Experimental

2.1 Kinetic Data Measurement

Although many fundamental studies have been performed on small spherical particles, we were aiming at fabricated shapes, and it was decided to approximate a real situation by the use of pressed pellets for our sintering studies. These pellets were about ½ inch in diameter and were prepared from thoria (99.9%) and yttria (99.99%) supplied by A.D. Mackay Inc., nickelous oxide (certified) from Fisher Scientific Company and zinc oxide (U.S.P., 99.5+%) from Bedesee Pharmaceutical Company. The proportions of thoria and yttria were based on a known good electrolyte composition. The selection of the amount of sintering aid will be discussed later. The raw powders for the selected compositions $Th_{.829}Y_{.146}Ni_{.025}O_{1.902}$ (TY.8N or TYN) and $Th_{.85}Y_{.15}O_{1.925}$ (TY) were ground in a 2 inch ball mill lined with latex rubber (gooch tubing). The mill contained ½ inch or 3/8" type 302 stainless steel balls. The TYN powders were milled for a minimum of 24 hours, and the TY a minimum of 72 hours. Other mixtures were prepared in an eccentric rotating mixer (made by Spex) of the type commonly found in dentists' offices. They were mixed in glass vials containing glass mixing beads and were sealed with polyethylene snap caps.

Single phase (solid solution or "alloyed") thoria-yttria powders were prepared in a tantalum resistance vacuum furnace manufactured by Brew & Company. This furnace is capable of reaching 2200°C, as measured by an optical pyrometer,

and operates at pressures below 10^{-5} torr. Sintered but unalloyed TYN pellets were also used as a source of powders. Fine-sized powders of the last two types were obtained by grinding in a Spex grinder for 50 minutes using a hardened steel cylinder with tungsten carbide caps and ball. A test for iron contamination was made using a control of known sintering behavior. No effect was observed and contamination was assumed negligible.

The powders for the pellets were always premeasured to about 0.25 c.c. and compacted at 50,000 psi in a ½ inch steel die with movable top punch and stationary bottom punch. The load was applied in a Loomis hydraulic press. After the load had relaxed to less than 25,000 psi, it was again raised to 50,000 psi, then quickly released. The die was inverted and the stationary punch removed. The sample was then ejected from the top. Many measurements were made on the "green" pellet size, and they were found to remain constant at 1.356±.003 cm.

A number of methods have been used to follow the change in dimensions of a compact being sintered. One of these is a dilatometer (R28, R41) which suffers from the need to make rapid contact with a push-rod to transmit the length change to the sensor. A second method employs accurate photography (R42), but has the disadvantage that results are delayed. The technique used in this work consisted of measuring the pellet size by means of a cathetometer or telescope mounted on an accurate scale. It has the virtue of simplicity, but requires

a great deal of tedious labor in reading dimensions.

The pellet, which had been pressed dry and without a binder, was strong enough to be handled without special care. It was placed on a zirconia holder shaped like a slitted L (see figure 2.1). The zirconia was ground down from a 1 inch zirconia rod supplied by Zircoa. The reason for the slit will be explained later.

The mounted specimen was put into the "intermediate zone" (approximately 600°C) of a tube furnace for at least 10 minutes. [The "intermediate zone" is the region outside of the constant temperature zone.] This was done for a threefold purpose; to degas the compact; to reduce thermal shock; and to reduce the time for the compact to reach the final temperature. Many tests run during this preheating at about 600°C showed that no dimensional change occurred. After 10 minutes in the intermediate zone, the specimen holder was pushed into the constant temperature zone of the furnace and placed close to a thermocouple. Dimensional measurements were taken immediately on the cathetometer capable of measuring within ± .002 cm. A series of statistical measurements on the pellet size calibrated the cathetometer when placed 30 inches from the specimen. The error was found to be 2.5% for a shrinkage of 12% (almost total shrinkage) of the ½ inch pellet.

The furnace, which was constructed in our laboratory, consisted of a horizontal 1" I.D. x 36" long mullite tube heated by four 27" x ½" Lifeline Globars connected in series. The heating chamber was 20 inches long and was

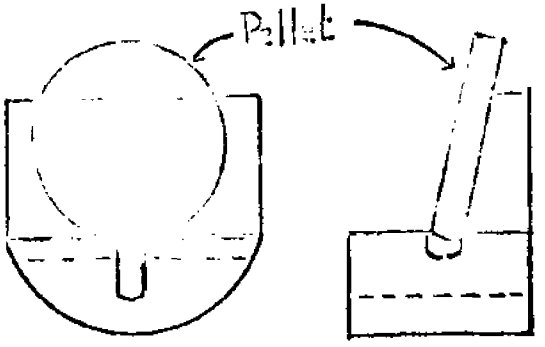

a) Front b) Side

Figure 2.1 - Specimen Holder

insulated by an unusually large thickness of at least 9 inches of refractory brick. This produced a constant temperature zone of 4½ inches. The furnace temperature was measured with a platinum/platinum-13% rhodium thermocouple placed within 1 inch of the specimen inside the mullite tube. Its EMF was measured with a Leeds and Northrup potentiometer. The system was calibrated at the melting point of gold (1063°C). The temperature was maintained by a Wheelco on-off controller connected to a platinum/platinum-10% rhodium thermocouple placed within the heating chamber but outside the mullite tube, so that the system response would be more rapid. This thermocouple was used for control purposes only. In order to keep fluctuations at a minimum, about 85% of the total power needed was applied continuously, while about 25% was used for fine control (see figure 2.2). In this way surges were kept at a minimum while the power oscillated between 85 and 110 percent of that needed to maintain the temperature. Temperatures as high as 1550°C were obtained and maintained within 2°C.

After the sample was pushed up to the thermocouple (which was positioned through the rear end to the rear side of the constant temperature zone), a timer was started. As soon as the cathetometer was focused, measurements were taken, using the telescope first on the top of the specimen, then on the bottom. Since above 1100°C, both the ZrO_2 holder and the thoria-based oxide mixtures were indistinguishable, the top and bottom of the specimen were rendered visible by means of the slit (see figure 2.1) which allowed viewing of the dark cold zone at the rear of the furnace. The first measurement

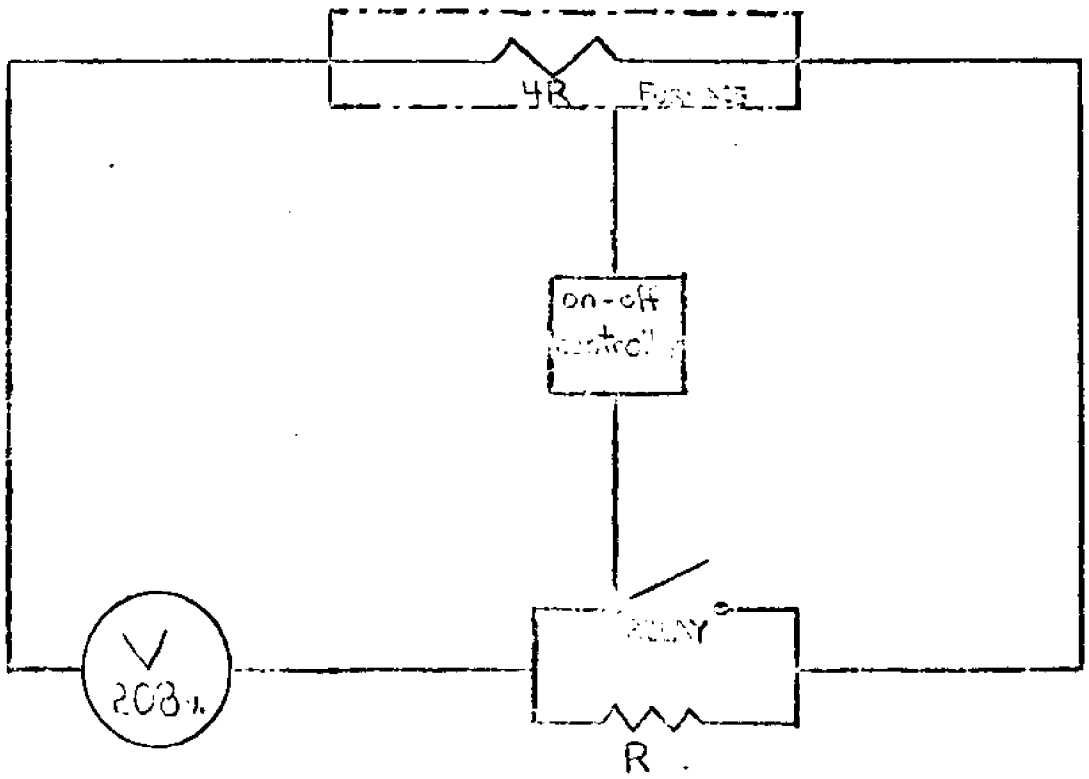

Figure 2.2 - Diagram, Furnace and Controller

was obtained at approximately 0.7 minutes. Subsequent readings were taken as needed. After the desired length of time, and after periodically checking the furnace temperature, the specimen was removed by pushing out from the rear into the intermediate zone, where it was allowed to cool for at least 5 minutes to minimize thermal stress. Then the pellet was removed, allowed to cool, and its properties measured.

2.2 Kinetic Shrinkage Rate Measurements

As previously stated, rate measurements are of obvious value in determining proper sintering conditions and may also be of value in explaining sintering behavior. But as mentioned earlier, the measurement of the rate of shrinkage of a disk undergoing sintering is not an easy matter. Because of a finite heat capacity, the time at which it reaches the approximate temperature of the test is ill-defined. Further, during this initial period, it is expanding because its temperature is rising and is shrinking because its density is increasing. To these difficulties is added the one relating the position of the pellet relative to the measuring instrument. Since it is undesirable to apply any stress, holding the specimen vertically is difficult. If it is put into a horizontal position, the measuring device or a prism must be above it, causing heating problems. In both cases, furnace tubes sag and so do supports so that one is not assured of reproducibility from test to test.

In the present research, the specimen was placed in a slightly inclined position with no effort made to measure

the angle of inclination. Instead, precise determinations were made of the sizes of the green compacts after pressing and of the sintered pellets after the desired time. Both of these were measured at room temperature. It was assumed that the inclination of the pellet remained unchanged during any run. Since the final hot size was also measured, it is obviously possible to relate the shrinkage during a run to the final cold size. Thus,

$$\underset{\text{observed length (hot)}}{Lc(t)} = \underset{\text{angular effects}}{\cos\theta}\underset{\text{cold length}}{[L(t)} + \underset{\text{thermal expansion}}{\alpha_L \Delta T L(t)}] + \underset{\text{edge effects}}{w \sin\theta[1+\alpha_L \Delta T]} \quad (25)$$

where θ is the tilt angle, L(t) the cold length at time t, w the thickness of the pellet and $\alpha_L \Delta T$ the fractional expansion due to heating. Noting that for our experiments $\alpha_L \Delta T \simeq .015$, $\theta \simeq 75^\circ$ and $w \geq .18L(t)$ yields

$$Lc(t) \sim 1.024\ L(t) \quad (26)$$

then as previously described when L is obtained by only using differences, the error introduced in the actual value is only 2.4%. Experimental checks found a maximum error of under 5%.

Final shrinkage and "green" (original) pellet size (L_o) were obtained by viewing the specimen outside of the furnace on an illuminated horizontal black field through the same cathetometer and a prism. When the compact was not friable, measurements were also made using a micrometer accurate to .001 cm. The latter method was found to be more consistent.

2.3 Physical Property Measurements

Density is an accurate measure of the extent of sintering. Density measurements were made to four places in a pycnometer made to specifications by Scientific Glass Apparatus Company. To find the density of a compact, first the dry pellet was weighed (PW), then the pellet was wetted in water and placed in a clean pycnometer filled with distilled water of known temperature (ambient). The pycnometer was tapped several times to remove entrapped air bubbles, then stoppered, scrupulously dried, and weighed (S). The pellet was then removed and its outside dried by wiping rapidly and it was then weighed at once (WP). The pycnometer was then visually observed for any specimen "chips". If they were present, then that pycnometer was weighed with the chips to get an actual weight (VP) or otherwise the clean pycnometer (after rinsing) was weighed (VP). The volume and density were respectively:

$$\text{Pellet Volume} = VP + WP - S \tag{27}$$

$$\text{Pellet Density} = PW/(VP + WP - S) \tag{28}$$

Also of interest was the accessible (wet) voidage, or volume percent water absorbed by the pores connected to the surface. This is given by

$$\text{wet voidage} = \frac{(WP - PW)/PW}{\frac{PW}{\rho_p} + \frac{(WP-PW)}{\rho_w}} \tag{29}$$

where ρ_w and ρ_p are the densities of water and the thoria-based mixture respectively. Some measurements of accessible pore volumes and sizes were also obtained under pressure on an AMINCO* mercury porosimeter.

*American Instrument Co.

The degree of homogeneity, or solution of yttria in thoria, was measured by x-ray diffraction. Lattice parameters were obtained either by use of a Debye-Scherrer powder pattern or by use of a Norelco diffractometer. Cu_{α} radiation, filtered by nickel, was used and measurements were made to four significant figures resulting in a scatter of .03%. Diffractometer specimens were either polished flat or the pellets ground down in an agate mortar. The latter method was found to be more reproducible. The x-ray machine was calibrated using CaF_2 as a standard.

A few micrographs were obtained on a Leitz metallurgical microscope with camera attachment capable of 2500X magnification. Specimens were prepared for microscopic examination by polishing on emery grit wheels and on automatic diamond polishing wheels with particle sizes as low as 3μ. Final polishing was with pure alumina. Specimens were etched with hot H_3PO_4, H_2SO_4 or molten $KHSO_4$ in less than 2 minutes.

Powder particle sizes were obtained on a Coulter Counter capable of measuring down to 1μ; by Andreisan pipette; by Fisher-Dotts, Stokes law apparatus and by scanning electron microscope. Scanning electron microscopy was also used to observe the particle behavior in various stages of sintering.

2.4 Scanning Electron Microscopy

In earlier sections (1.3 and 1.4), the use of kinetic sintering data, i.e. $\Delta L/Lo$ vs. a function of time, was described as a test of the mechanism of sintering. Although this approach has been employed widely, it is of dubious value for the elucidation of mechanisms (R11). It is highly suspect when more than one mechanism is operative and is of almost no value when the shapes of the powder particles depart greatly from spherical. When, in addition, the system is multicomponent, this further complexity makes reliance on kinetic data alone virtually impossible. Therefore, a different approach is needed.

Microscopy would appear to be a good investigative technique. However, the particle sizes of the powders are so small, that microscopy by visible light with its limited resolution and very small depth of focus is of little real value. Hence, it was abandoned after a few early attempts.

Fortunately, scanning electron microscopy (SEM) has been developed to a high level of quality in the past few years (R33). It is capable of magnifications in the range of 1000-20,000X and possesses an immense depth of focus as compared with light microscopy. This method has a disadvantage in that specimens must be conductive to avoid "charging" by electrons and accompanying loss of resolution.

Since an SEM unit was not available locally, specimens were prepared and taken to Structure Probe, Inc. at West Chester, Pa. There, they were fractured as necessary, and vacuum coated on a tilting stage coating unit with about 200 Å of a gold-palladium alloy to eliminate charging. They

were then examined on a JSM3U3 scanning electron microscope and projected on a large T.V. receiver. Specimens were photographed on 4"x5" Polaroid film. The photos were reduced to 3¼"x4½" for this report.

3. Experimental Results

3.1 Introduction

Since the primary purpose of this research was the reduction of the sintering temperature from the usual 2100°C to about 1500°C or less, the initial effort consisted of the exploratory screening of a variety of sintering aids. Without any a-priori theory or hypothesis, the selection was necessarily quite random. However, a number of guidelines were employed: oxides and halides that had been found to aid the sintering of thoria or zirconia were tried, as were closely related compounds; compounds that had the same type of fluorite structure; or oxides that might form solid solutions based on Hume-Rothery's criteria.

An initial exploratory survey was made of the effects of a number of additive oxides and fluorides. These tests were run en masse in a Lindberg furnace at its maximum operating temperature of about 1370°C (2500°F) as measured by a chromel-alumel thermocouple. The pellets were prepared as previously described and placed on alumina dishes. Nickelous oxide (NiO), zinc oxide (ZnO), copper oxides (CuO and Cu_2O) and cobalt oxide (Co_3O_4) were found to aid sintering excellently when air fired for two hours as described. Other additives were found to have no effect on the sintering (see Table 3.1 describing the results with thoria-yttria). As a result of this screening survey, nickel oxide and zinc oxide were selected as the primary reference additives to be studied in detail. Copper oxide, though it is a good sintering

aid, forms a liquid at 1235°C. This could cause deformation of the electrolyte at high temperatures, or cause liquid junction potentials. Cobalt oxide was dropped because of the numerous oxidation states of cobalt. These might physically harm the electrolyte or induce electronic conduction.

At first it was suspected that the ThO_2-Y_2O_3-NiO system might form an eutectic thereby causing activated liquid-phase sintering. To investigate this, a series of ThO_2-NiO, Y_2O_3-NiO, and TY-NiO mixture compacts ranging in composition from 2 wt % up to 90 wt % NiO in increments of about 9 wt % were fired at 1370°C for four hours. The specimens were then examined for any visual evidence of liquid formation which might be shown by smoothing of sharp edges or surfaces, or rounding of flash. No such evidence of liquid formation was found. (It will be shown later that the addition of 2.5 mole percent NiO to ThO_2 or TY improves the sintering considerably. Since the melting point of ThO_2 is 3300°C and that of NiO is 1990°C, it is extremely unlikely that a liquid phase is formed in this case at 1370°C.)

Table 3.1 Effect of 2 wt % Additions on the Sintering of TY Fired at 1370°C for 2 Hours

Additive	Oxid. state	Cationic rad.	Elec. neg.	Final percent accessible voids
NiO	+2	.78	1.8	6
Co_3O_4	+2,3,3	.78, .63	1.8	5
Fe_3O_4	+2,3,3	.76, .64	1.8	-
ZnO	+2	.74	1.6	0
CuO*	+2	.69	1.9	6
CaF_2	+2			>20
LiF	+1			>20
Cr_2O_3	+3	.69	1.6	>20
SiO_2	+4	.41	1.8	>20
TiO_2	+4	.68	1.5	>20
MgO	+2	.65	1.2	>20
Ta_2O_5	+5	.73	1.5	>20
ZrO_2	+4	.80	1.4	>20
Al_2O_3	+3	.50	1.5	>20; .05μ~16
CdO	+2	.97	1.7	>20
BaO	+2	1.35	.9	>20
SrO	+2	1.13	1.0	>20

*forms a liquid

3.2 Effect of Additives on Sintering

As already stated, the purpose of this research was to reduce the sintering temperature of thoria-yttria (TY). The extent of that effect should be shown more quantitatively than in Table 3.1. Figure 3.1 shows a comparison between the kinetic shrinkage curves of thoria-yttria-nickel oxide, thoria-yttria-zinc oxide and thoria-yttria. All specimens were fired at temperatures between 1370 and 1385^{o}C. It should be noted that maximum density corresponds to a fractional shrinkage of 0.126. This graph shows that at 1370^{o}C, additions of 0.8 wt % ZnO or NiO cause a rise in shrinkage from 40% of the total possible shrinkage to well over 90%. Examination of Figure 3.1 will show that the bulk of the effect of the additive occurred within the first two minutes during which time the specimen may not yet have reached steady state. It also indicates an unexpected shape to the curve, since the Kuczynski model is expected to yield a straight line on a log-log plot (see Figure 3.2). Instead, the quick initial rise followed by a fairly horizontal zone implies more than one transport mechanism. The shrinkage curve compared to that for a well known material, alumina, is shown in Figure 3.3. Alumina sintering follows a bulk diffusion mechanism with a sintering index "m" of 0.37.

The reference mixtures for the present study were chosen on the basis of optimizing both the additive effect and the operable oxygen pressure range of the electrolyte. Thoria-15 at % yttria ($Th_{.85}Y_{.15}O_{1.925}$) was selected

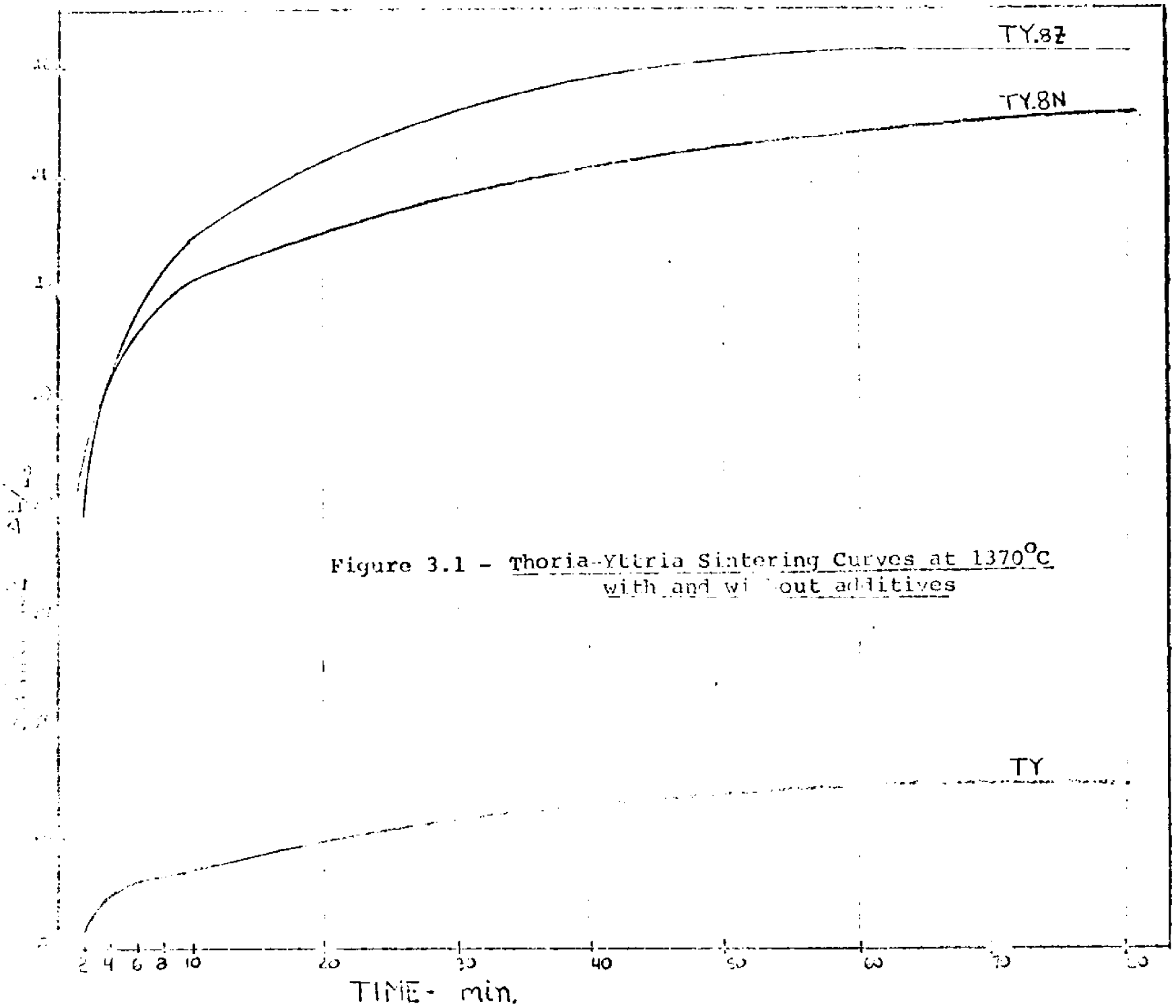

Figure 3.1 - Thoria-Yttria Sintering Curves at 1370°C with and without additives

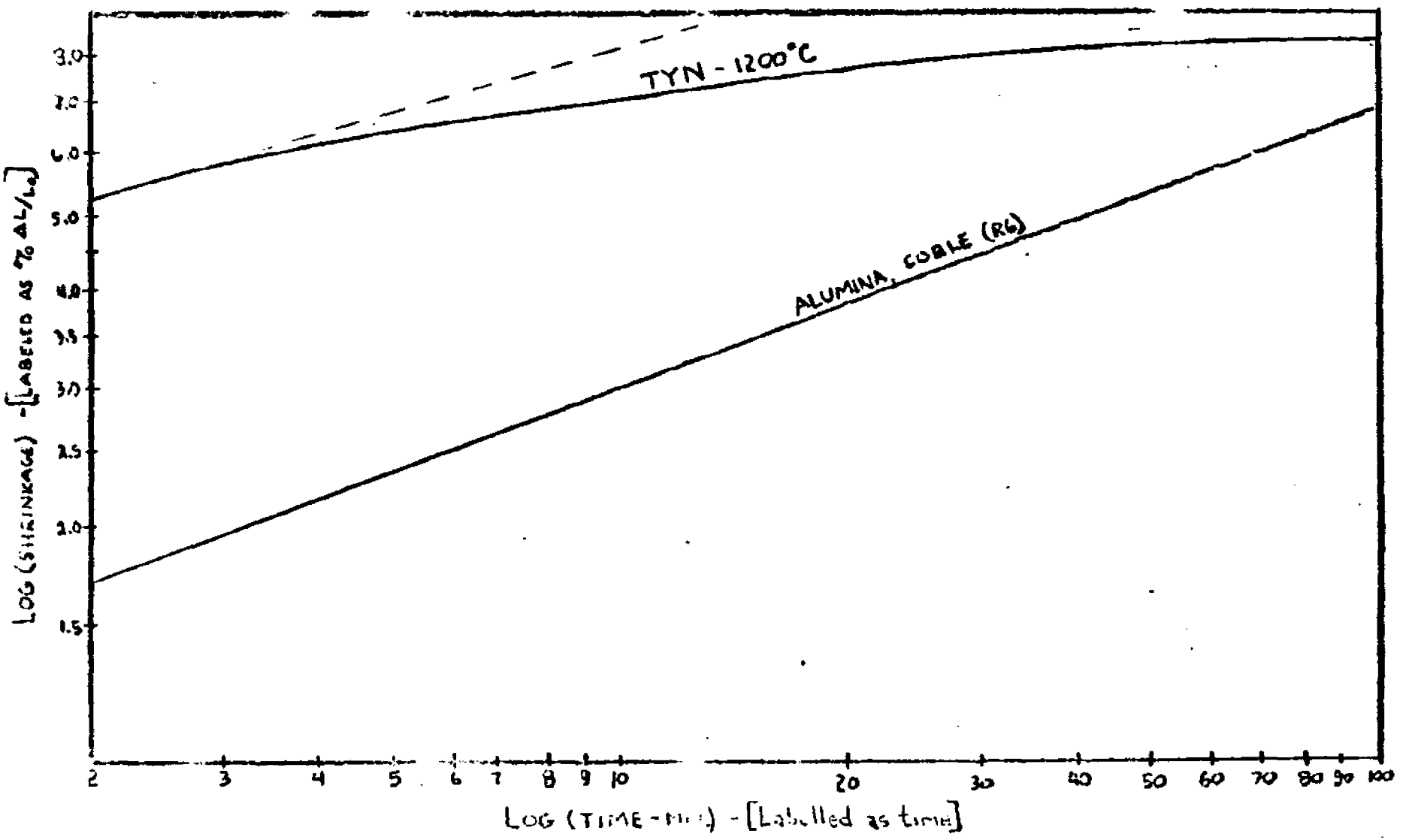

Figure 3.2 - Log-Log Kinetic Shrinkage Curve, Coble vs. TYN

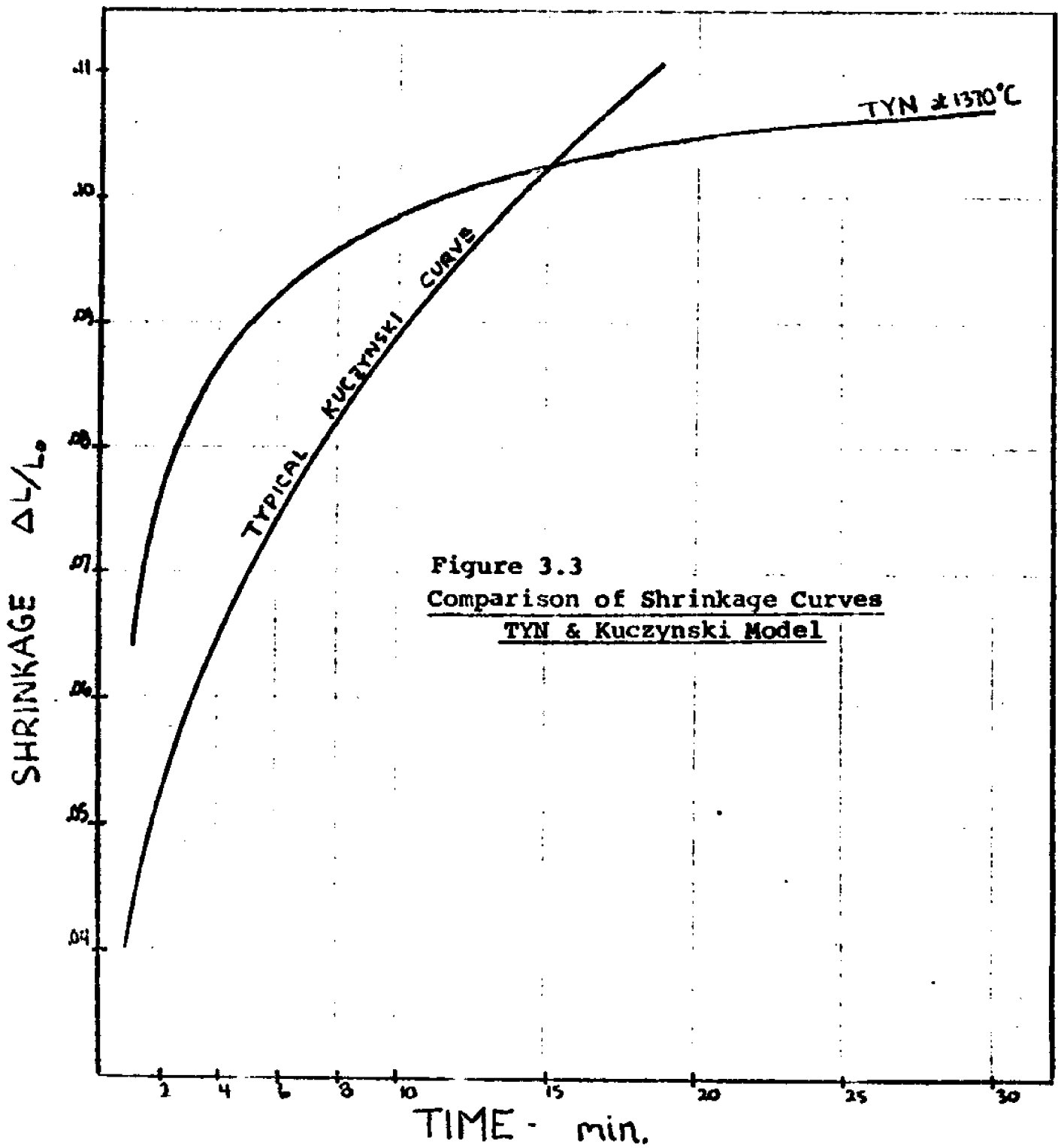

Figure 3.3
Comparison of Shrinkage Curves
TYN & Kuczynski Model

because this was the material used previously by Levine (R1) and shown by Steele and Alcock (R37) to have the widest range of oxygen partial pressures for anionic conduction. The amount of additive was chosen on the basis of studies conducted in this laboratory (see Figures 3.4, 3.5, 3.6 and 3.7). In these Figures, percent additive is plotted both against accessible (wet) voidage (residual water left in internal pores after rapid drying of the surface) and shrinkage. For both materials and methods, a marked effect is noted with up to 0.2 to 0.4 wt. percent additive. Thereafter, increasing the amount of additive has no appreciable effect. This kind of behavior is typical for additives. Eight tenths of a percent was chosen because it was far enough into the "plateau" region of the additive curve so that it would produce the best sintering despite inhomogeneity of the mixed powders. It is expected to be small enough to produce no appreciable electronic conduction (R51).

Figure 3.8 compares the effect of nickel oxide on the sintering of thoria and thoria-yttria mixtures at 1370°C for times up to 100 minutes. Note that nickel oxide greatly increases the shrinkage rate of both thoria-yttria and thoria, with T.8N sintering to a higher density than TY. Again the major difference in shrinkage occurred in the initial heat-up period, where non-steady state conditions are prevalent.

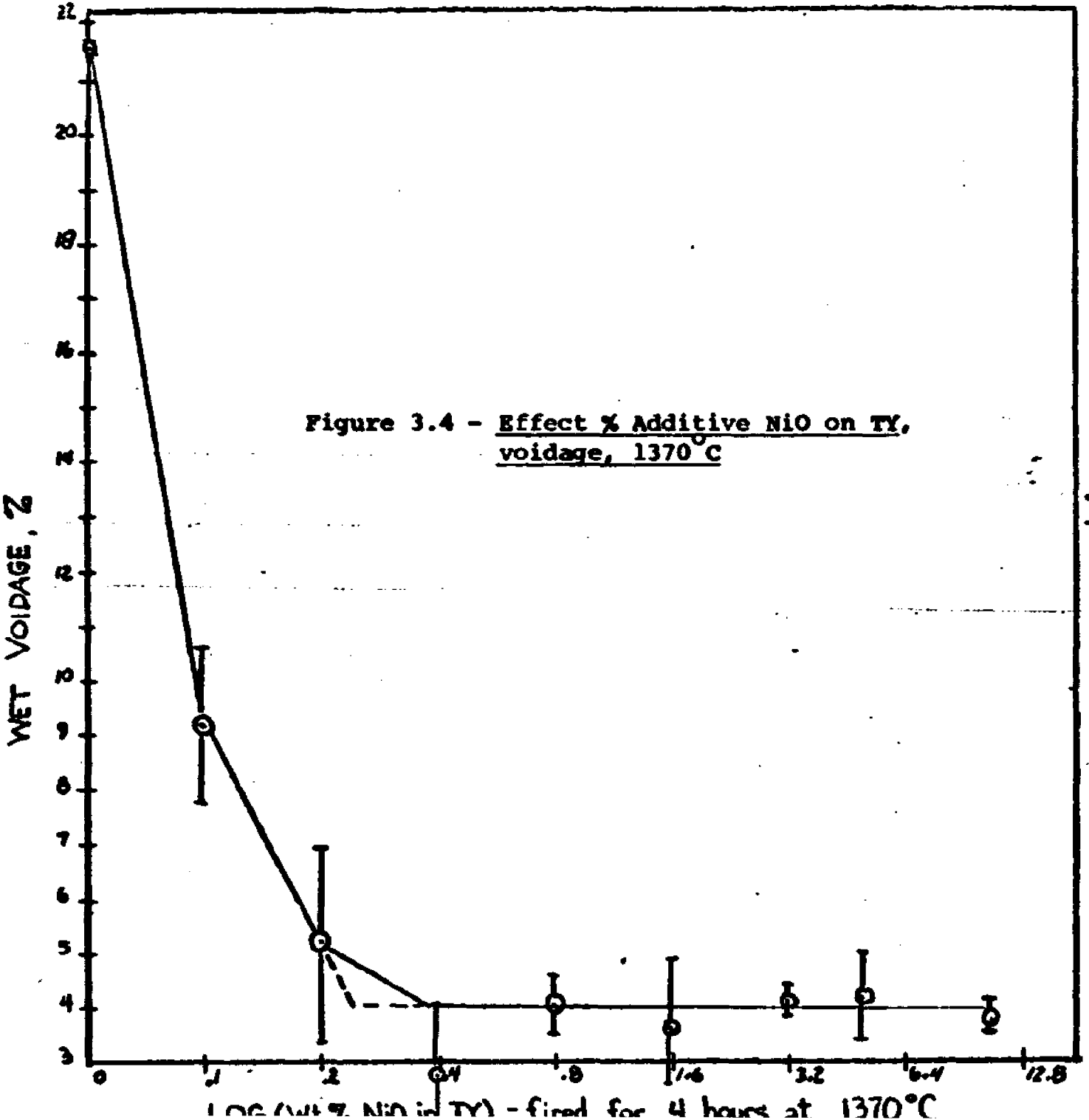

Figure 3.4 - Effect % Additive NiO on TY, voidage, 1370°C

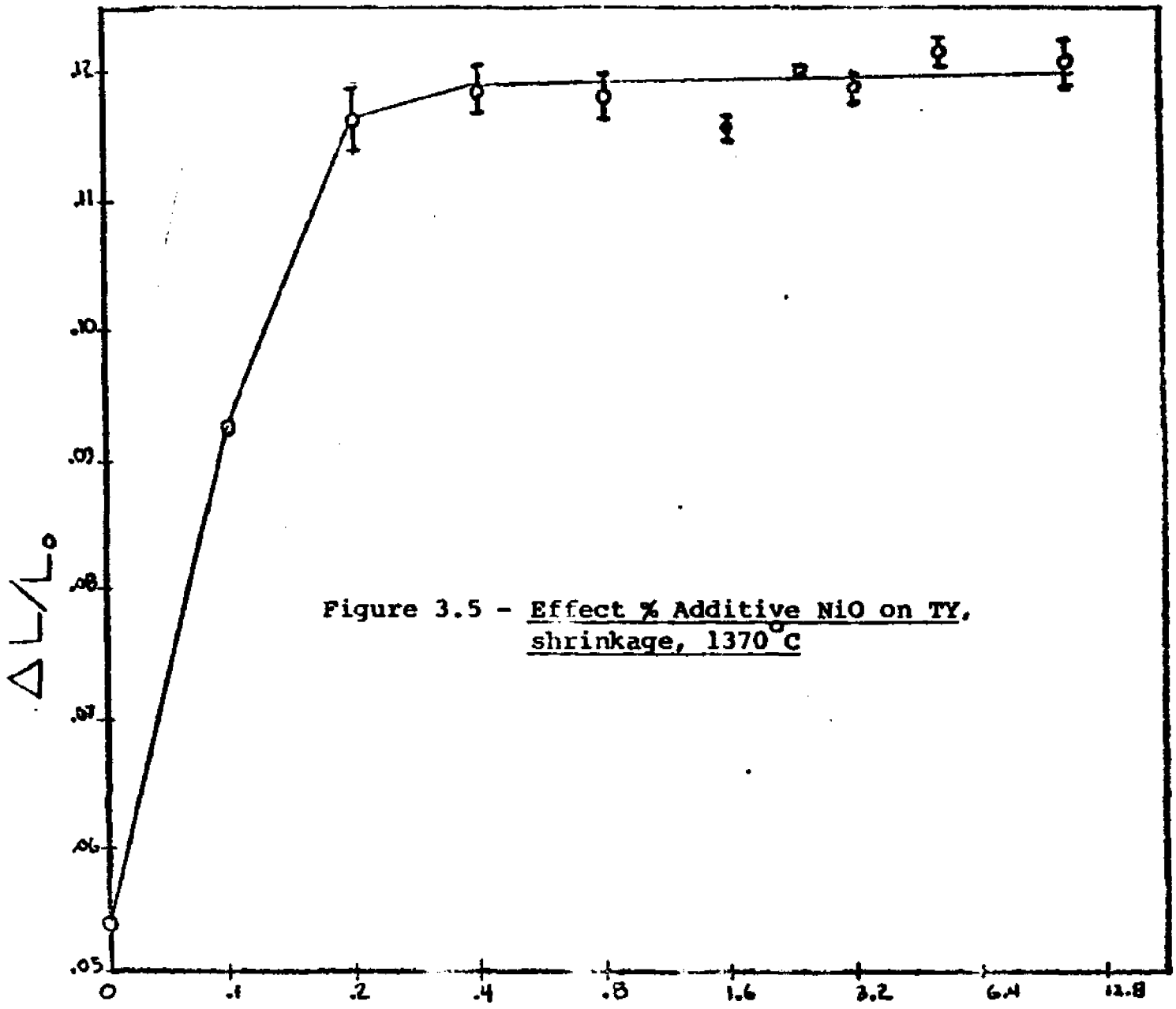

Figure 3.5 - Effect % Additive NiO on TY, shrinkage, 1370°C

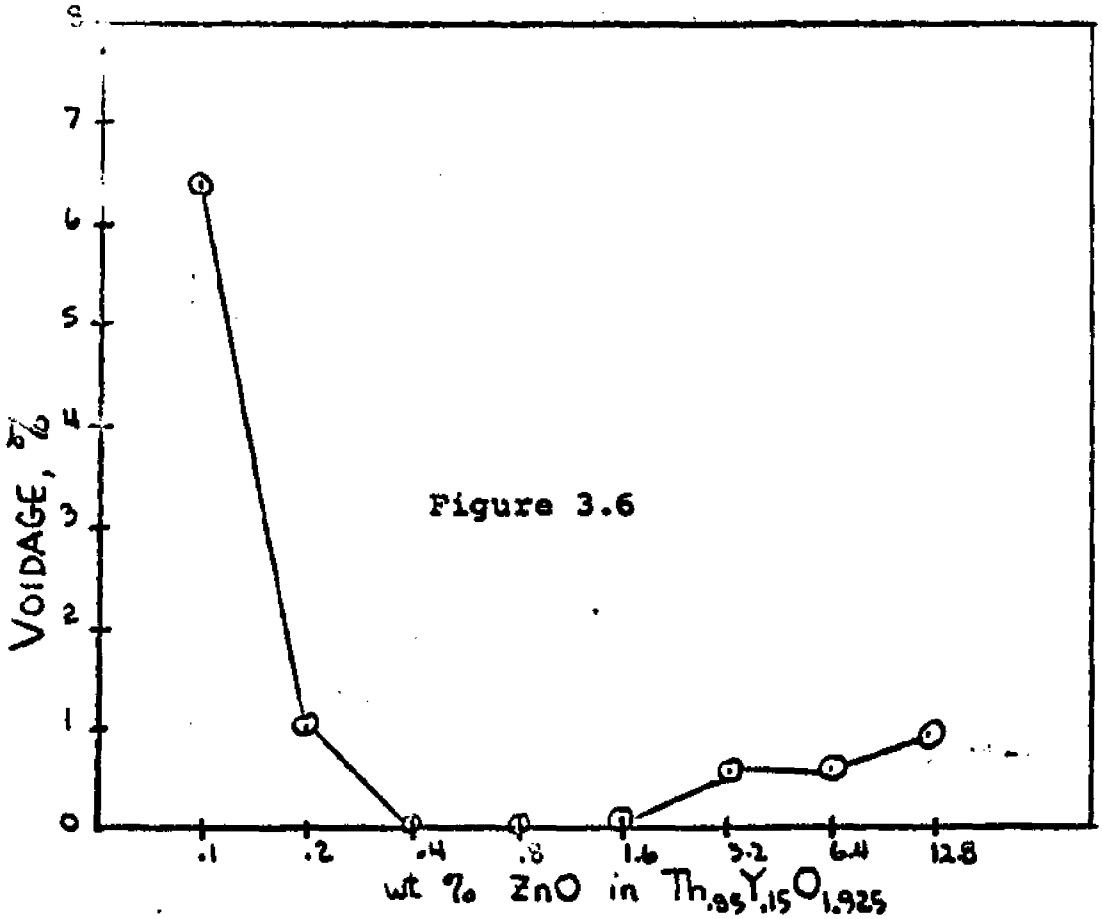

Figure 3.6

Effect of ZnO Concentration on Sintering at 1370°C for 100 minutes

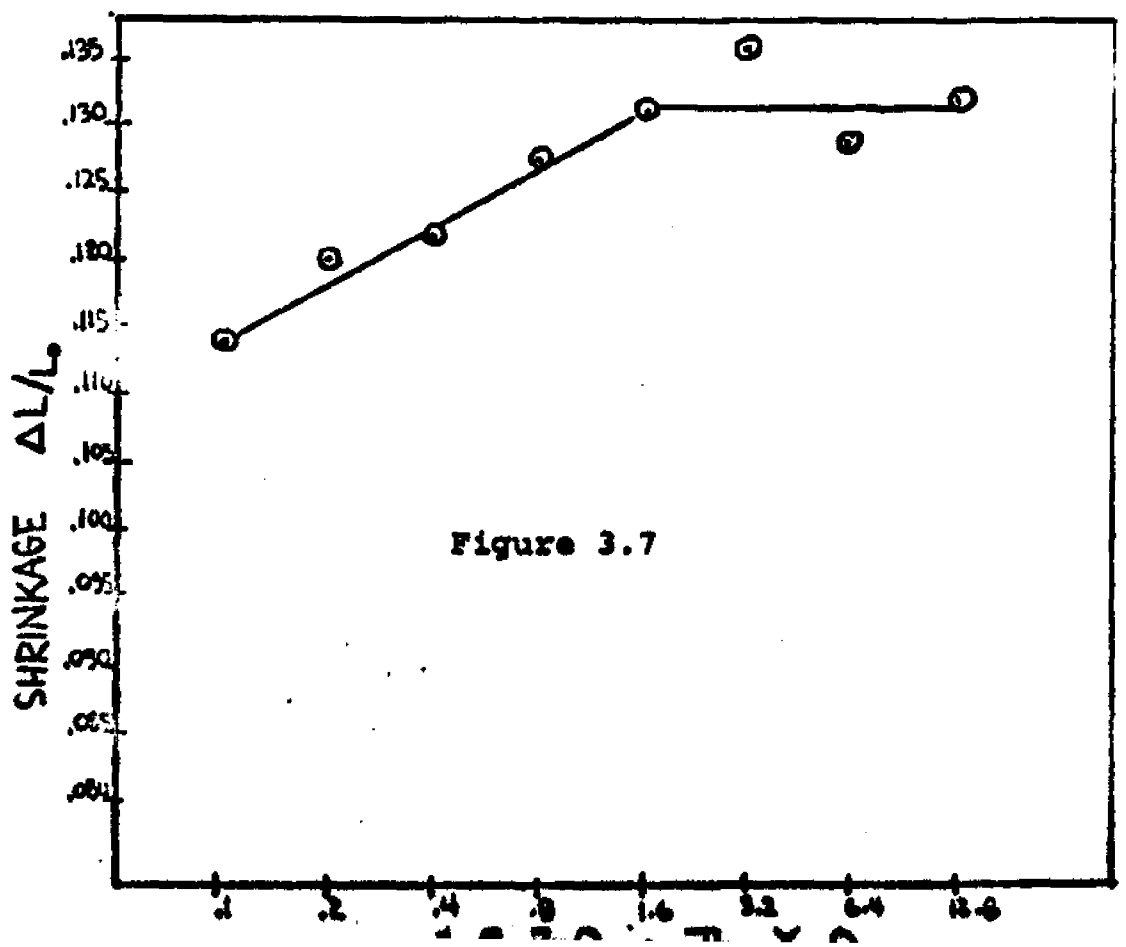

Figure 3.7

This page is blank.

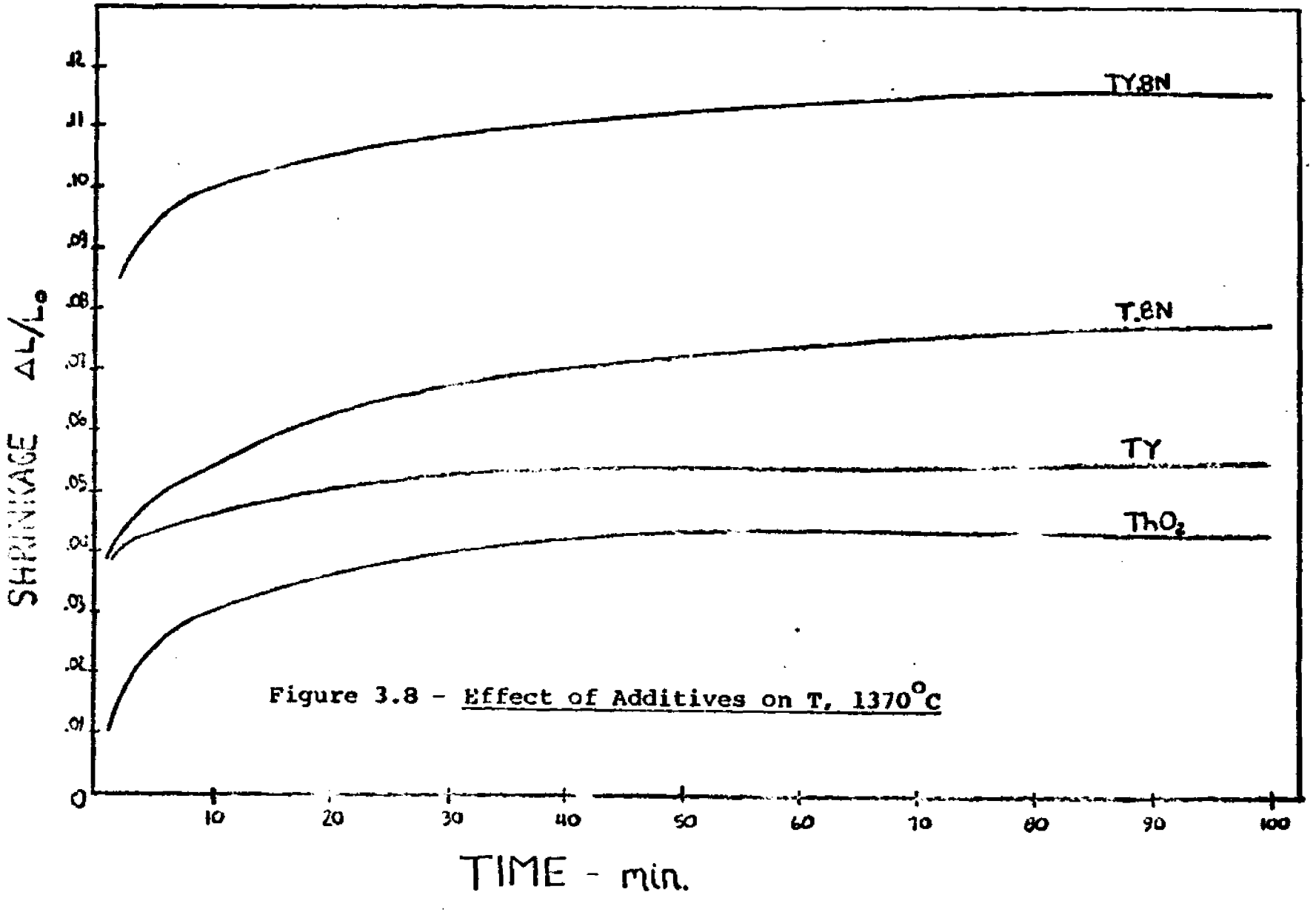

Figure 3.8 - Effect of Additives on T, 1370°C

3.3 Effect of Temperature

In an effort to select the most suitable conditions for sintering and to help elucidate the mechanism, a series of kinetic shrinkage curves for TY.8N were run at different temperatures (see Figure 3.9). Each curve in Figure 3.9 represents the average of at least three runs. The data at 1450, 1370 and 1300°C represent the average of eight separate runs. The extent of scatter in the shrinkage data is displayed at the 10 and 100 minute times. It is quite evident that an apparent end point in density exists for these moderate times. This density is essentially dependent on temperature alone and is independent of time. This is similar to the results of Morgan's group (R29, R30, R38). Once again, the obvious major difference among the kinetic curves is the events of the first two minutes where temperature gradients are high and non-steady state exists. Indeed, it appears that the superposition of the 1300, 1370 and 1440°C curves from .7 minutes on yield but one curve.

Similar runs have been made on TY.8Z (see Figures 3.10 and 3.11). Each curve here represents the average of three runs made at the designated temperature. Here again apparent temperature-dependent, time independent end points were noted, with the behavior differing substantially only during the first minute.

To check on the method of estimating the actual dimensions and to further clarify the initial behavior during heat-up, short-time runs were made on TY.8N at

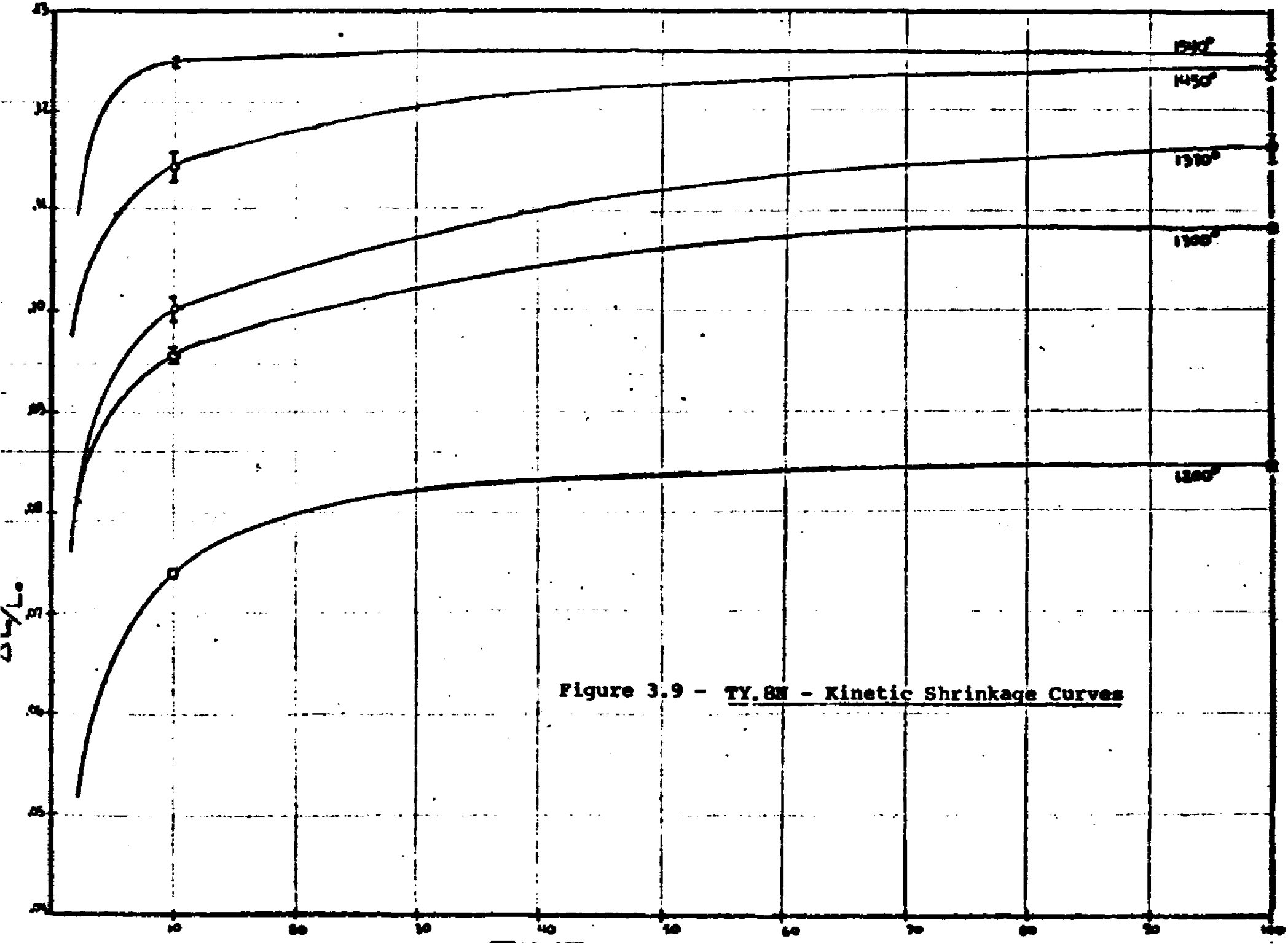

Figure 3.9 - TY.8M - Kinetic Shrinkage Curves

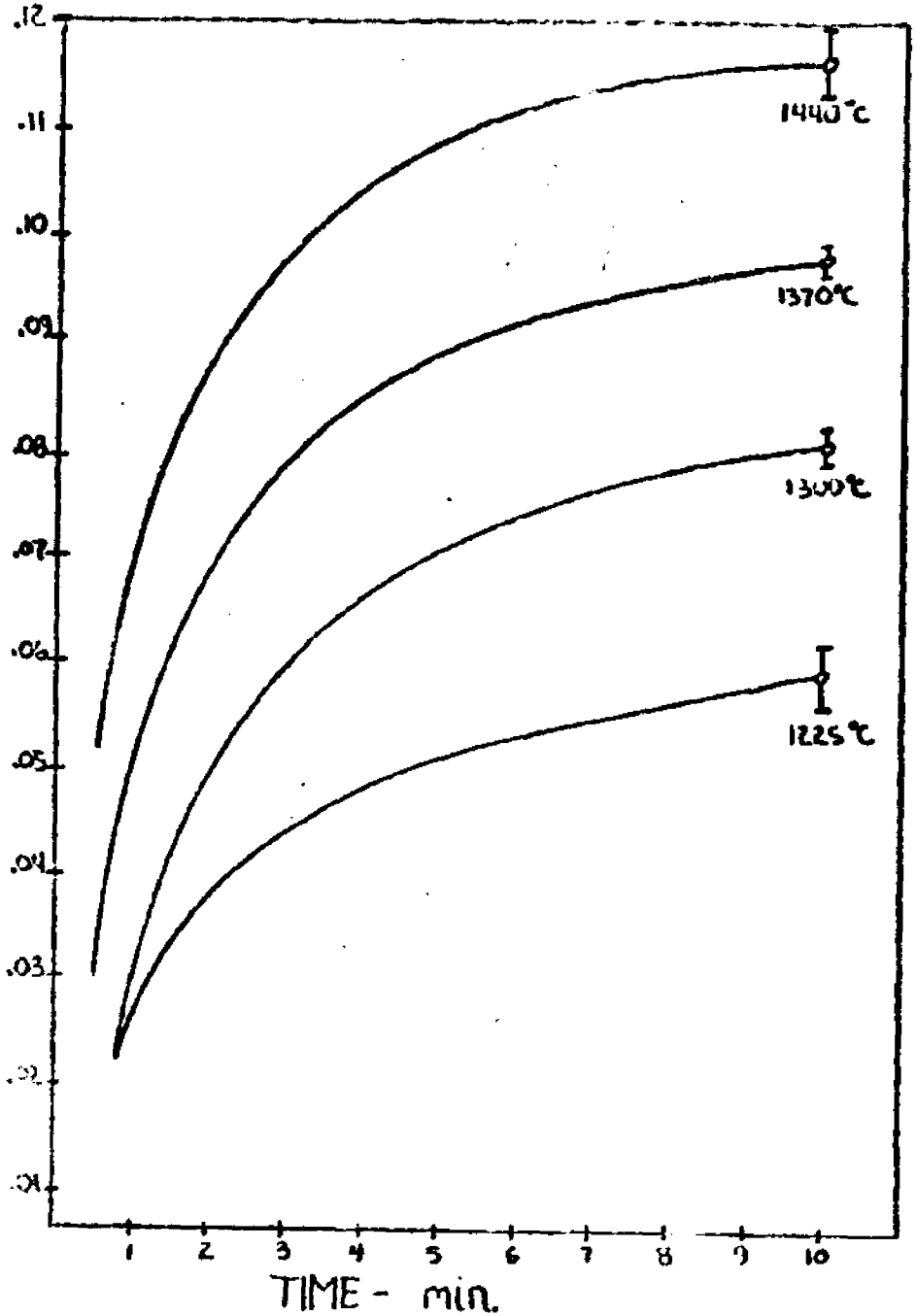

Figure 3.10
Kinetic Shrinkage Curve
TY.8Z

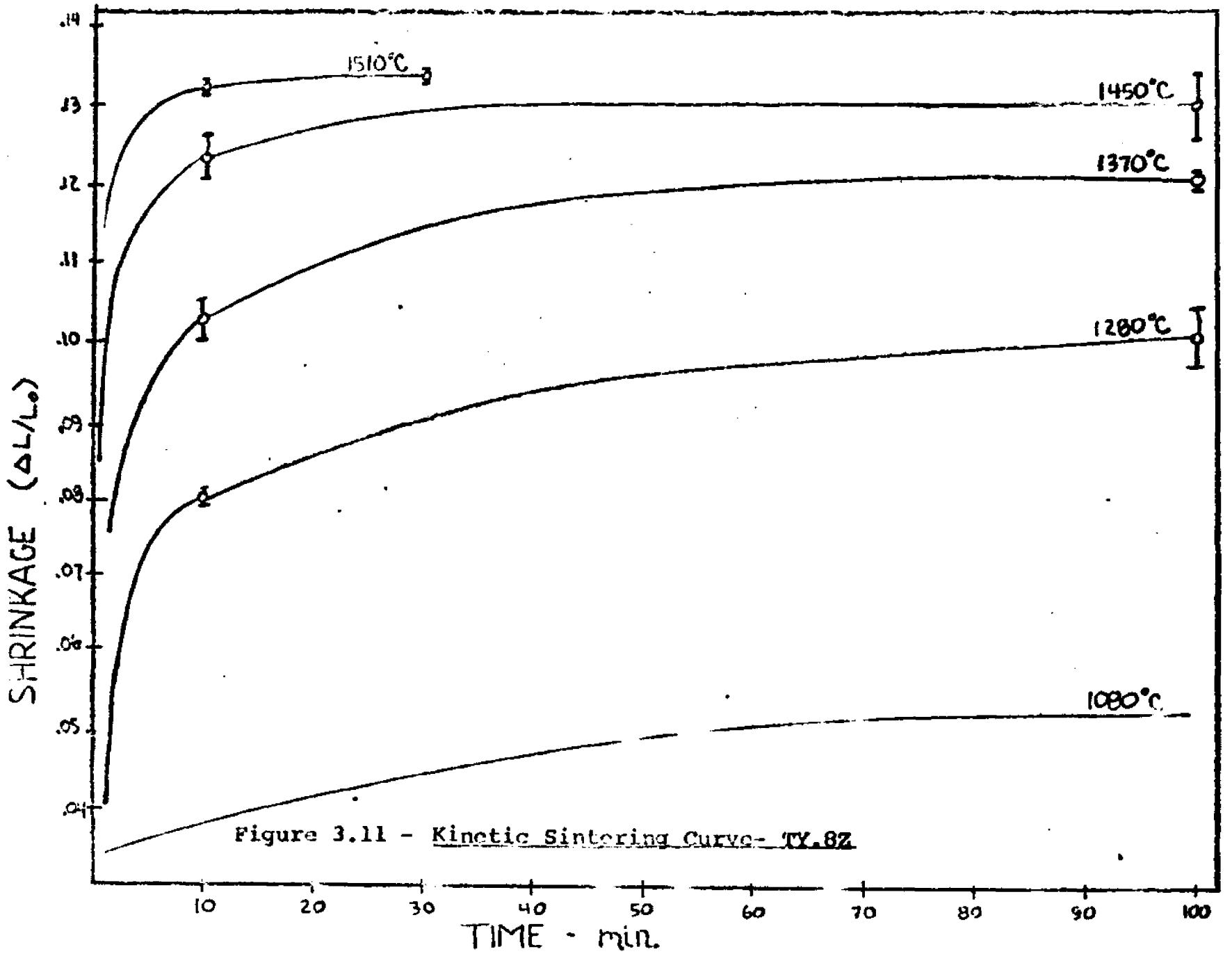

Figure 3.11 - Kinetic Sintering Curve- TY.8Z

1370°C. These consisted of inserting the pellet in the hot zone of the furnace for a length of time varying from 15 sec to 8 minutes, then rapidly removing it. The data for these runs are given in Figure 3.12. Each data point was obtained on two different pellets. For the 2, 4 and 8 minute samples, one pellet was heated continuously for the indicated time, and the other was previously heated for a shorter length of time and incrementally heated to the indicated time. Each value of $\Delta L/Lc$ is the total shrinkage for the indicated time. Comparison with two points obtained from earlier continuous in situ measurement of the same temperature, shows essentially no difference.

Some runs were made for one thousand minutes. The overall curve is shown in Figure 3.13. This shows that despite an apparent temperature-dependent end point at short times, densification proceeds close to theoretical ($\Delta L/Lo \approx .126$) when sintered for long times even at lower temperatures. Similar results were obtained at 1440°C. The difference in end point at 100 minutes and later approach to one single density indicates two different mechanisms, the slower one dominant at longer times.

Wet (accessible) voidages were also measured on samples of TYN at the end of 10, 30 and 100 minute runs (see Section 2.3). These data, plotted as 1/T versus wet voidage, are shown in Figures 3.14 and 3.15 for TYN and TYZ. Theoretically, they should be plotted as an Arrhenius-type plot ($1/T$ vs. $\ln(\Delta v)$), but note that it yields a relatively straight line on a $1/T$ vs. ΔV plot.

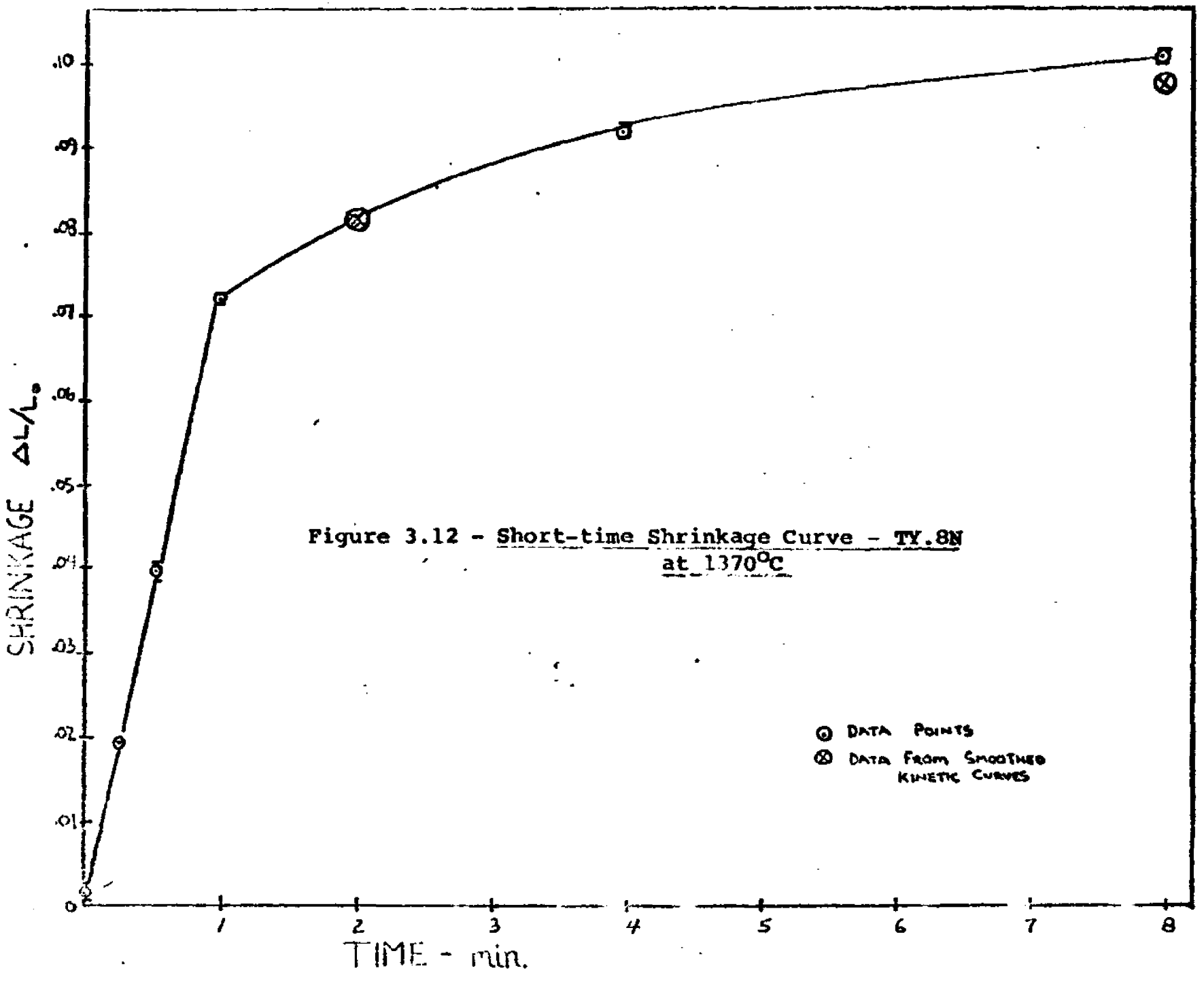

Figure 3.12 - Short-time Shrinkage Curve - TY.8N at 1370°C

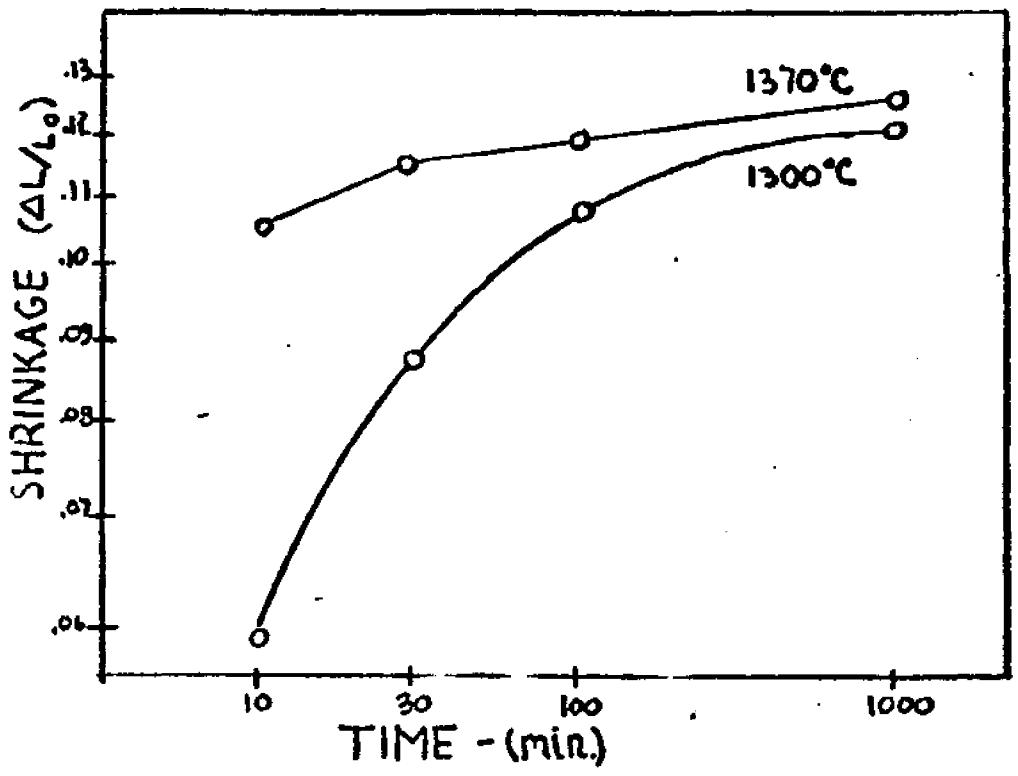

Figure 3.13 - Log-Log Kinetic Shrinkage Curve

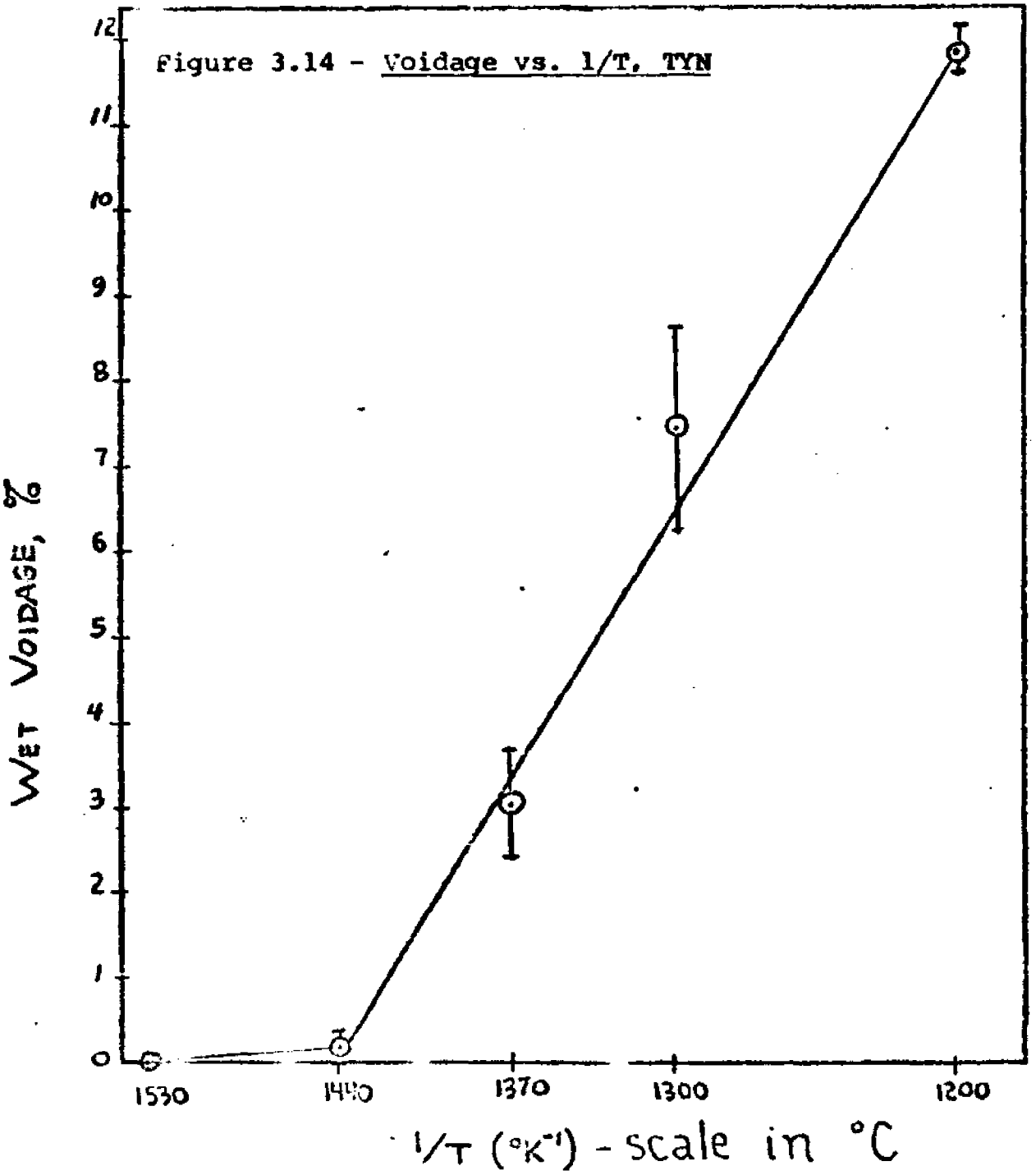

Figure 3.14 - Voidage vs. 1/T, TYN

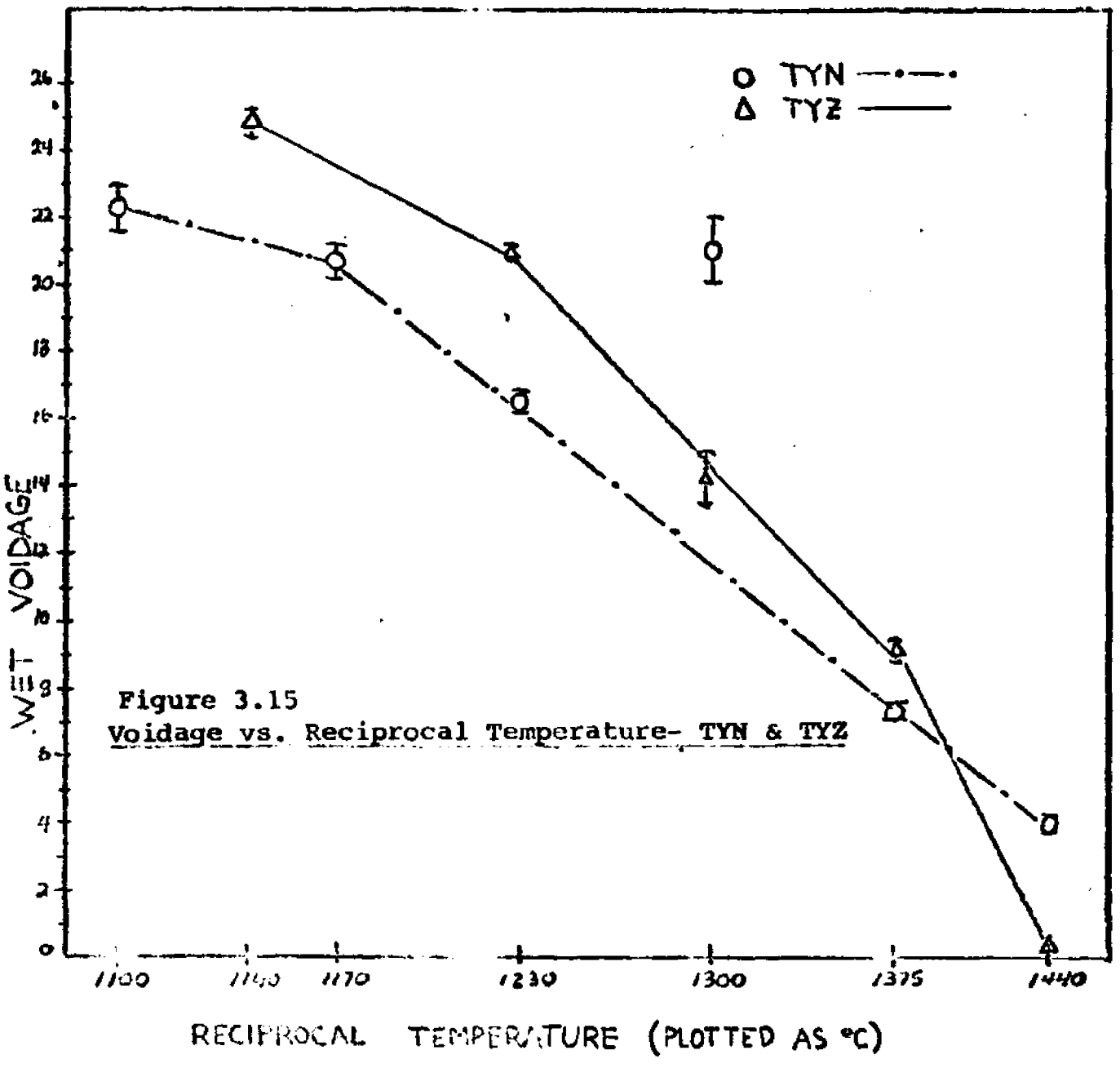

Figure 3.15
Voidage vs. Reciprocal Temperature- TYN & TYZ

The abrupt increase in shrinkage which occurs in the first few minutes and which is followed by a period of much slower rate of shrinkage might be explained in terms of a time limited effect of the additive. For example, the additive might be effective only when present in high concentrations on the surface of the thoria and/or yttria. Once diffused into the TY, it would then be expected to lose its power. If this explanation were correct, a specimen that had reached an apparent end point in shrinkage at one temperature should show no abrupt increase in shrinkage when rapidly raised in temperature.

This theory was tested in a series of runs made on T, TN, TYN and TYZ. The pellets were fired at one temperature, cooled and measured by a micrometer, then refired at a higher temperature. The results are shown in Figures 3.16 through 3.19. Each curve represents at least 10 data points taken at each temperature and with each run being duplicated at least once. It will be observed that on reaching the higher temperature, the specimen approached the fractional shrinkage to be expected from continuous heating at that temperature. In other words, the additive apparently does not lose its potency by diffusion into the body of the electrolyte material, while TY and TYZ exhibit no such initial jump.

It is fairly common in the sintering of multicomponent powders such as mixed oxides or carbides of nuclear fuels, to find that although a high density is attained, the individual components do not interdiffuse or "alloy" completely to form

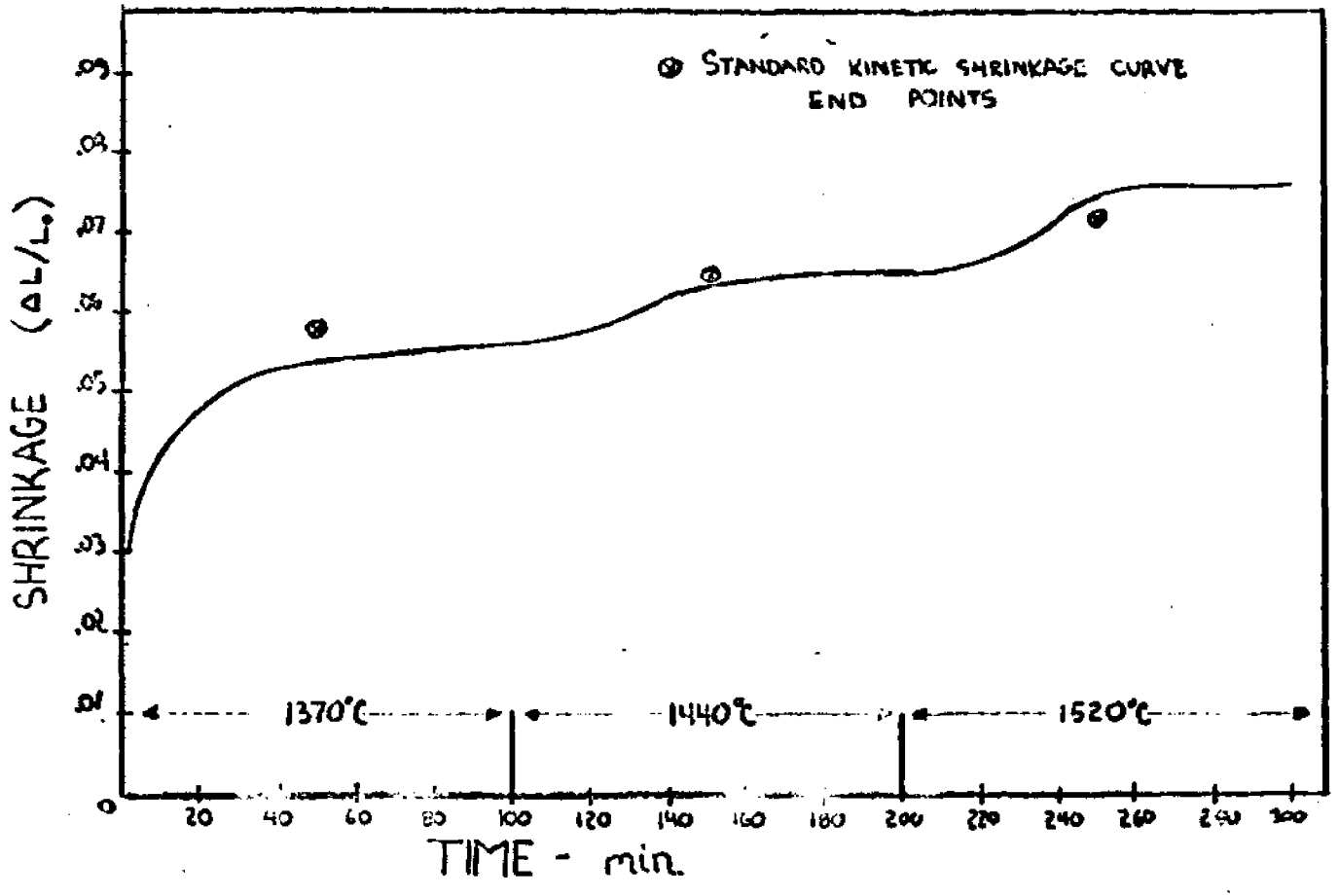

Figure 3.16 - Discontinuous Runs, ThO_2; 1370, 1440, 1520°C

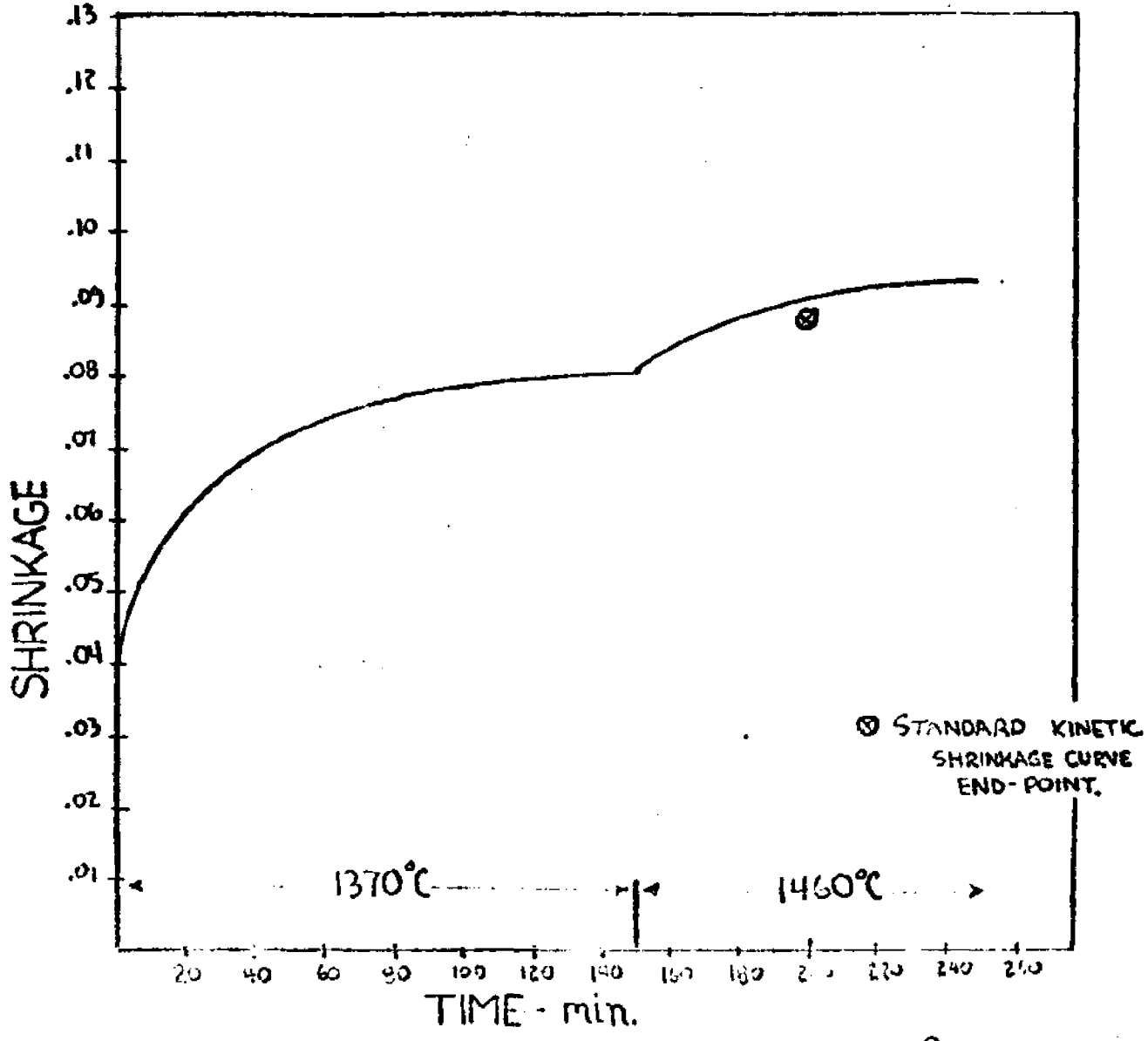

Figure 3.17 - Discontinuous Run, TN; 1370, 1460°C

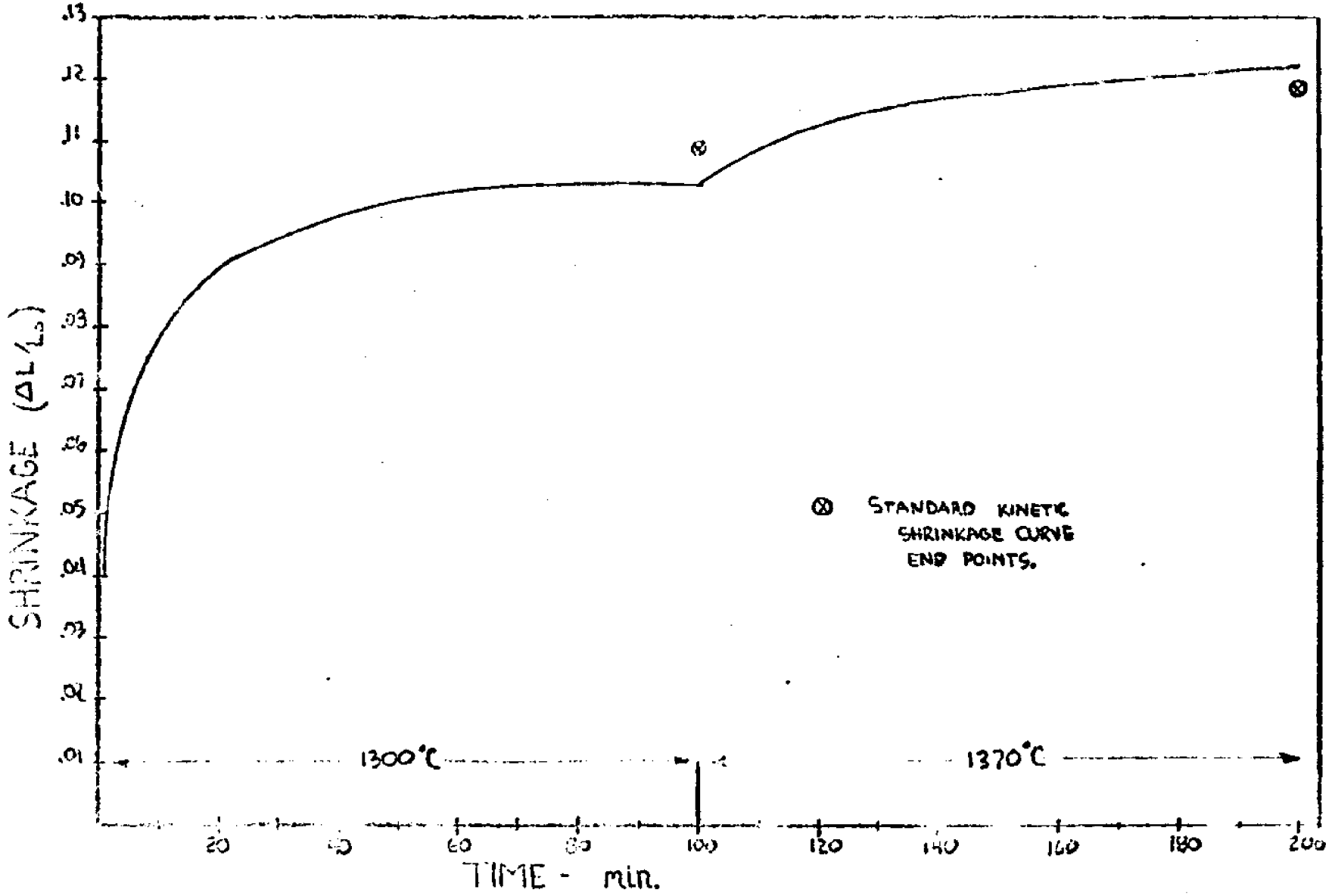

Figure 3.18 - Discontinuous Run, TYN; 1300, 1370°C

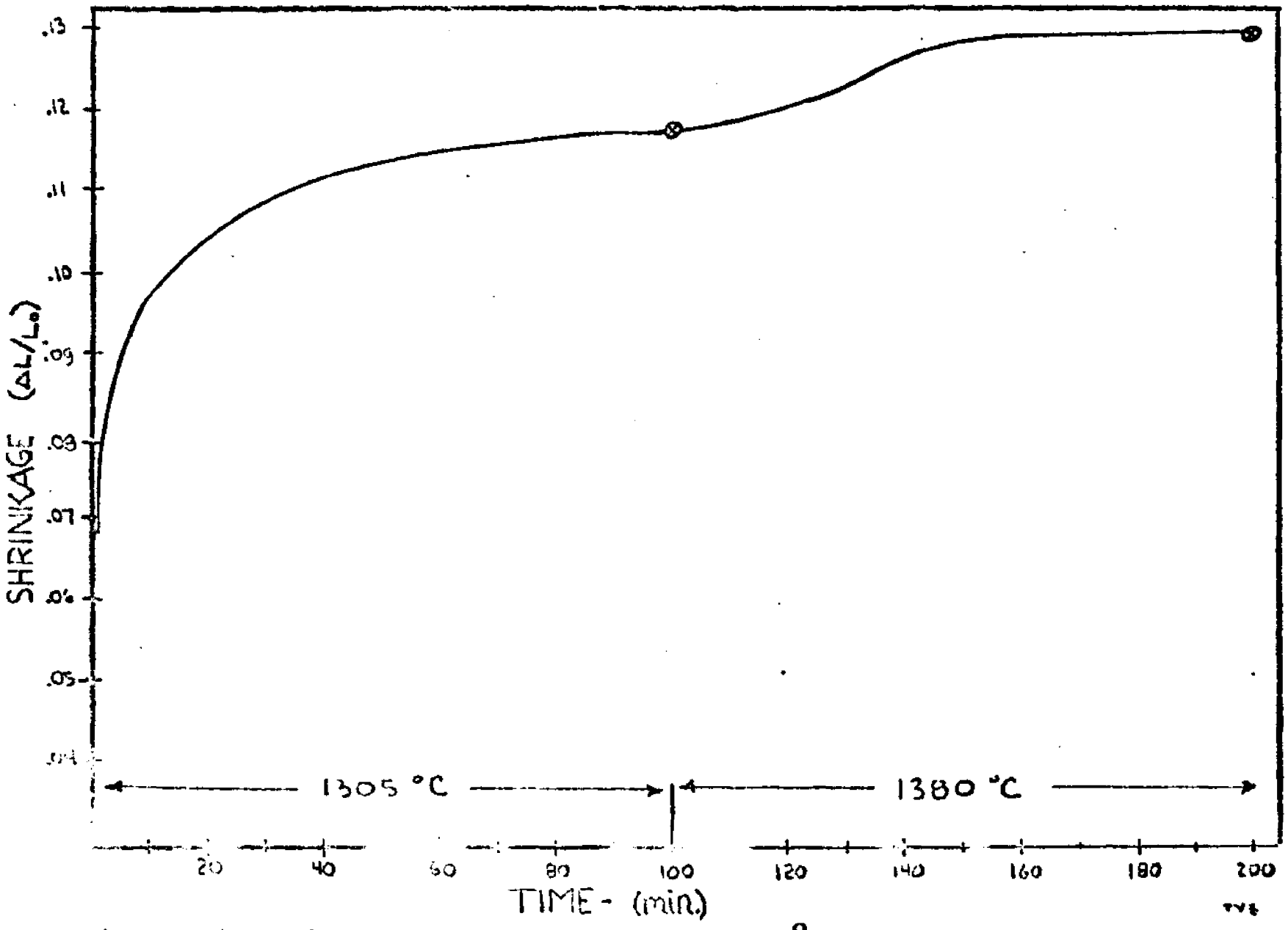

Figure 3.19 - Discontinuous Run, TYZ; 1305, 1380°C

a solid solution. This matter is of particular consequence in the case of thoria-yttria, because the conductive and electrolytic properties depend upon the replacement of thorium ions by yttrium ions in the thoria lattice. The extent of alloying may be followed by x-ray measurements for, as previously shown in Figure 1.6, the lattice parameters of thoria and yttria are different. Thus that of pure thoria (as measured by our laboratory) is 5.602Å and for ThO_2•15 mol % Y_2O_3, the parameter is 5.57.

Figure 3.20 shows the effect of temperature on the alloying of TYN, TY and TYZ, where lattice parameters are plotted against temperature. On these curves, 2 phases are noted by two markers connected with a vertical dashed line. These data appear to show that ZnO does not aid alloying, while NiO does, the alloying occurring at a lower temperature than for TY.

3.4 Effect of Sintering Atmosphere

In an earlier Section 1.10, it was shown that both NiO and ZnO are semiconductors, non-stoichiometric oxides, but of opposite types. Nickel oxide is a metal-defect (oxygen surplus) p-type conductor, while ZnO is a metal excess n-type conductor. It was also shown that the vacancy concentration in each depends in entirely different ways on the ambient oxygen partial pressure. Hence, although the amount of additive used in this work was small, an effort was made to determine whether its behavior was sensitive to

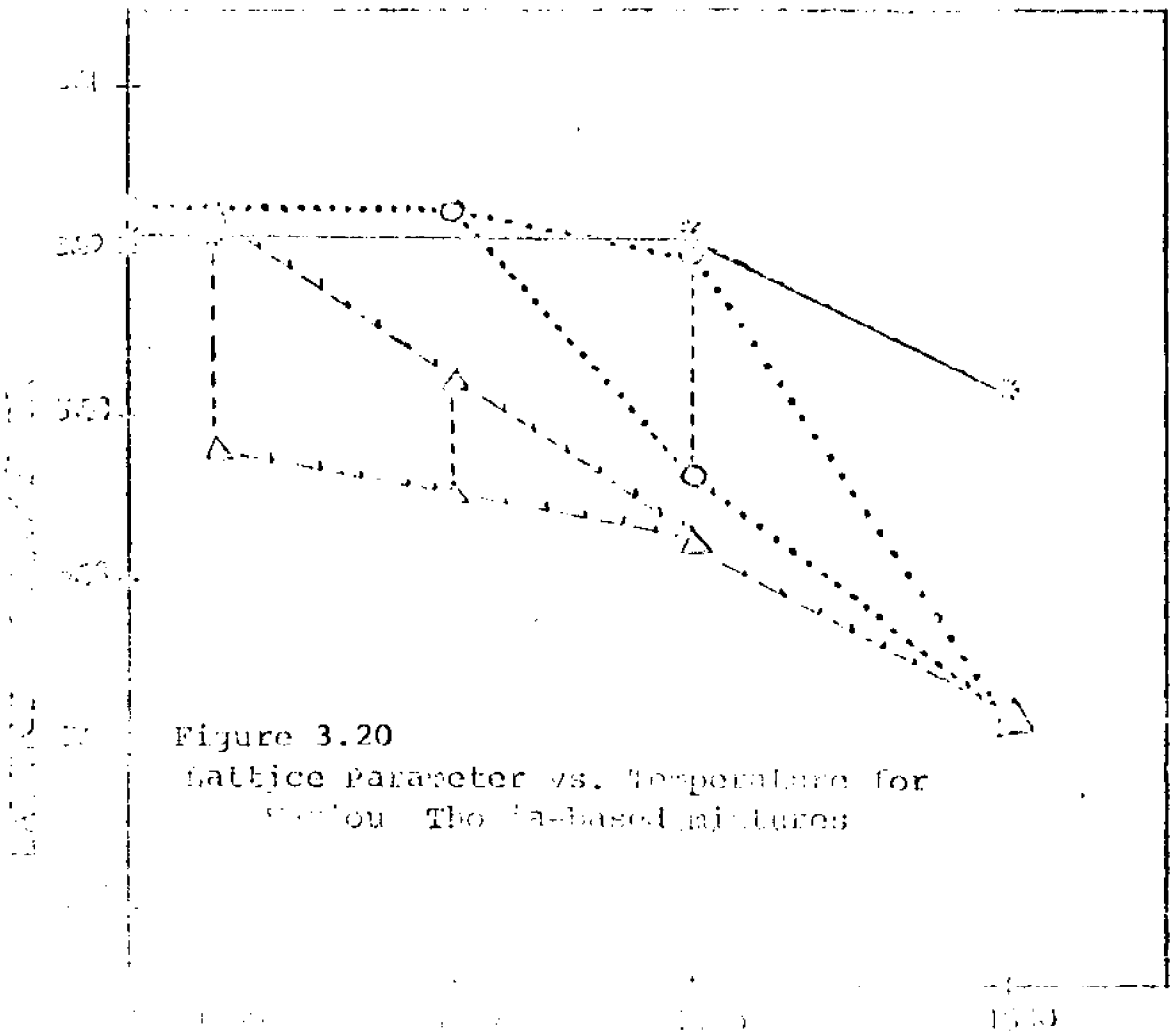

Figure 3.20
Lattice Parameter vs. Temperature for
Various Tho Ta-based Mixtures

○ ThO_2
○ TY ·····
Δ TYN - - -
* TYZ ——
– – – Indicates two phases

the oxygen partial pressure. Toward this end, TYN was tested by firing three pellets in air, three in argon and three in nitrogen at 1330°C. This data lend themselves to a comparison utilizing an analysis of variance (ANOVA). The results are given in Tables 3.2 and 3.3

Table 3.2 Data for Atmosphere Effects

	Data: Shrinkage	Data: Wet Voidage	(1) $(\Delta L/Lo)_{Ave.}$	(2) $\bar{\epsilon}_{A.V.}$
Air	.122, .112, .110	2.8,6.3,6.1	.115	5.1
Argon	.096, .104, .104	9.4,3.8,7.2	.101	6.8
Nitrogen	.111,.100,.102	7.9,9.1,7.6	.104	8.2

Table 3.3 ANOVA on Atmosphere Effects

	df	SS(1)	SS(2)	EMS(1)	EMS(2)	F_{test}
Effect of Atm.	2	.00003	14.4	.000015	7.2	
Error	6	.0003	24.1	.00005	4.2	
Total	8	.00033	38.5			
				.3	1.75	

$$\left\{ \begin{array}{l} F_{.75,\ 2,\ 6} = 1.76 \\ F_{.90,\ 2,\ 6} = 3.46 \end{array} \right\}$$

These show that the atmospheres tested have no statistical effect on the sintering of TYN.

The effect of atmosphere and temperature were checked using either air or argon at 1140, 1300 and 1440°C, with three

samples fired for 10 minutes at each combination of conditions. The raw data are given in Table 3.4 where the measurements were obtained by the cathetometer prism method.

Table 3.4 Data for Atmosphere Effects, Shrinkage

	1140	1300	1440
Air	.041 .043 → .042 .043	.080 .083 → .082 .083	.113 .122 → .117 .117
Argon	.048 .047 → .048 .050	.097 .080 → .089 .050	.126 .117 → .119 .116

Section 3.5 Scanning Electron Microscopy

The cost of scanning electron microscopy (SEM) at a commercial laboratory limited the number of specimens that could be examined. In an initial set, the powders were examined and exploratory tests were performed on TY.8N specimens sintered at 1370°C. Although these tests provided valuable information on the nature of the starting materials and the effect of mixing, it was decided that the sintering behavior of a three component mixture was too complex. Accordingly, a substantial number of additional SEM runs were performed with thoria and T.8N in an attempt to isolate the effect of the sintering aid.

The results are displayed in Plates 1 through 9 in the form of copies of the 4"x5" Polaroid photos taken directly on the SEM. For display, the photos have been reduced to

3¼"x4¼". In the process, the linear dimensions have been reduced by a factor of about 1.16, so that any length measured on these photos should be multiplied by this amount before using the magnification factor to estimate the size. (At 3000x, 1 cm $\simeq$ 3.9μm and at 10,000x, 1 cm $\simeq$ 1.2μm.)

In examining these micrographs, it must be remembered that, except for Plate 1, they represent fracture surfaces and that fracture is most likely to occur on weak planes which may not be representative at the bulk material. Secondly, the surfaces have been coated with about 200Å of gold-palladium alloy (0.02μm), but this is small compared with the thoria particle dimensions. Thirdly, because of cost limitations, only one specimen was usually used as representative of the experimental conditions. Lastly, the pictures displayed are photocopies of original photos (not made from the same negative) and have therefore lost some of their clarity. However, despite these limitations, the method is very powerful and the micrographs will repay very careful study.

The plates are arranged for the easy study of variables. Hence, where necessary, photos have been repeated on different plates. Although magnifications from 1000x to 15,000x were used, the 3000x and 10,000x appeared most useful.

<u>Plate #1</u> This shows both the individual powders that were the basic starting materials at 3000x and then the powders as mixed in the Spex mixer. Several interesting facts are

Plate #1 - The Sintering Powders, 3000X

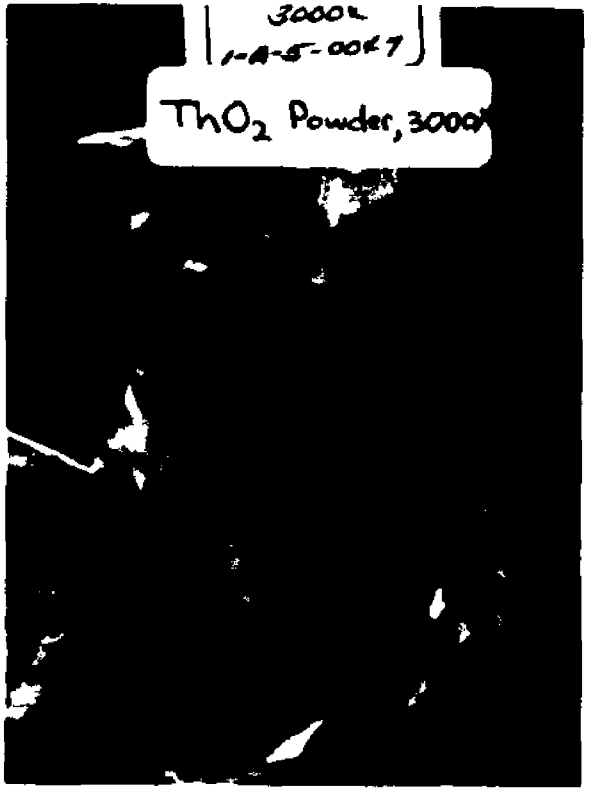

ThO_2 Powder, 3000X

Y_2O_3 Powder, 3000X

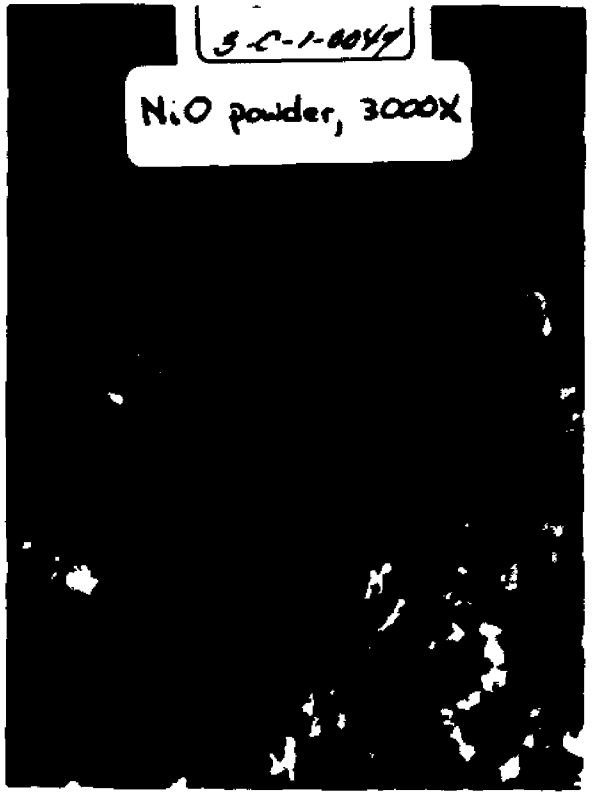

NiO Powder, 3000X

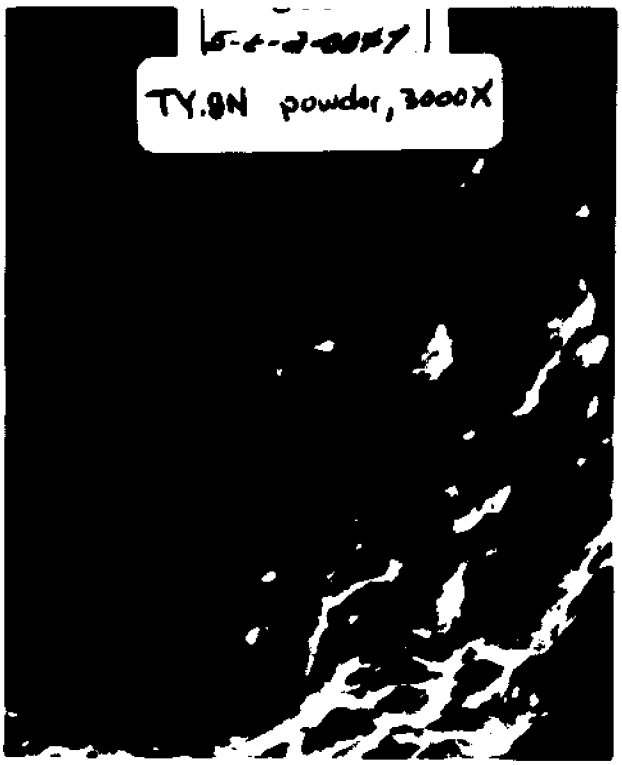

TY.8N powder, 3000X

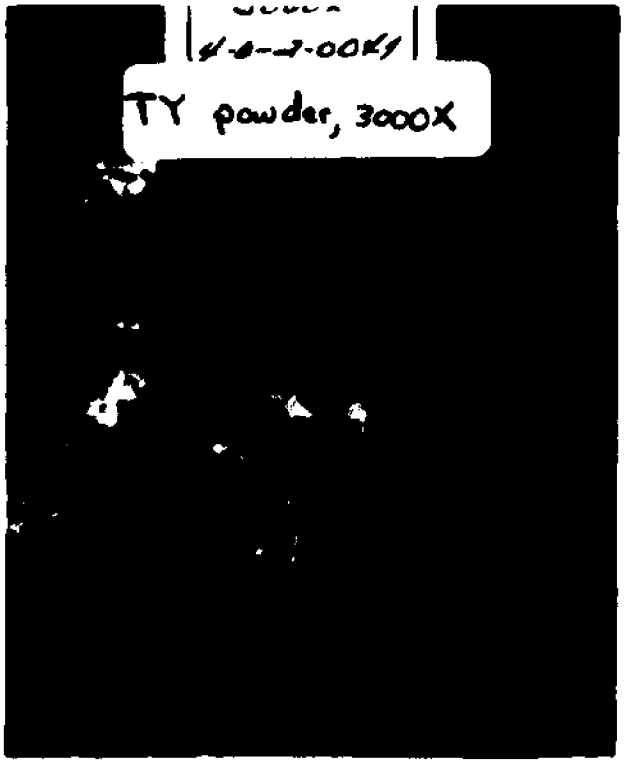

TY powder, 3000X

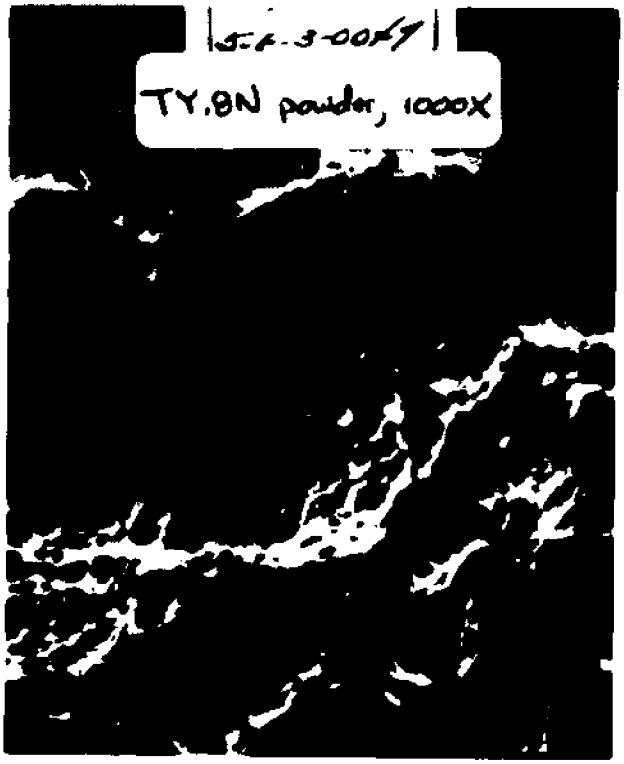

TY.8N powder, 1000X

TY 10N powder, 1000X

evident. First, the thoria is obviously in the form of flat, monocrystalline plates (perhaps more clearly shown in Plate 2). The plate size of the thoria is in the range from 0.6 to 5.0μm and consists of some large plates and some "burrs" that look as if they were broken off the plates. The yttria is also plate-like, but smaller and containing more burrs, while the NiO consists of very fine, more spherical powder of about 0.5μm diameter. The NiO powder agglomerated into larger clusters.

Upon mixing of the powders, they gathered into large individual clusters about 20-25μm in size. These clusters no longer retain a flat plate-like shape on the surface, but rather appear as if small particles were stuck onto a viscous substance. It would appear that NiO aids this aggregation process if the difference in appearance of TY.8N and TY10N is real. The thoria plates seem to be buried in these clusters. Of course, it is these inhomogeneous clusters that are cold-pressed to form the green compact, but as shown in Plate 1, they have only been mechanically mixed and not heated.

Plate #2 This plate, with both macro and micro photos, depicts sintering without pressing, i.e., stress-free sintering. The powders were simply put into alumina dishes as shown in the macro photos and leveled off with a spatula. They were heated simultaneously in a Lindberg box furnace at about 1370°C for the designated times. This plate

Plate #2 - Sintering of Unpressed Powders, 1370°C

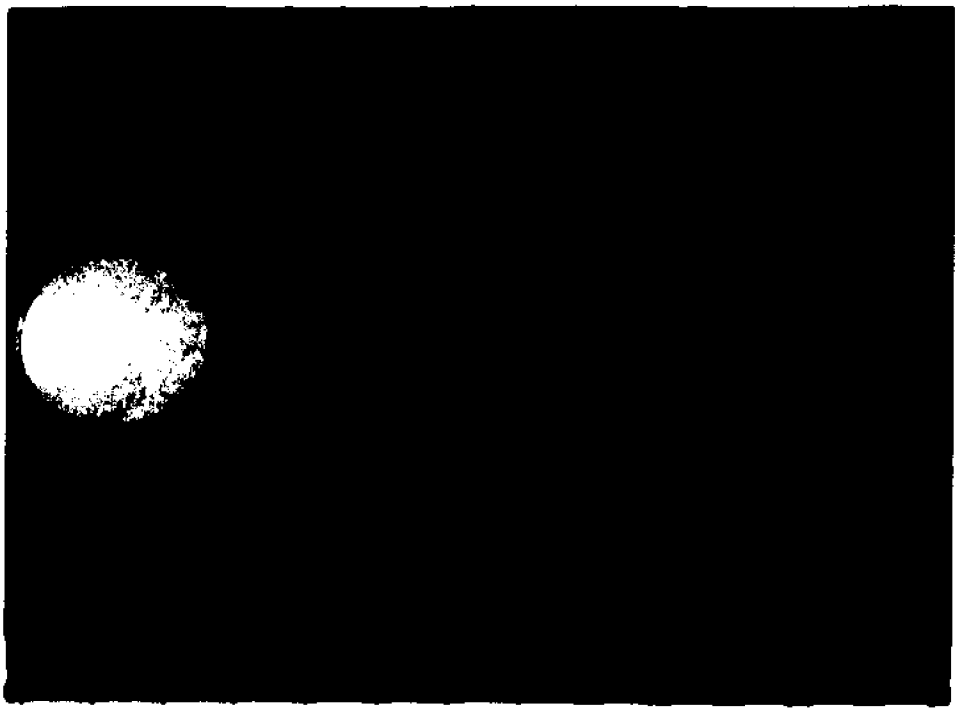

Macrophoto - unstressed powders

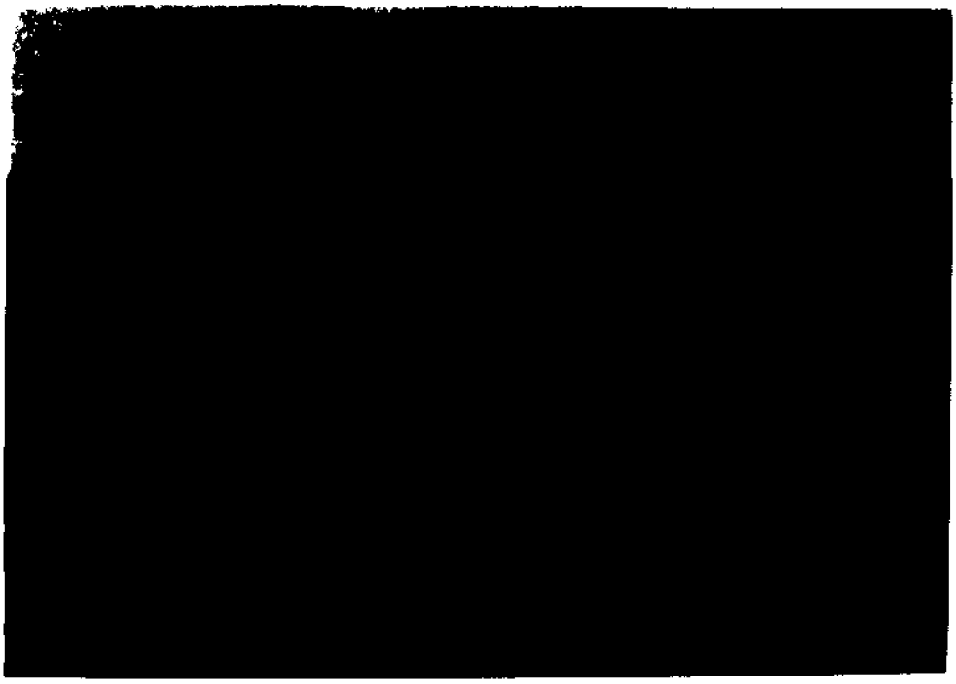

Macrophoto - unstressed powders

Plate #2 - Sintering of Unpressed Powders, 1370°C

ThO_2 - unpressed, 3000X

TN - unpressed, 3000X

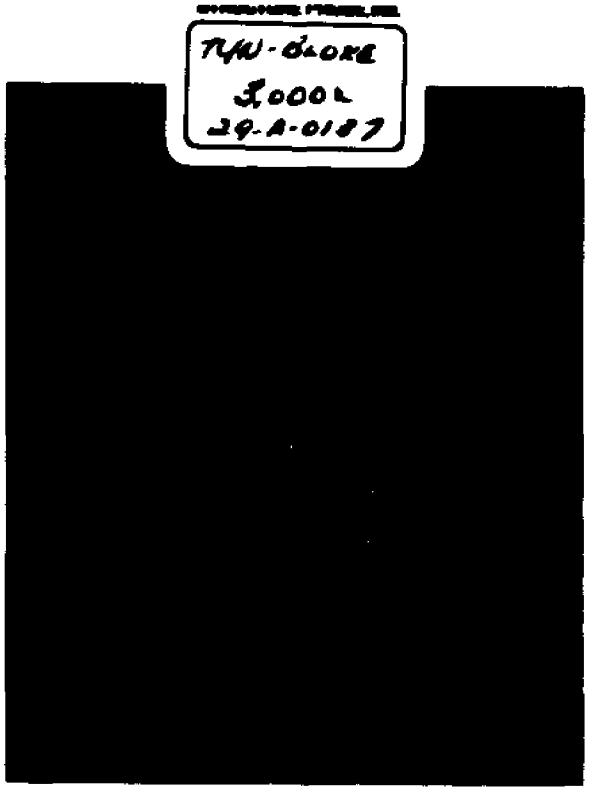

TYN -- unpressed, 3000X

Plate #2 - Sintering of Unpressed Powders, 1370°C

ThO_2 - unpressed, 10,000X TN - unpressed, 10,000X TYN - unpressed, 10,000X

Plate #2 - Sintering of Unpressed Powders, 1370°C

ThO_2 - unpressed, 15,000X

TYN - unpressed, 15,000X

compares the behavior of pure thoria, thoria containing 0.8 wt % NiO (T.8N), and the reference 3-component mixture of TY.8N, the effect of ZnO additions is also depicted in the same macropicture.

The effects of adding yttria and/or sintering aids is very evident. It is estimated that the original total voidage was 33%. The macroscopic photographs show that the pure thoria had shrunk essentially not at all under these conditions. In marked contrast, the addition of yttria or sintering aids were very effective as shown in Table 3.5.

Table 3.5 Shrinkage and Additives for Unstressed Thoria and Mixture

	T	TY	TN	TZ	TYN	TYZ
$\Delta L/Lo$ (%)	0	2%	14%	9%	15%	16%
time (hrs)	10	10	10	6	10	6

A great difference in behavior is also apparent in the micrographs of Plate 2. The plate-like character of the thoria powder is again evident. It is also clear that there was essentially no joining of the ThO_2 plates at 1370°C in 6 hours and that a random, unaligned configuration is maintained. By contrast, the addition of only 0.8 wt % NiO has greatly altered the appearance and the extent of consolidation of these urpressed sintered powders. The thoria plates are clearly visible in many areas and there appears to be evidence of their orientation in a stacked form. The amount of fine powder present cannot

be accounted for on the basis of NiO alone. The reason for this is as of yet, unanswered. The TYN specimen shows evidence of major sintering in both the macro and microscopic views. At 3000x, ThO_2 plates are visible, but the overall rounding, expecially of the finer material, is characteristic of the kind of structure that will be seen in more densified pure thoria and in T.8N (c.f. Plate 3, specimen 34; Plate 5, specimen 37). It can be seen in Table 3.5 and in the macrophotographs that TN and TYZ sintered appreciably too. Also shown are micrographs of thoria and TYN treated as before at 15,000x. Though the resolution of the TYN is poor because of electron charging, a configuration indicative of massive flow is evident which is not the case for pure thoria. The pure thoria at 15,000x has sharp edges, but there appears to have been a roughening of the surface and lines reminiscent of cracks. These are not visible in untreated pure thoria at high magnification (micrograph not shown).

Plates #3 and 4 These two plates are arranged to display the effects of time and temperature on pure thoria. Plate 3 consists of micrographs taken at 3000x while Plate 4 was at 10,000x. The two temperatures used were 1370°C (2500°F) and 1530°C (2786°F), and times ranged to six hours. A sintering time of 1 minute was investigated because the kinetic data showed major changes occurring at about that time.

Examining Plates 3 and 4, specimen 24 depicts the fractured, cold-pressed compact before heating. The thoria plates are intermixed with a substantial amount of fines,

Plate #3 - ThO_2 Effect of Temperature and Time, 3000x

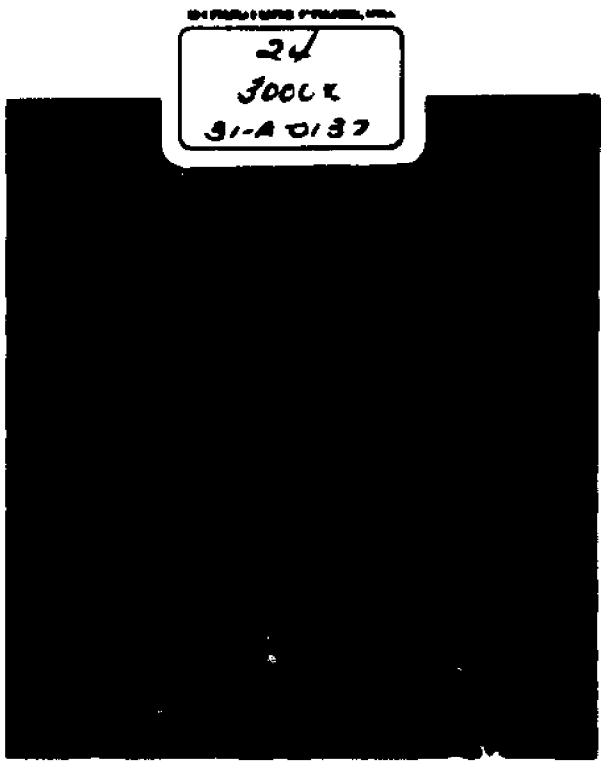

ThO_2, 1370°C for 0 min.

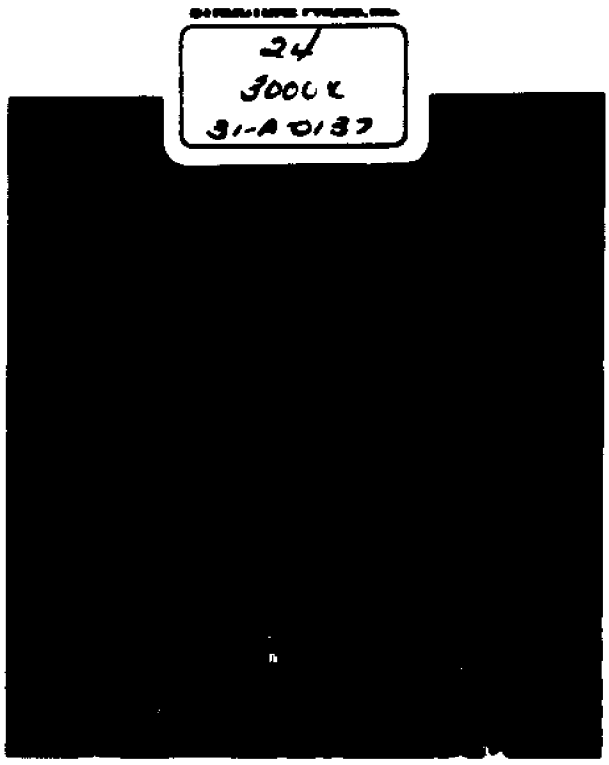

ThO_2, 1530°C for 0 min.

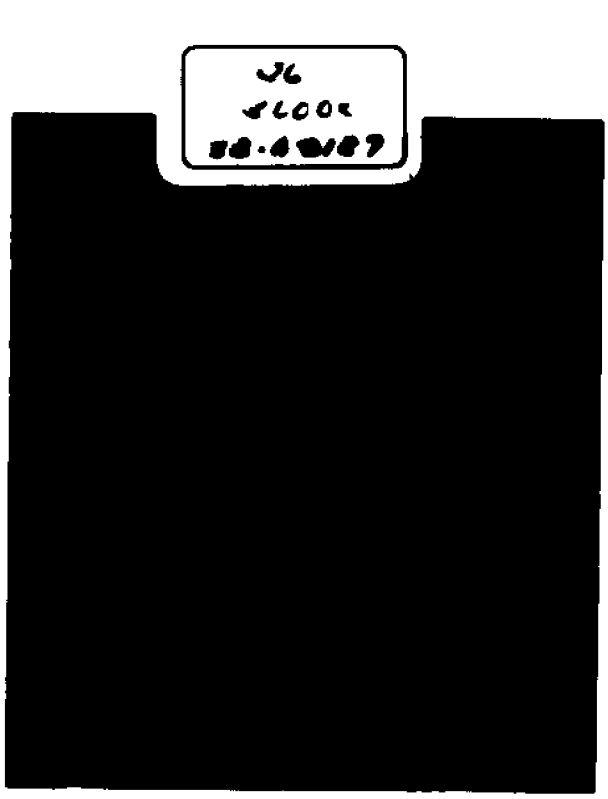

ThO_2, 1370°C for 1 min.

ThO_2, 1530°C for 1 min.

Plate #3 - ThO_2 Effect of Temperature and Time, 3000x

ThO_2, 1370°C for 20 min.

ThO_2, 1530°C for 20 min.

ThO_2, 1370°C for 6 hours

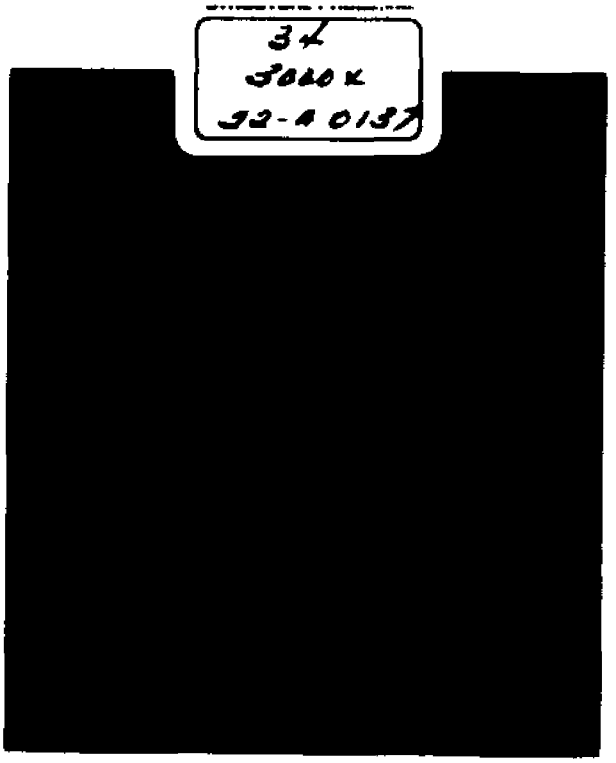

ThO_2, 1530°C for 6 hours

Plate #4 - ThO_2 Effect of Temperature and Time, 10,000x

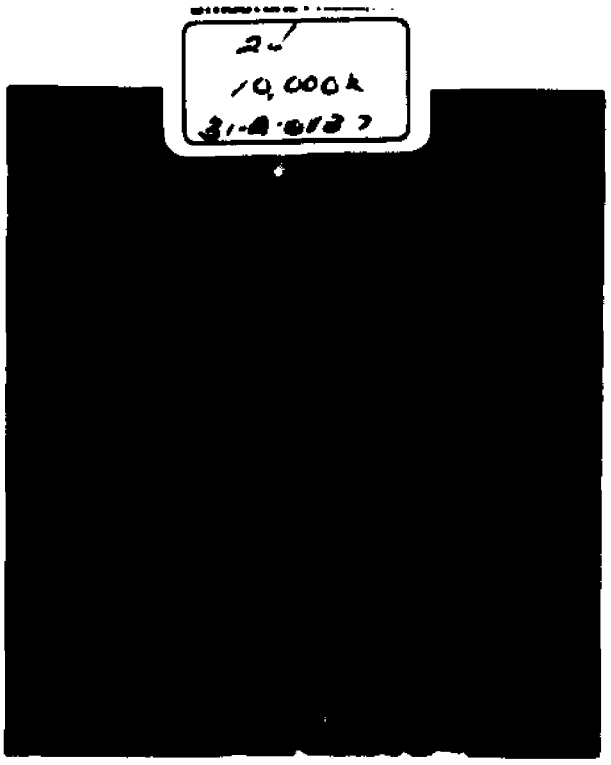

ThO_2, 1370°C for 0 min.

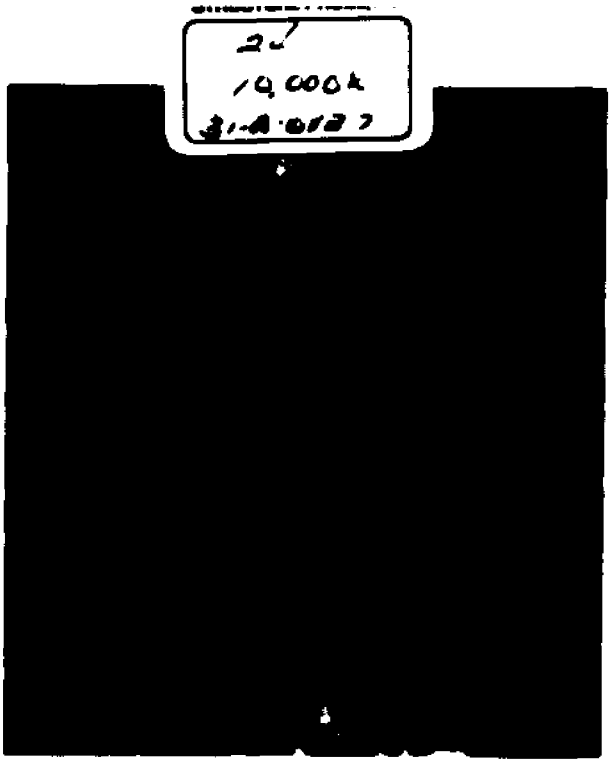

ThO_2, 1530°C for 0 min.

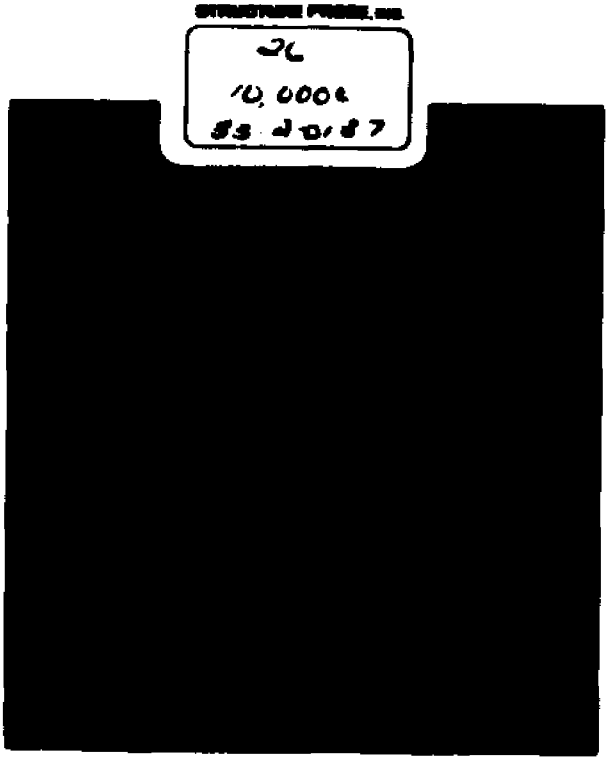

ThO_2, 1370°C for 1 min.

ThO_2, 1530°C for 1 min.

Plate #4 - ThO_2 Effect of Time and Temperature, 10,000X

I

ThO_2, 1370°C for 20 min.

I

ThO_2, 1530°C for 20 min.

I

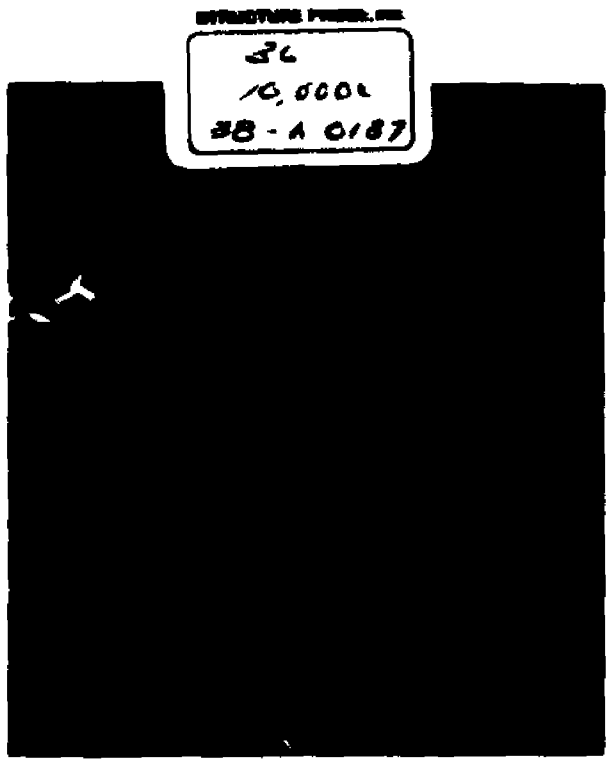

ThO_2, 1370°C for 6 hours

II

ThO_2, 1530°C for 6 hours

probably resulting from both Spex mixing and compaction fractures. At 1 minute, there is little discernible change, even at 1530°C (yet the kinetic data show a substantial shrinkage). However, after 20 minutes, the 1370°C and 1530°C specimens are very different. In the 1370°C specimen (No. 28), consolidation appears to have taken place, but individual thoria plates with sharp edges are clearly visible, especially at 10,000x. But at 1530°C, the change is readily apparent. Even at 3000x, densification is noticeable, while the 10,000x magnification discloses a marked alteration of the thoria plates. In addition, the "fines" or "burrs" seem to be rounding off and there appears to be fewer of them. Although some remnants of the original thoria may be observed, it is clear that true sintering has occurred; the material seems chunkier, new crystals appear to be forming and the particles are definitely interconnected.

Finally, after sintering for about 6 hours, a very considerable change is manifest even in the 1370°C specimen (No. 36). At 10,000x especially, its appearance becomes close to that of the 20 minute 1530°C specimen (No. 32). [If No. 36 and 32 had truly reached identical states, the respective temperatures and times would correspond to an activation energy of about 100,000 cal/mole]. Inspection of the micrographs of No. 34 (6 hours at 1530°C) makes it obvious that a really profound change has taken place. The thoria has formed new massive crystals from the thin flat plates, while no fines whatsoever are in evidence. It is apparent,

however, that there is a great deal of porosity. Specimen #36 seems to show agglomeration and smearing of fines onto the surface of the larger plates. This is a precursor step to recrystallization and an explanation of the disappearance of fines in #34.

Plates #5 and 6 These two plates at 3000x and 10,000x respectively, show the effects of NiO sintering aid and yttria dopant on the sintering of thoria at the low temperature-1370°C. There appears to be little noticeable difference among the three kinds of green compacts (0 minutes). However, after 1 minute at 1370°C, the TN specimen (No. 27) appears to show some sintering or orientation of the ThO_2 plates as compared with the pure thoria (No. 26). This is more evident at 10,000x. There can be no doubt that the 2 minute TYN sample (9-B-2-0047) displays advanced sintering. Note the lack of massive voids and depth while the surface is flat indicating plate orientation.

After 20 minutes at temperature, the difference becomes easily perceived. Although there is some rounding and sintering of the small particles in pure thoria (No. 28), this effect is obvious at a glance for T.8N (No. 29). Also noticeable, especially at 10,000x is the agglomeration of the separate plates and fines into groups that are probably the basis of the newer, larger crystallites noted on Plate 4. The sintering of the TYN specimen 10-c-2-0047 has gone very far. Indeed, this specimen is close in structure to TY sintered at 2000°C for an hour (see No. 47, Plate 9).

Plate #5 - Thoria and Dopant/Additives, 1370°C, 3000x

ThO_2, 1370°C for 0 min.

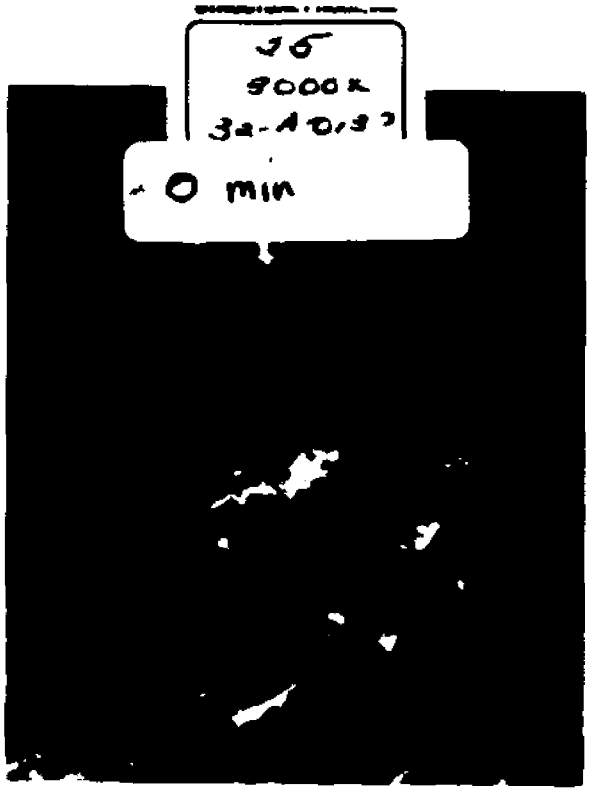

TN, 1370°C for 0 min.

TYN, 1370°C for 0 min.

Plate #5 - Thoria and Dopant/Additives, 1370°C, 3000x

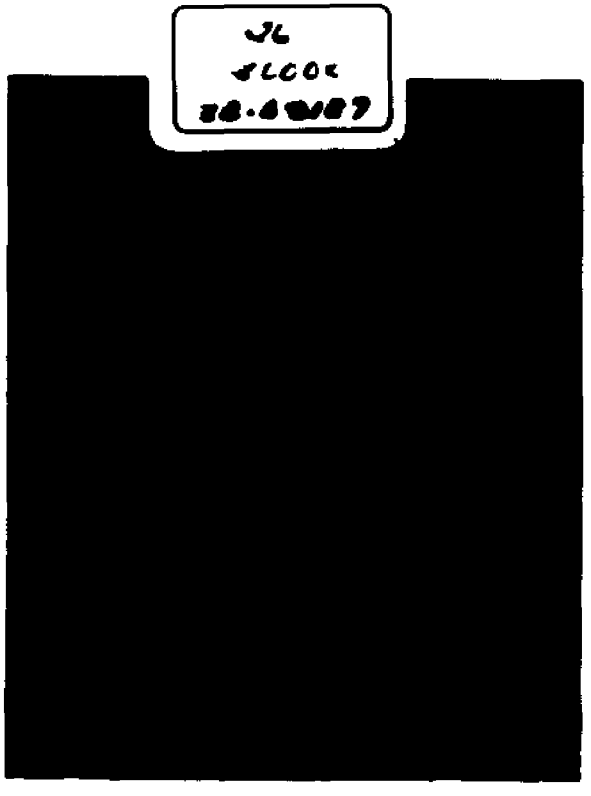

ThO_2, 1370°C for 1 min.

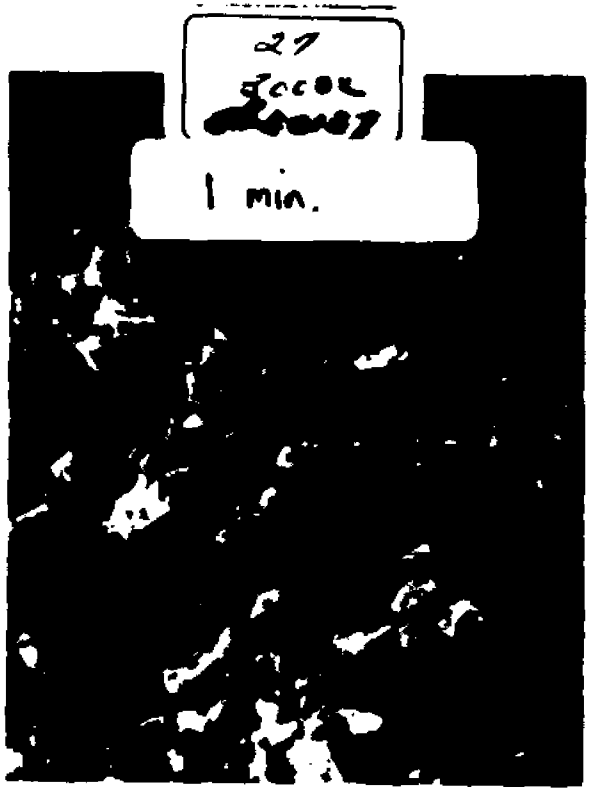

TN, 1370°C for 1 min.

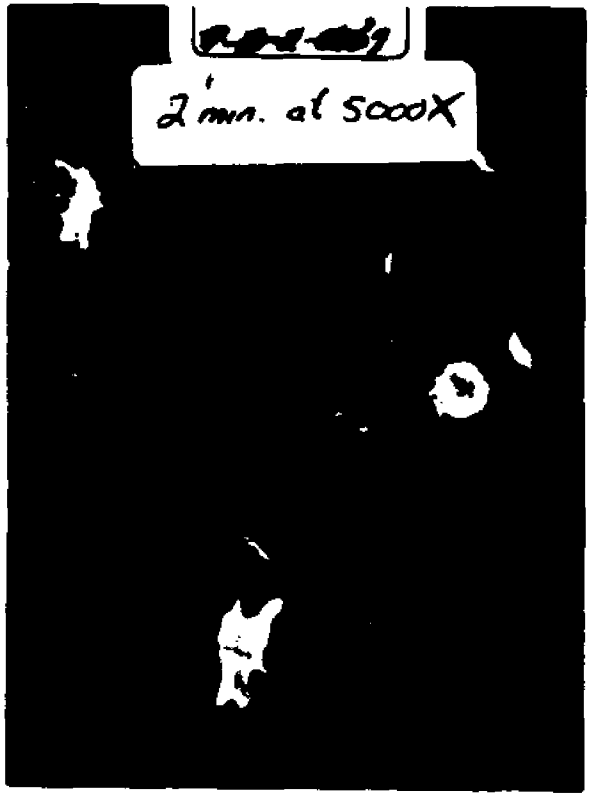

TYN, 1370°C for 2 min.

Plate #5 - Thoria and Dopant/Additives, 1370°C, 3000x

ThO_2, 1370°C for 20 min.

TN, 1370°C for 20 min.

TYN, 1370°C for 20 min.

Plate #5 - Thoria and Dopant/Additives, 1370°C, 3000x

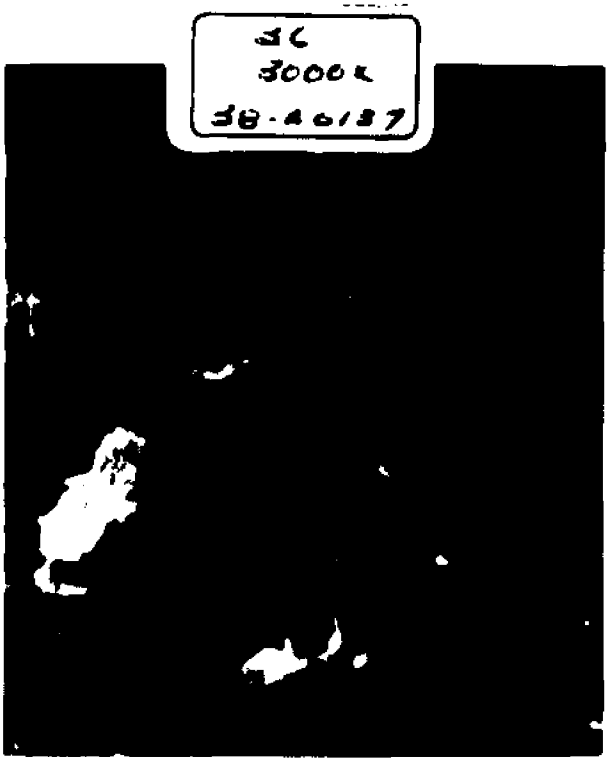

ThO_2, 1370°C for 6 hours

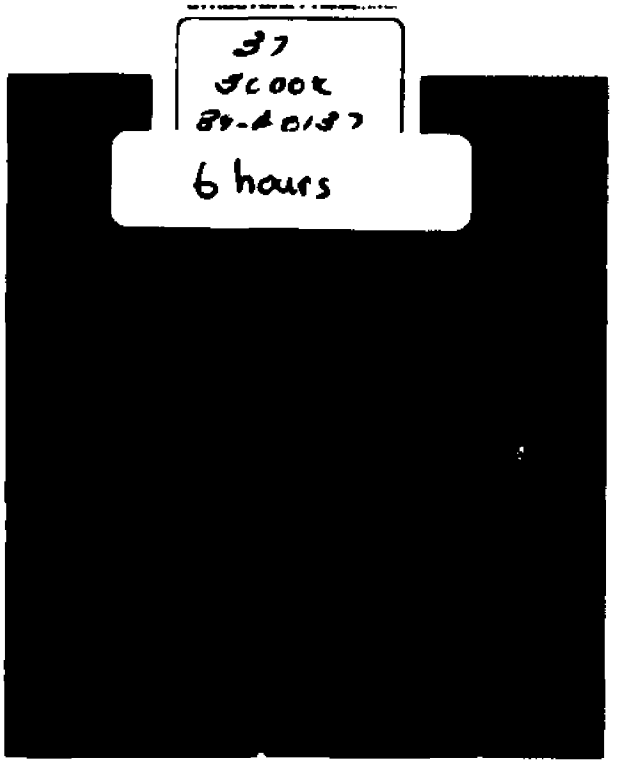

TN, 1370°C for 6 hours

Plate #6 - Thoria and Dopant/Additives, 1370°C, 10,000x

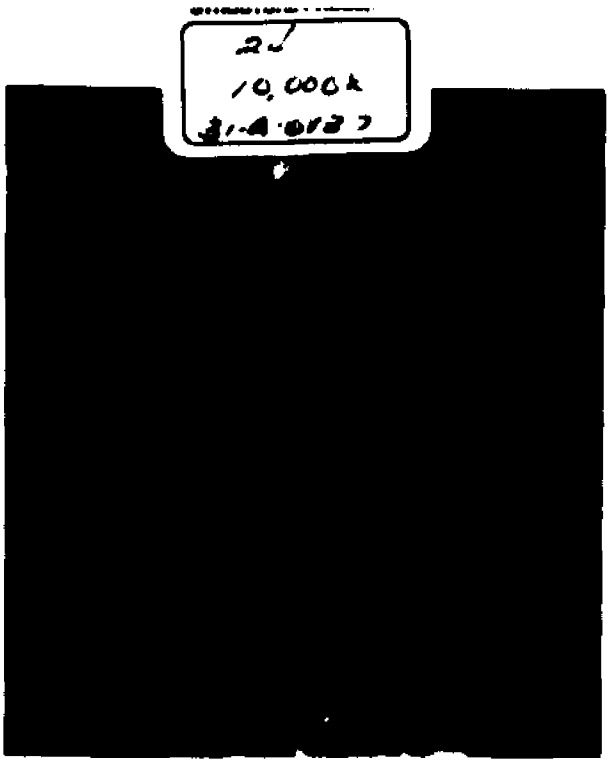

ThO_2, 1370°C for 0 min.

TN, 1370°C for 0 min.

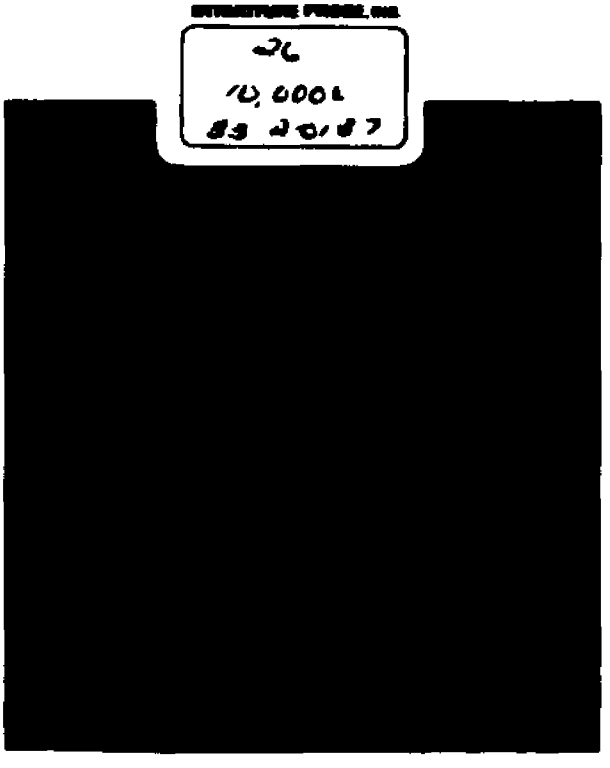

ThO_2, 1370°C for 1 min.

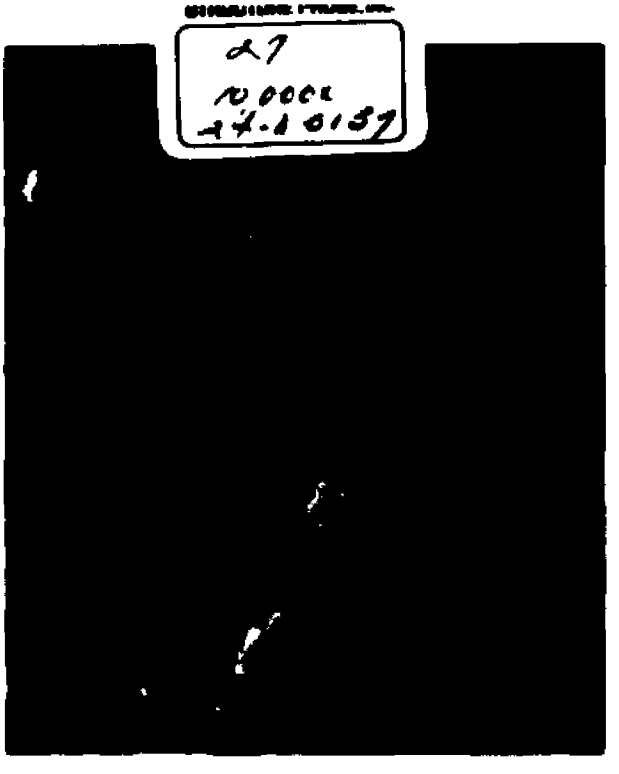

TN, 1370°C for 1 min.

Plate #6 - Thoria and Dopant/Additives, 1370°C, 10,000x

ThO_2, 1370° C for 20 min.

TN, 1370°C for 20 min.

TYN, 1370°C for 20 min.

Plate #6 - Thoria and Dopant/Additives, 1370°C. 10,000x

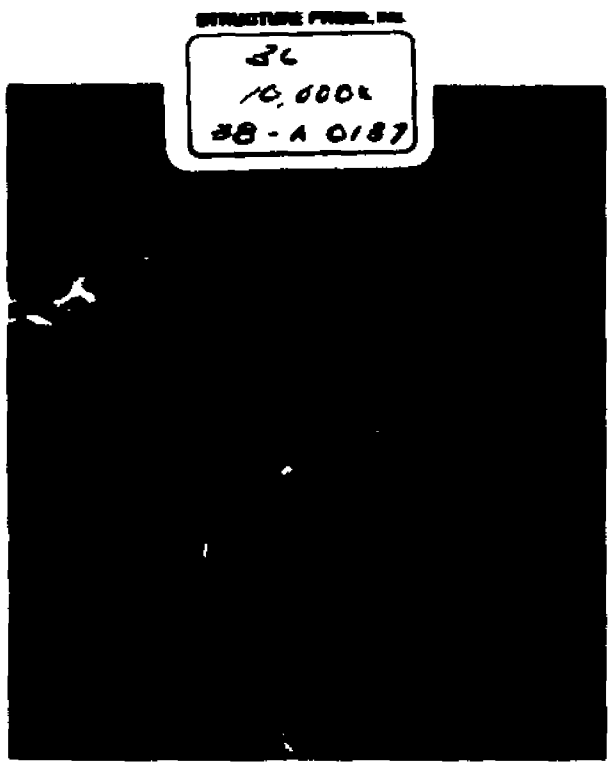

ThO_2, 1370°C for 6 hours

TN, 1370°C for 6 hours

Finally, after 6 hours at 1370°C, some sintering has taken place in the pure thoria (No. 30), but the fines and plates still have their irregular shapes. In contrast, the T.8N specimen (No. 37) is well advanced in forming new crystals and has begun to resemble thoria heated for the same time at 1530°C (c.f. with No. 34 Plates #3 and 4).

Plates #7 and 8 These two plates are the 1530°C analogs of the previous two plates. The starting compact is still the same. After heating for 1 minute, sintering is not observable in thoria. Now, though, after 20 minutes, substantial sintering has occurred in the T.8N sample (No. 33). This is evidenced by the formation of large crystallites and the total disappearance of fines. Interestingly, this 20 minute T 8N resembles the 6 hour TN at 1370°C (No. 37 Plates # 6 and 7), tending to confirm the relationship previously described for pure thoria.

Now when the specimen is heated at 1530°C for 6 hours, truly effective sintering has occurred in the T.8N and the TYN specimens. This TYN specimen was not produced from the individual green powder directly. Instead, TYN powder was pressed into a pellet and fired for 100 minutes at 1440°C and then ground. Thereafter it was treated in the usual way. The pores in the TN are no longer interconnected but are instead small and rounded Recrystallization is very apparent The TYN has the look of a viscous fluid at 3000x.

Plate #7 - Thoria and Dopant/Additives, 1530°C, 3000x

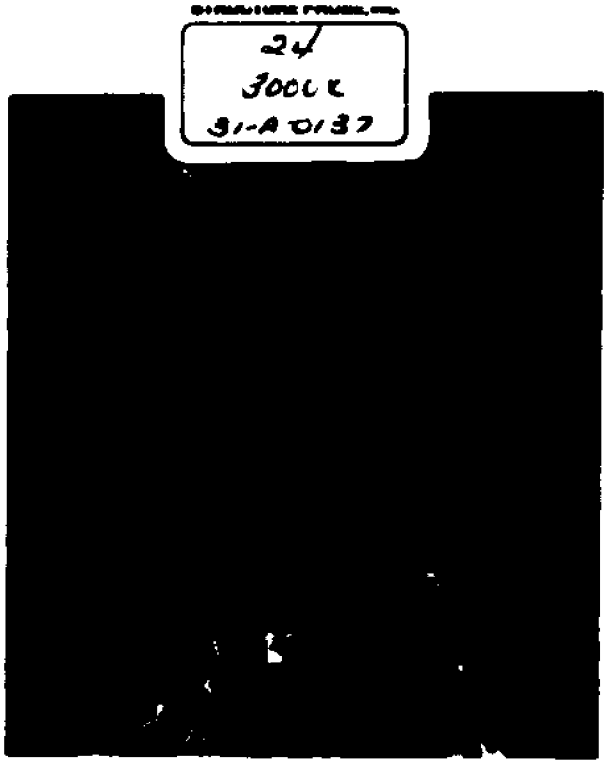

ThO_2, 1530°C for 0 min.

ThO_2, 1530°C for 1 min.

Plate #7 - Thoria and Dopant/Additives, 1530°, 3000x

ThO_2, 1530°C for 20 min.

TN, 1530°C for 20 min.

Plate #7 - Thoria and Dopant/Additives, 1530°C, 3000x

ThO_2, 1530°C for 6 hours

TN, 1530°C for 6 hours

TYN, 1530°C for 6 hours

Plate #8 - Thoria and Dopant/Additives, 1530°C, 10,000x

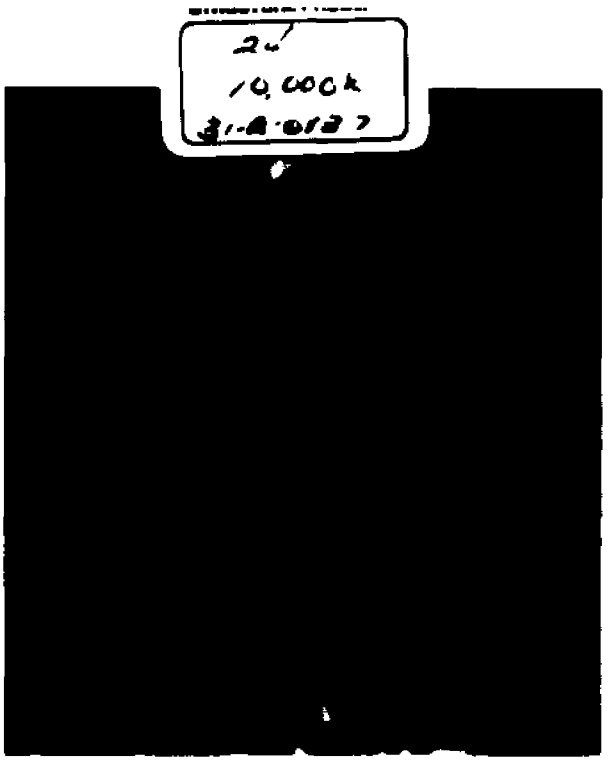

ThO_2, 1530°C for 0 min.

ThO_2, 1530°C for 1 min.

Plate # 8 - Thoria and Dopant/Additives, 1530°C, 10,000x

ThO_2, 1530°C for 20 min.

TN, 1530°C for 20 min.

Plate #8 - Thoria and Dopant/Additives, 1530°C, 10,000x

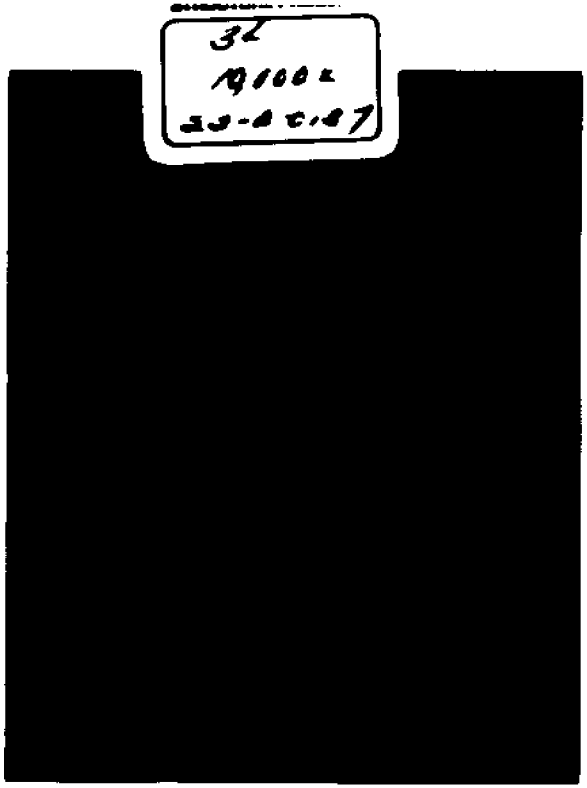

ThO_2, 1530°C for 6 hours

TN, 1530°C for 6 hours

TYN, 1530°C for 6 hours

but at the higher magnification (10,000x) is seen to consist of very well-formed, albeit rounded grains.

Plate 9 The first three horizontal sets of micrographs on this Plate depict similar structures obtained under different operating conditions. The bottom set shows products of different compositions. The top two horizontal sets make it reasonably clear that 20 minutes at 1530°C produces a result much like 6 hours at 1370°C. This is true both for pure thoria and for thoria-NiO. Of course, the sintering in the latter is greater. Unfortunately, no such sets of photographs exist for TY or TYN.

The third set shows similar structures obtained in TYN in 20 minutes at a low temperature of 1370°C and TY for an hour at 2000°C in vacuum. Either NiO is more effective in the presence of yttria or vacuum sintering is slower, than the sintering in air. Both may be true. These two figures compare the final electrolyte material with and without additives after different times. It is quite noticeable that these samples look as if they are the same, despite the specimen with the 0.8% additive being heated for one third the time at 600°C lower temperature!

Lastly, the bottom set of three micrographs compares the "fully sintered" final products in TY, TN and TYN (which was prealloyed, see this section, Plates 7 and 8). It is evident that nickel oxide aids sintering better than yttria and that a combination of both is best. It is also clear that a continuous non-porous ceramic phase can be produced better

Plate #9 - Some Comparisons, 10,000x

ThO_2, 1530°C for 20 min.

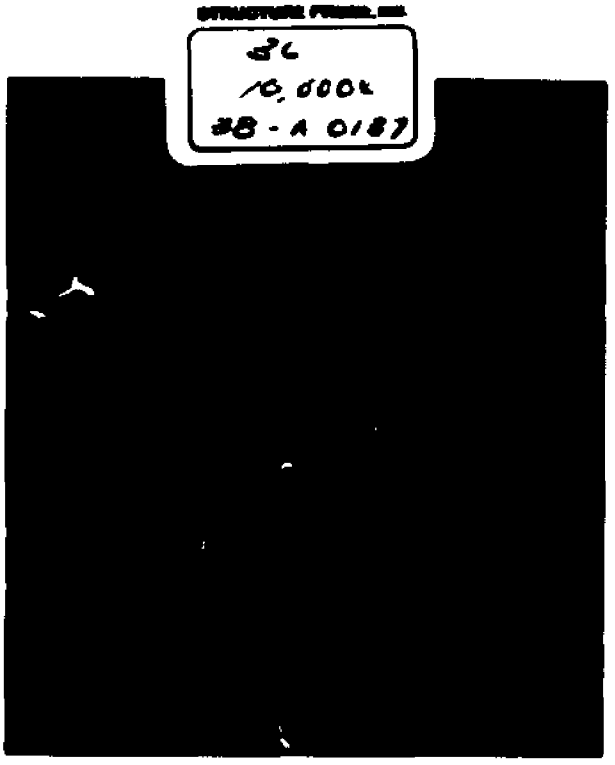

ThO_2, 1370°C for 6 hours

TN, 1530°C for 20 min.

TN, 1370°C for 6 hours

Plate #9 - Miscellaneous Micrographs, 3000x
Effect of Additives, Comparison

TYN, 1370°C for 20 min.

TY, 2000°C for 60 min.

Plate # 9 - Miscellaneous Micrographs, 10,000x
Comparison Finished Products

TY, 2000°C for 60 min.

TN, 1530°C for 6 hours

TYN, 1530°C for 6 hours

and at much lower temperatures, by the use of small amounts of additives. However, electrolytic behavior must also be investigated to ascertain the applicability of this final product as an ionic electrolyte.

4. Discussion

4.1 Research Objective

As has been previously stated, the main object of this research was to produce a solid thoria-yttria electrolyte that could be fabricated at temperatures below 1550°C. This electrolyte was for use in oxygen concentration cells to measure thermodynamic properties. The choice of a thoria-yttria electrolyte was based on the excellent electrolytic conduction characteristics of this material. It is known that in the low oxygen pressure (10^{-30}<P(atm)<1) and high temperature (600<T (°C)<1100) domain, thoria-yttria conducts anionically with anion transport number close to unity.

The need to fabricate the electrolyte at temperatures below 1550°C was necessitated by the physical hardness and friability of some of the electrode materials of interest. Hence it appeared that total encapsulation of the electrode within the electrolyte was highly desirable. This would allow the creation of a probe that could be used within a closed environment where the overall oxygen partial pressure would reach equilibrium. It was apparent that the high sintering temperature (>2000°C) normally needed for thoria-yttria electrolytes precluded the use of most normal reference electrodes (e.g. FeO+Fe, NiO+Ni, Cu_2O+CuO, etc.) due to their low melting points. In addition, electrical lead-throughs of exotic materials would be necessary since 2000°C is also far above the melting points of oxidation-resistant alloys, including those based on platinum.

In order to drastically lower the sintering temperature, various solid oxides and halides were tested as sintering

"activators." Since solid solution formation would not necessarily aid the sintering, and very little previous work has been done on the thoria-metal oxide phase systems, no a-priori approach was attempted. A review of the literature for sintering aids in related materials was found to be rewarding. Exploratory tests showed that additions of nickel oxide (NiO) and zinc oxide (ZnO) greatly reduce the sintering temperature of a premixed, unalloyed ThO_2+15 mole % $YO_{1.5}$. Though both produce excellent sintering in air at 1370°C when fired for one hour, it was found that their behavior with respect to the alloying of ThO_2 and Y_2O_3 was different. Since it is essential for the electrolyte to be nearly single phase in order to have oxygen ion defects present, criteria for the production of electrolyte materials were further investigated. It was found that for thoria-yttria-nickelous oxide, and thoria-yttria-zinc oxide, probable electrolyte grade material (alloyed, density>95% theoretical, nonporous) could be fabricated at 1530°C after air firing for two hours for the NiO material and six hours for the ZnO aided ceramic. It was also found that, although ZnO is perhaps a better aid in densifying the electrolyte, it appeared to hinder the alloying of the thoria and yttria phases.

The results of this research lead to the following recommended procedures for fabricating thoria-yttria solid electrolyte bodies:

1) Grind 99.9% pure, 2μ diameter ThO_2 with 14.6 mole % $YO_{1.5}$ (99.99% pure) of comparable size and 2.5 mole % NiO (99.5% pure and much smaller than the thoria) in a rubber lined ball mill for at least 48 hours using

stainless steel balls.

2) Press the dry mixture in a die at approximately 50,000 psi with the pellet thickness to diameter ratio of 1 :
3) Preheat to about 600°C for a minimum of 10 minutes, and for longer times for thicker sections.
4) Fire at 1500°C for at least two hours. Remove from hot zone of furnace allowing to cool in "preheat" zone for at least two minutes (longer for larger sections) before removing.

or, using zinc oxide as the additive:

1) Mix the ThO_2, Y_2O_3 and ZnO (99.5% pure, ~0.1 μ diameter) in a glass jar containing glass mixing beads on a Spex mixer for about 45 minutes.
2) Press the dry mixture in a die at approximately 50,000 psi with the pellet thickness being not more than one fourth the diameter.
3) Preheat to about 600°C for a minimum of 10 minutes, and for longer times for thicker sections.
4) Fire at 1500°C for at least six hours. Remove from hot zone of furnace allowing to cool in "preheat" zone for at least two minutes (longer for larger sections) before removing.

The major objective of the research having been achieved, the investigation turned to the nature of the activation mechanism of the sintering aids. In an effort to explain this behavior, a study was undertaken of the sintering behavior of this system using both classical shrinkage rate techniques and modern scanning electron microscopy.

4.2 Isothermal Kinetic Shrinkage Models

It is very common to first measure the rate of a chemical or physical process and then conceive a mechanism that approximately predicts the experimentally measured rate. If the agreement is reasonably good, it is very tempting to believe that the postulated mechanism is the true one. Apart from the obvious fallacy in logic, this approach of relying almost exclusively on kinetic measurements is almost certain to fail when the real situation differs from the model in important respects, or when a number of processes are occurring simultaneously, at changing rates. Nevertheless, for more than two decades, kinetic studies have been employed as a means of identifying the mechanism of sintering. Relatively simple models have been refined and corrections have been applied to rate measurements in an effort to determine the major mechanisms. The most important of these will be tested against the experimental rates measured in this research.

In section 1.3, the general form of the Kuczynski model was derived using the following assumptions:

1) that the particles are monosized
2) that the particles have a regular shape
3) that thermal heating effects (transient non-steady state) are negligible
4) that the shrinkage occurs by a vacancy flux between pores and vacancy sinks
5) that only one path is operable (only one type of vacancy)
6) that no other driving forces exist (e.g. stresses, concentration gradients, etc. to cause sintering)

The resulting shrinkage rate equation was

$$\left(\frac{\Delta L}{Lo}\right) = \left(\frac{K\beta\gamma V}{RTr^{n}}\, t\right)^{m} \qquad (14)$$

Various values of m and n were listed, dependent on the mechanism of transfer and on the paths taken.

In section 3.3, linear plots of the data of the kinetic shrinkage curves were given for TYN and for TYZ. If the assumptions made in the derivation of equation (14) are true then the data, when plotted on log-log coordinates, should yield a straight line of slope m. This test is applied in figures 4.1, 4.2 and 4.3, which are log-log plots of the shrinkage data for TYN (at two temperatures), TY and TYZ (at four temperatures). [Shrinkage plots for TYZ were drawn at four temperatures because of the interesting behavior of the break point (the time when the first two straight lines intersect). This will be discussed later. No such interesting behavior was noted with TY or TYN.] Obviously, these plots do not yield straight lines. In figures 4.2 and 4.3, for short times it would appear that the data can be plotted either as two or possible three straight lines. These consist of an initial steep rise in shrinkage followed by a slower increase. The latter is in turn followed by a region where almost no shrinkage occurs.

For TYZ, the break point (α), or time when the two linear extrapolations meet, appears to obey the simple relationship

$$\left(\frac{1}{\alpha}\,\frac{\Delta L}{Lo}\right)_{\text{break point}} \simeq .02\ \text{min}^{-1} \qquad (30)$$

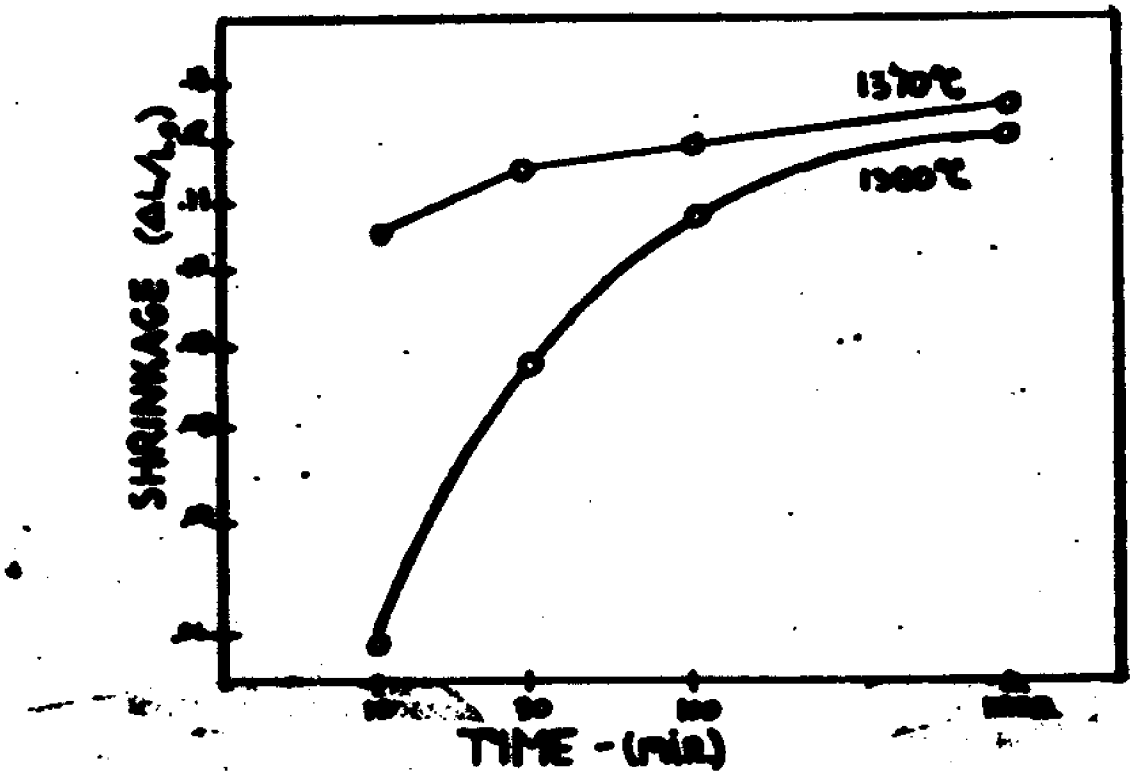

Figure 4.1 - Log-log Kinetic Shrinkage Curve

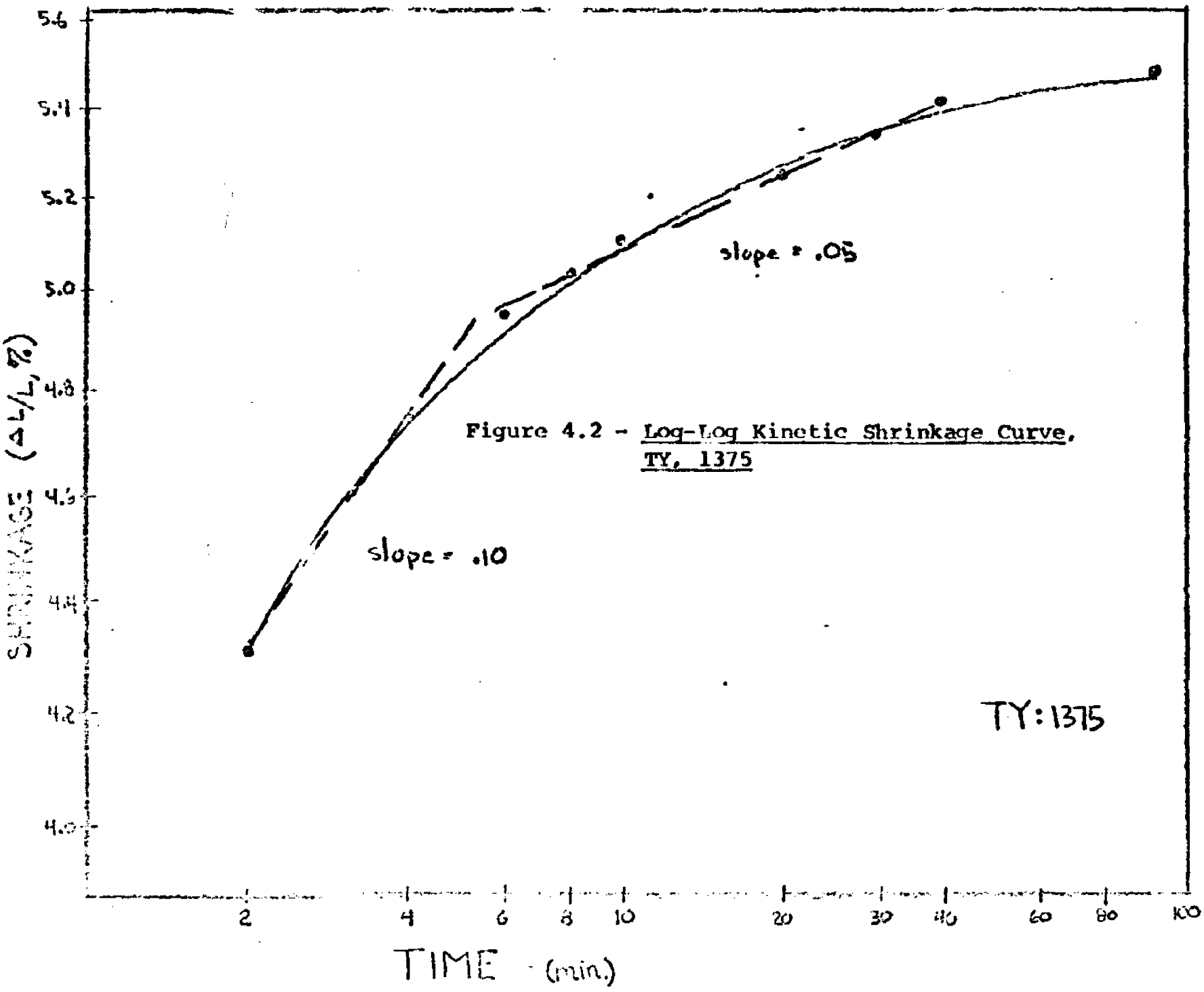

Figure 4.2 - Log-Log Kinetic Shrinkage Curve, TY, 1375

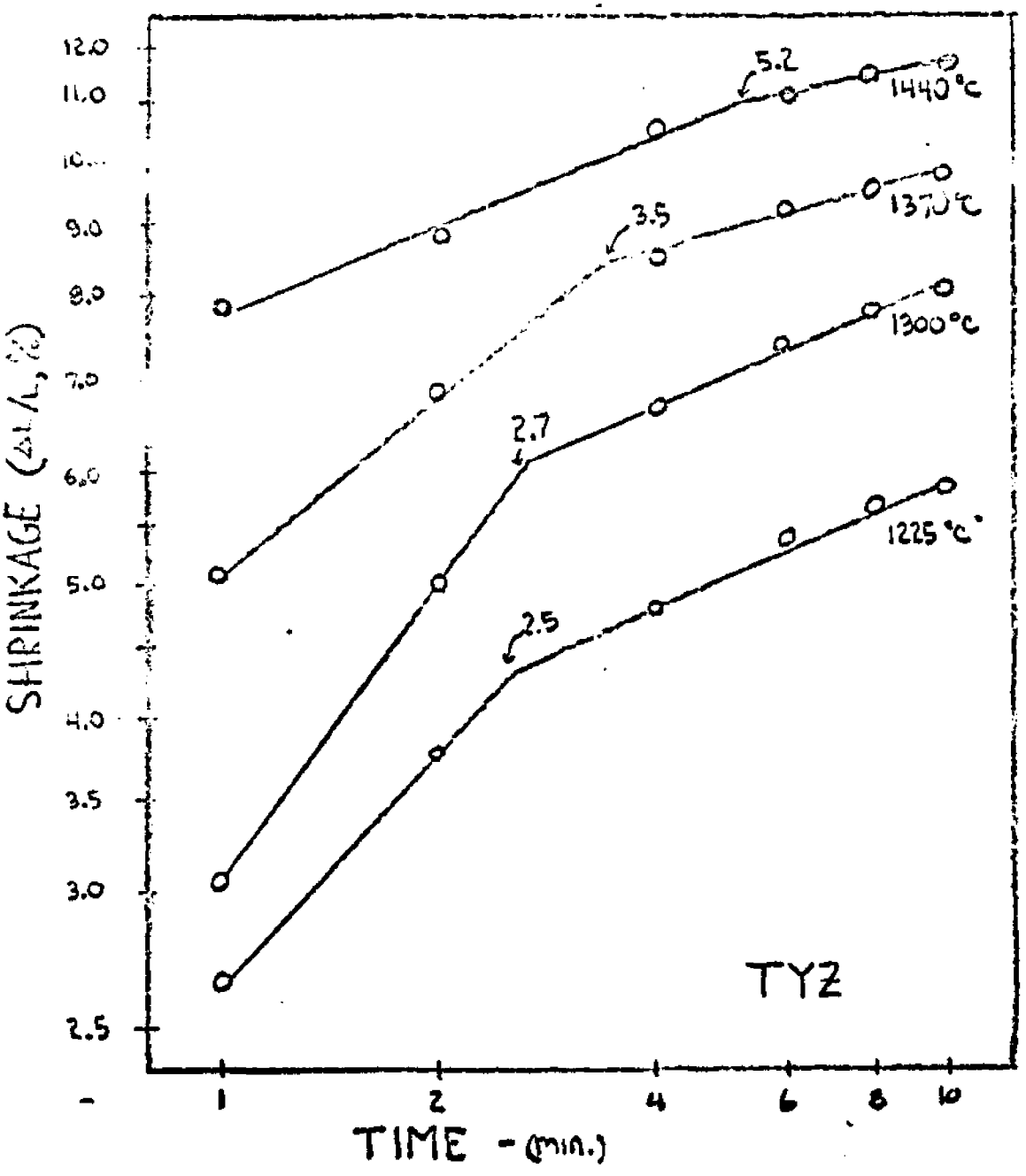

Figure 4.3
Log-Log Kinetic
Shrinkage Curve
TYZ

at every temperature. This indicates that the "break point" occurs at increasing time with increasing temperature. This type of behavior was not noticed with TYN, where the values of $\left(\frac{1}{\alpha}\frac{\Delta L}{Lo}\right)_{b.p.}$ ranged from .007 to .02. Instead, the "break points" appeared to be at about 9 minutes in each case. This behavior could be due to the nature of the log-log plot and not ascribable to the phenomena.

For TYZ, if $\left(\Delta L/_{\alpha Lo}\right)_{b.p.}$ is a constant, then a linear equation of the form

$$\left(\frac{\Delta L}{Lo}\right) = \beta t \qquad (31)$$

is suggested as the governing equation of the initial period. It should be remembered that the data on the short-time runs for TYN (figure 3.12) showed a linear relationship for the first minute at 1370°C. The only model that this corresponds to would be the liquid phase model of Kingery (R8). For TYN, a constant value for the "break point" could indicate that in all cases a constant time is necessary for the initial rearrangement. Apart from the qualitative aspects, conclusions based on the "break points" are doubtful at best.

The observed non-linearity of the log-log plot would indicate that one or more of the six assumptions made above are incorrect.

As was explained earlier, it is usually impossible to establish the starting time and length during the initial heating interval when the specimen has not yet reached the steady-state temperature. Various attempts have been made to correct mathematically for these deviations. One method of rendering the correlation less sensitive to the initial conditions is the

Johnson-Cutler method of finding an "effective" heating time and an "effective" initial shrinkage to correct for non-ideal behavior in the beginning. This is accomplished by using an expanded form of equation 14.

$$(L_o - \delta L) - L(t) = (L_o - \delta L)\left\{\frac{K\Theta\gamma V}{RTr^n}(t-\delta t)\right\}^m \qquad (32)$$

or

$$L(t) = (L_o - \delta L)\left[1 - \left\{\frac{K\Theta\gamma V}{RTr^n}(t-\delta t)\right\}^m\right] \qquad (33)$$

where δt is the required correction in starting time and δL is the corresponding correction in length, and plotting $(t-\delta t)^m$ vs. L to get a straight line. The time error, δt, is determined graphically as the value necessary to straighten the L vs. $(t-\delta t)^m$ isotherm. The deviation in length, δL, is then the difference between Lo as measured and the intercept at $(t-\delta t)=0$. The value of the sintering index, m, can be obtained from the log-log plot of the raw data if the corrections are small. In this method, the time correction is analogous to the incubation time and the length correction to the correction factor for having non-uniform powders. Figures 4.4, 4.5, 4.10 and and 4.11 consist of two sets of plots. The upper sets labelled Johnson-Cutler plots are the log-log plots of $\frac{Lo-L}{Lo}$ vs. log $(t-\delta t)$. This should yield a straight line of slope m if equation (14) holds. These plots are analogous to the previously mentioned L vs. $(t-\delta t)^m$ plots and are justified when $\delta L \ll Lo$. Typical values

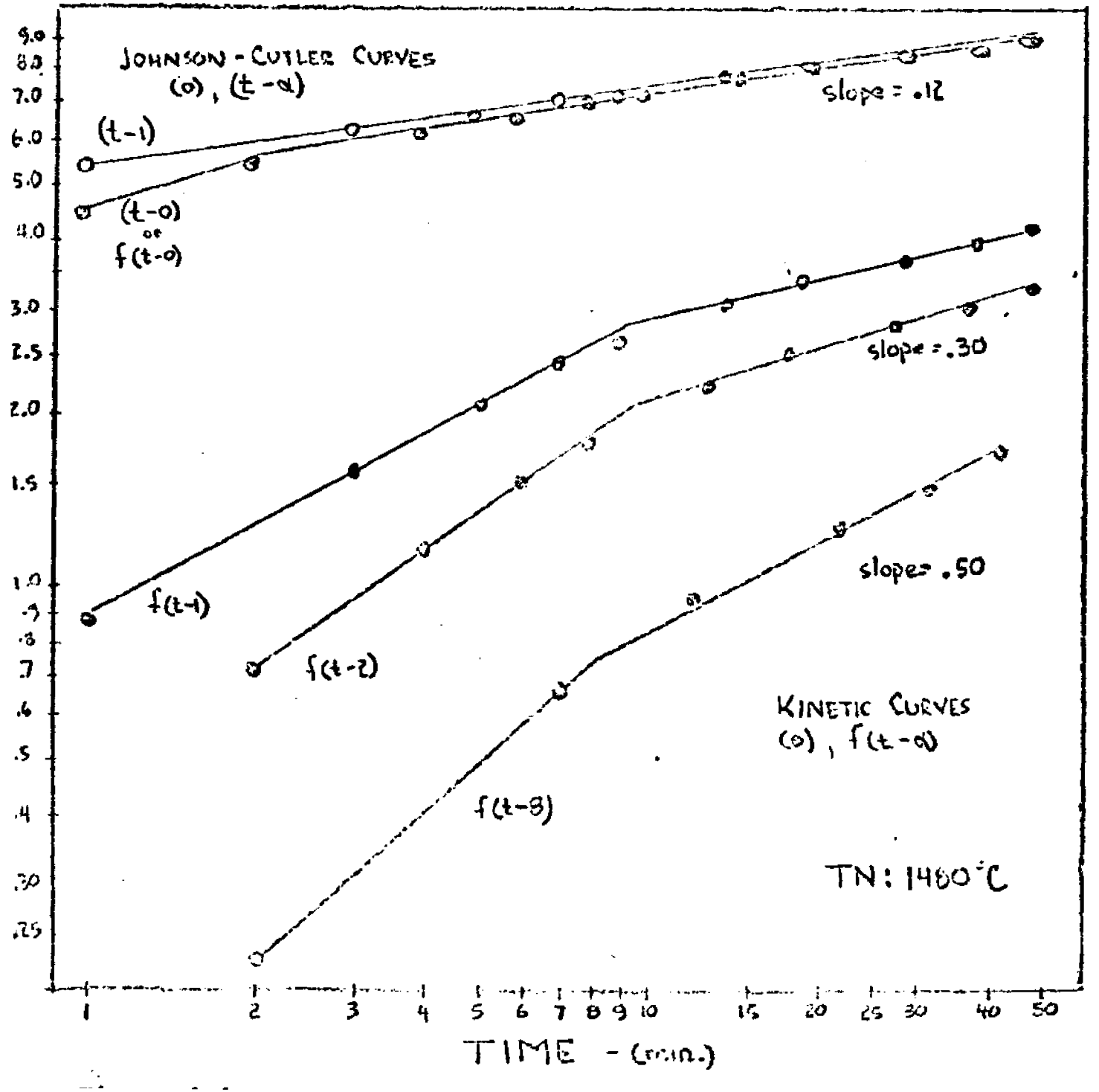
JOHNSON - CUTLER CURVES
(o), (t - α)
slope = .12
(t-1)
(t-0)
f(t-0)
slope = .30
slope = .50
f(t-1)
f(t-2)
f(t-3)
KINETIC CURVES
(o), f(t - α)
TN: 1480°C
9.0
8.0
7.0
6.0
5.0
4.0
3.0
2.5
2.0
1.5
1.0
.9
.8
.7
.6
.5
.4
.30
.25
1
2
3
4
5
6
7
8
9
10
15
20
25
30
40
50
TIME - (min.)

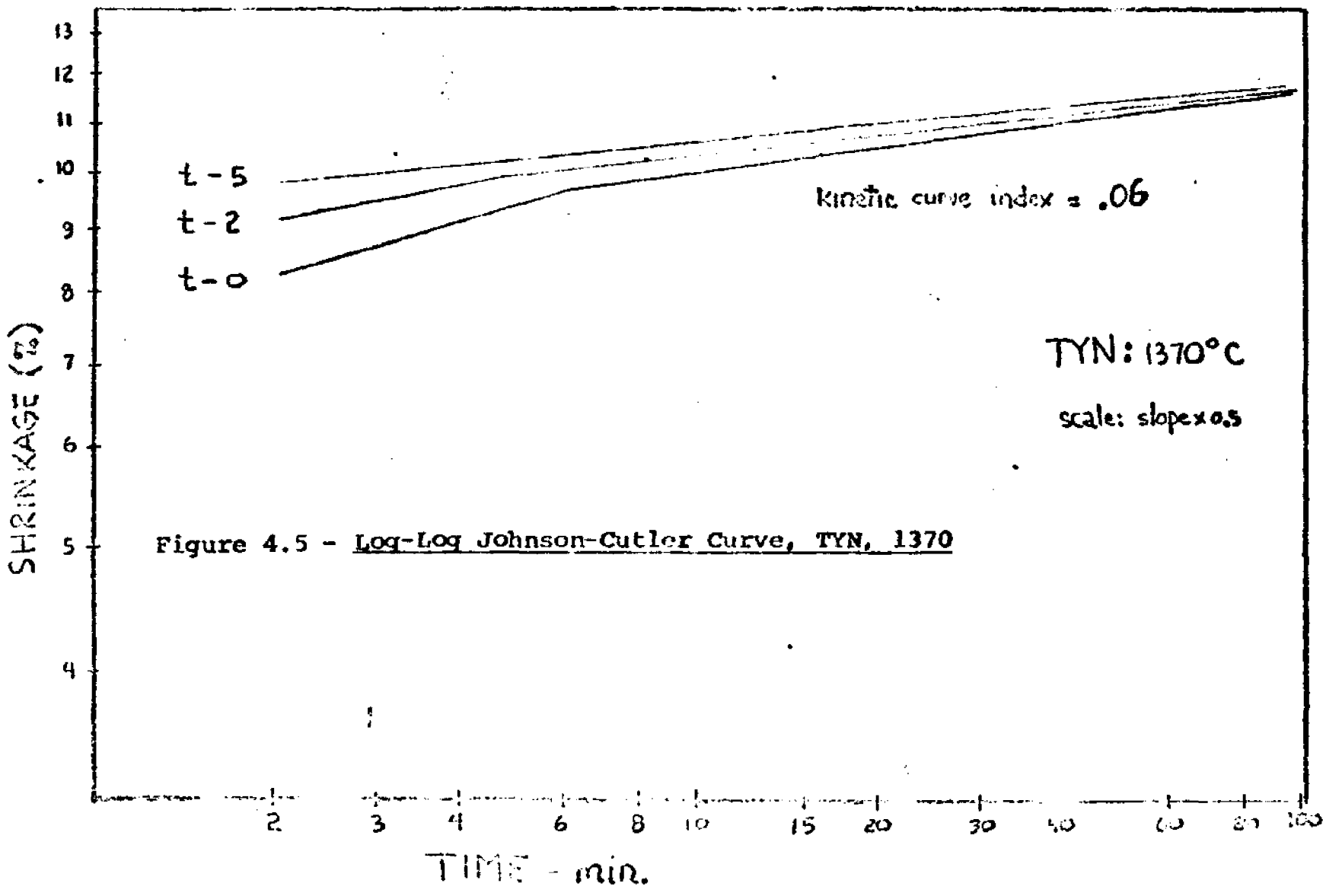

Figure 4.5 - Log-Log Johnson-Cutler Curve, TYN, 1370

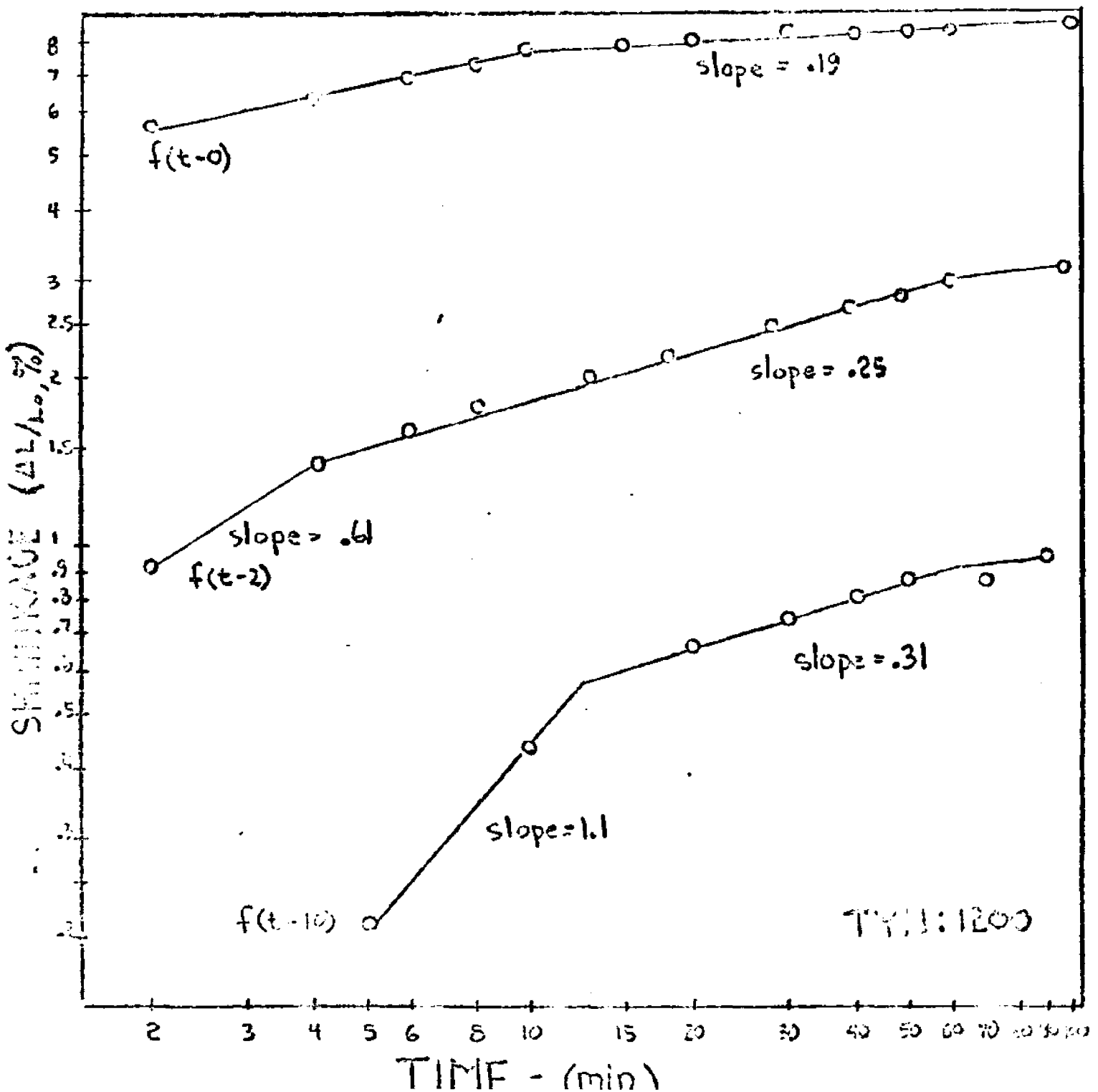
SHRINKAGE (ΔL/L0,2%)
TIME - (min)
f(t-0)
slope = .19
f(t-2)
slope = .61
slope = .25
f(t-10)
slope = 1.1
slope = .31
TYT: 1200

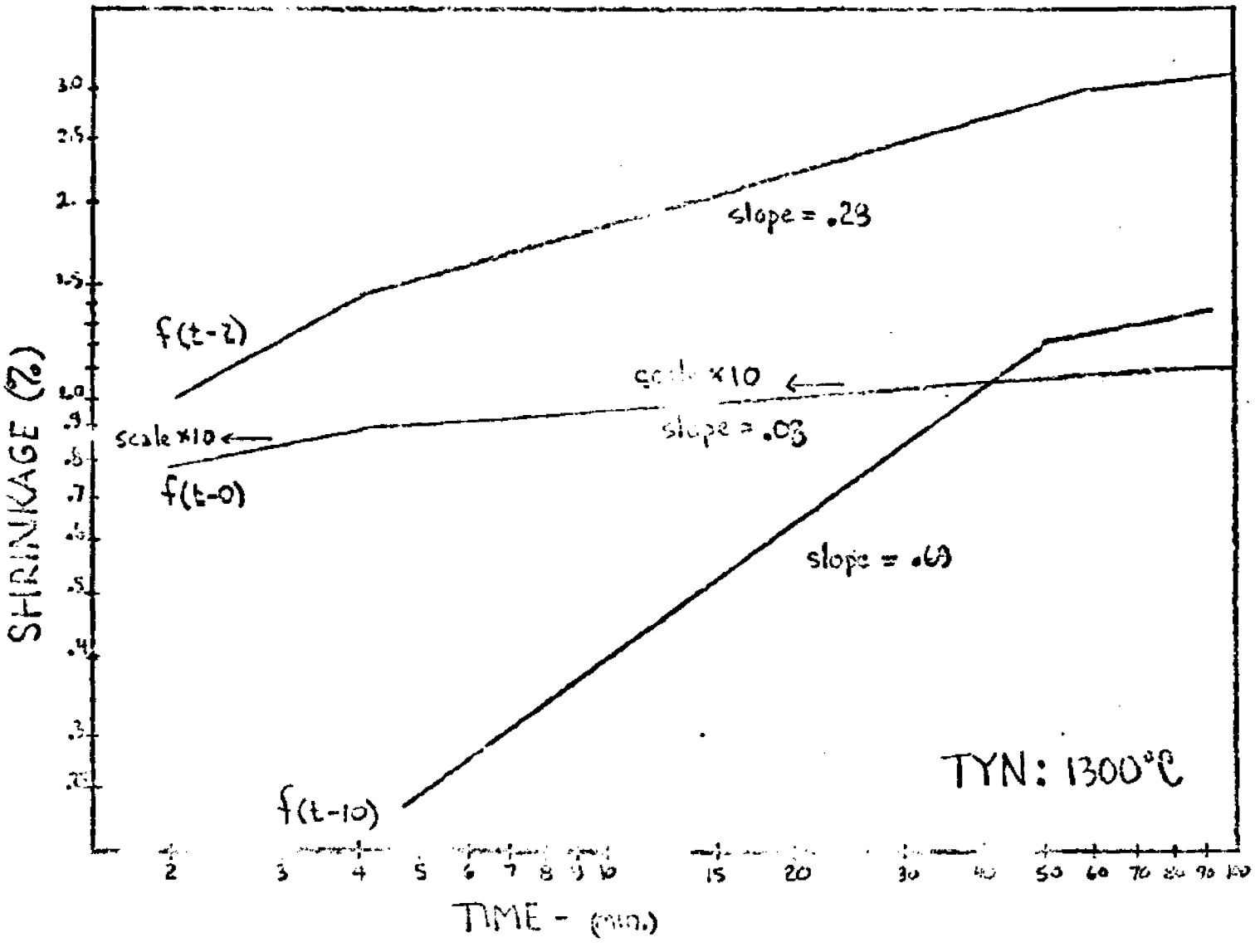

Figure 4.7 - Non-linear Translated Curves, 1300

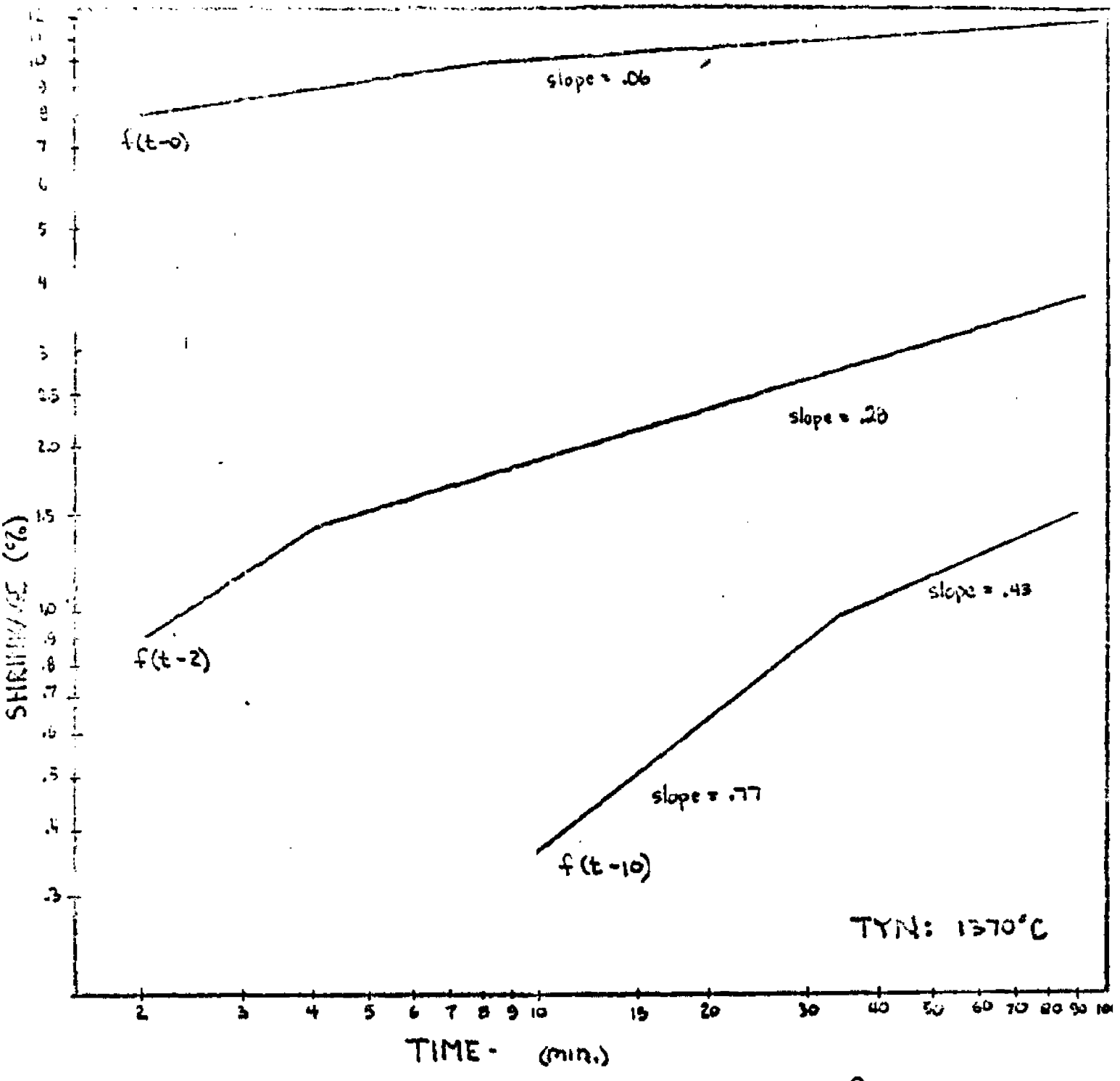

Figure 4.8 - Non-linear Translated Curves, TYN, 1370°C

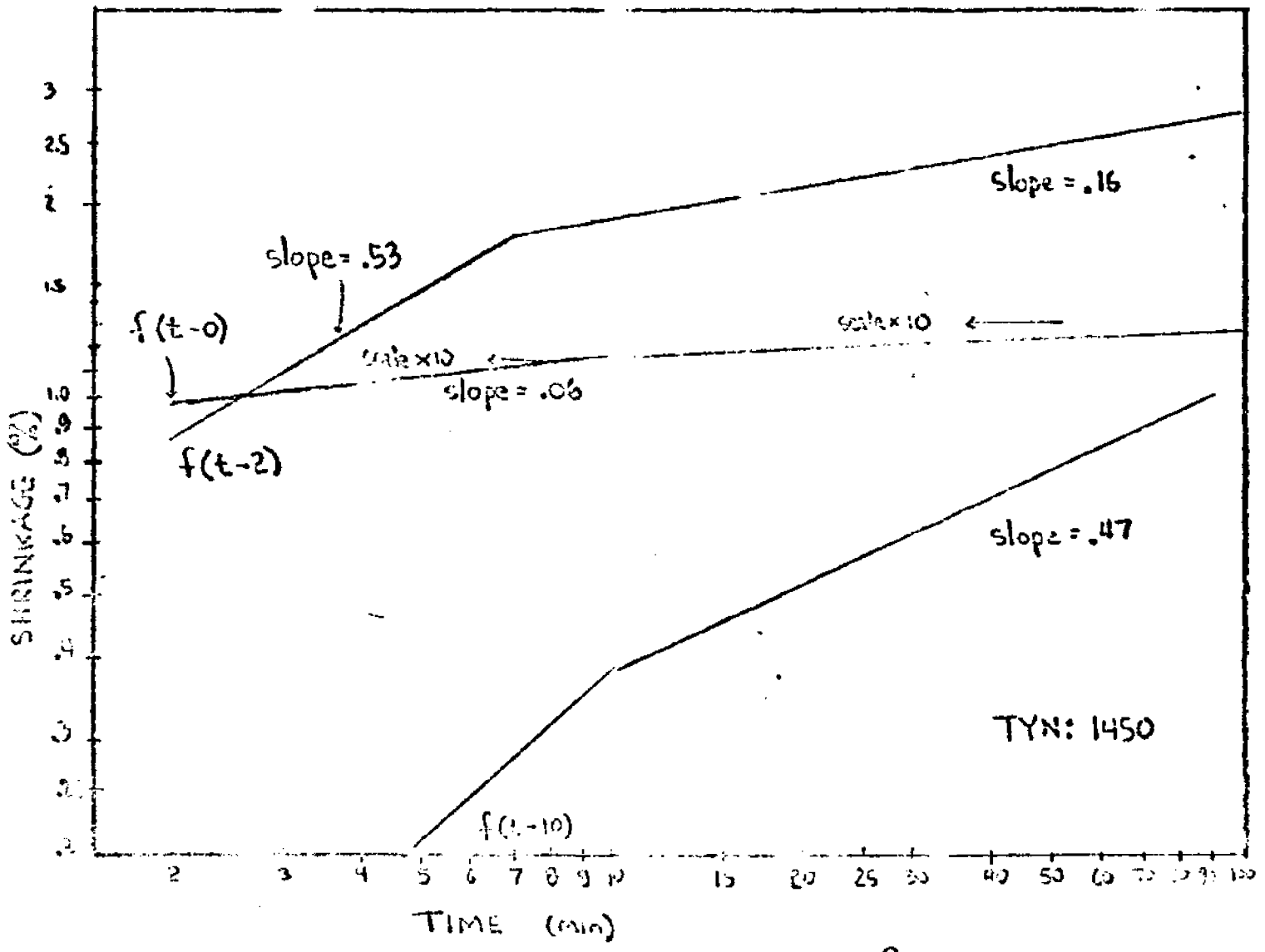

Figure 4.9 - Non-linear Translated Curves, 1480°C

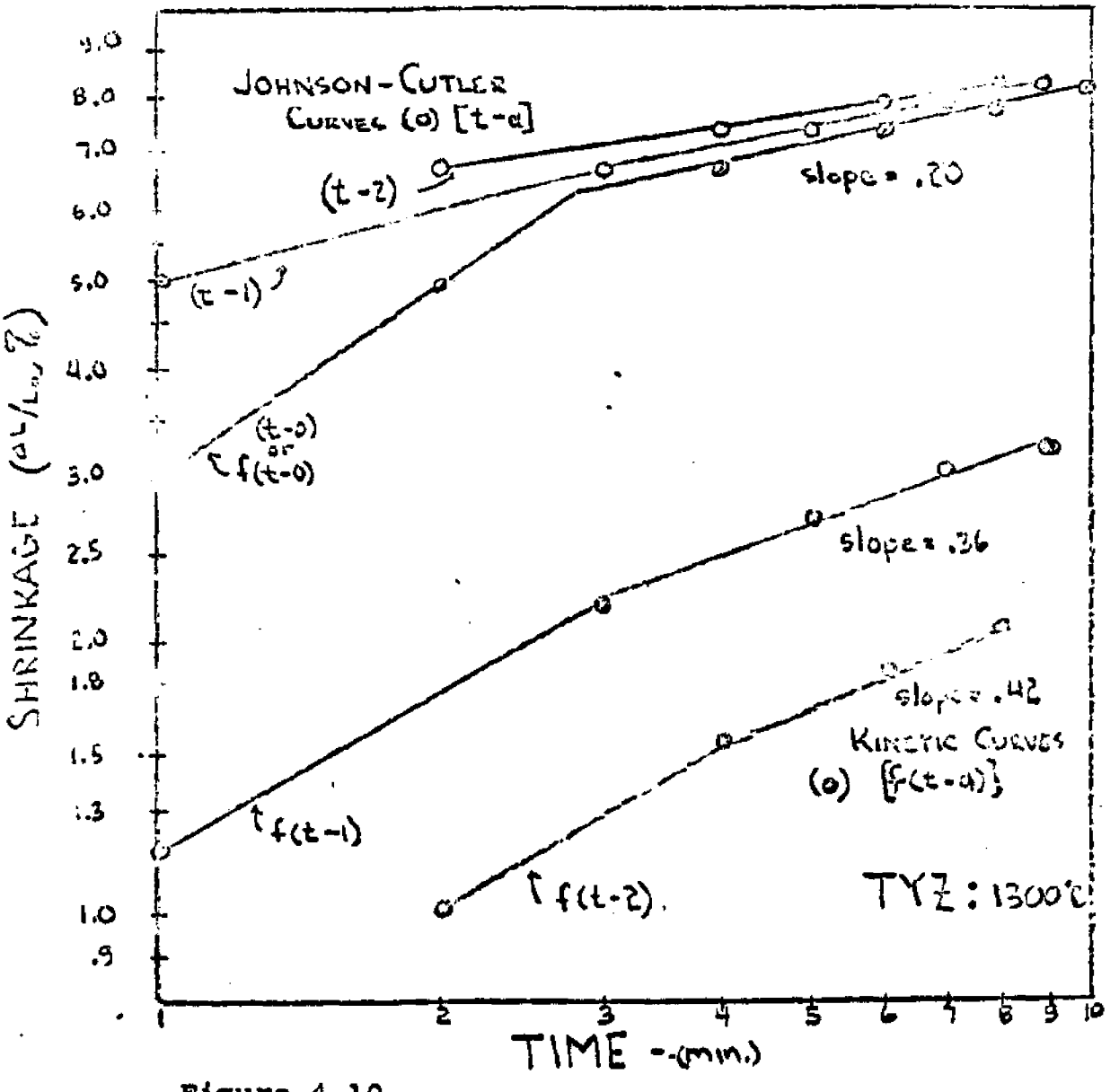
JOHNSON-CUTLER
CURVES (o) [t-a]
(t-2)
(t-1)
(t-0)
or
f(t-0)
slope = .20
slope = .36
slope = .42
KINETIC CURVES
(o) {f(t-a)}
f(t-1)
f(t-2)
TYZ: 1300°C
SHRINKAGE (ΔL/L₀, %)
TIME - (min.)
9.0
8.0
7.0
6.0
5.0
4.0
3.0
2.5
2.0
1.8
1.5
1.3
1.0
.9
1
2
3
4
5
6
7
8
9
10

Figure 4.10

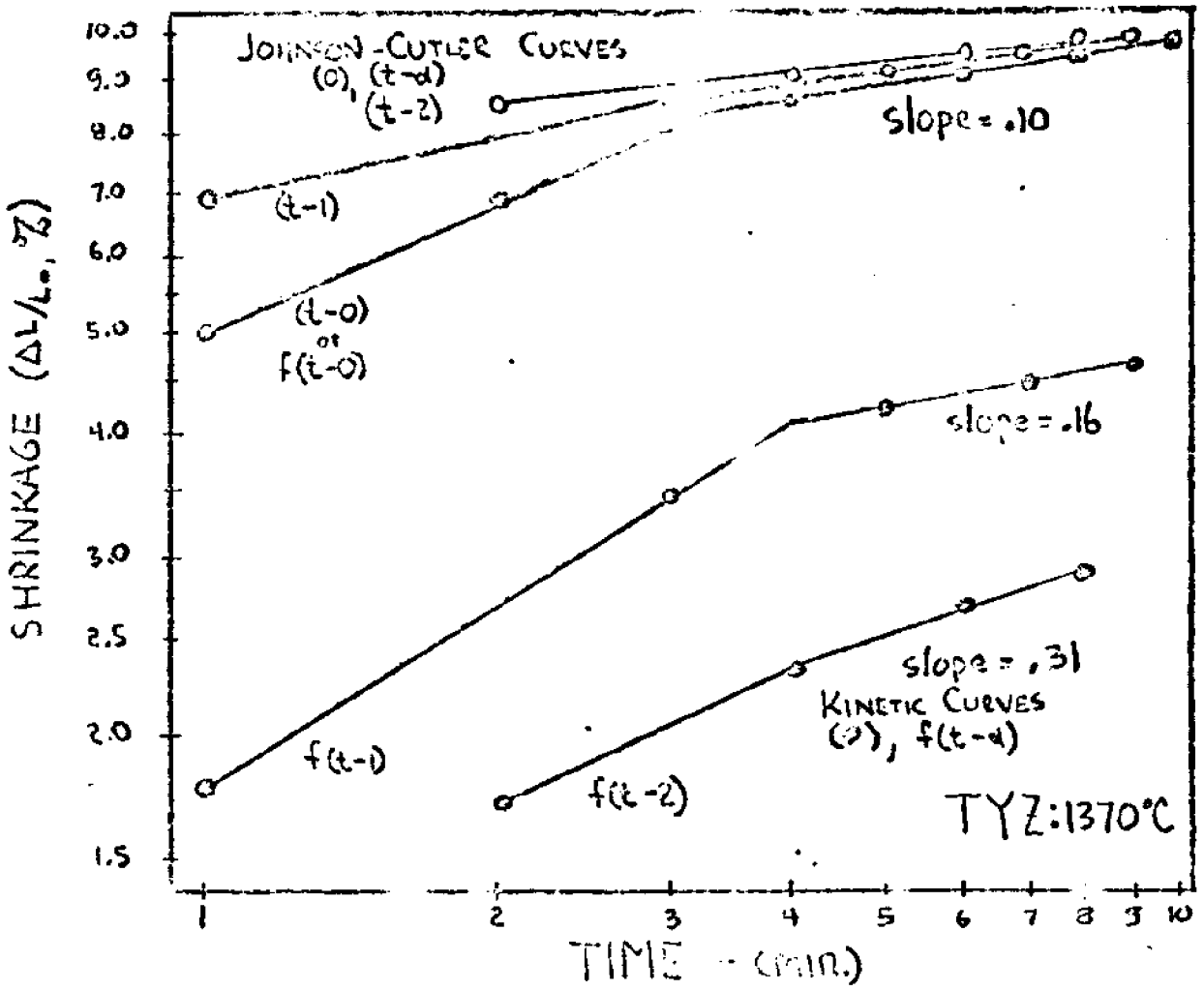
JOHNSON-CUTLER CURVES
(O), (t-d)
(t-2)
slope = .10
(t-1)
(t-0)
or
f(t-0)
slope = .16
slope = .31
KINETIC CURVES
(O), f(t-d)
f(t-1)
f(t-2)
TYZ:1370°C
SHRINKAGE (ΔL/L°, %)
TIME - (min.)
10.0
9.0
8.0
7.0
6.0
5.0
4.0
3.0
2.5
2.0
1.5
1
2
3
4
5
6
7
8
9
10

Figure 4.11

determined from L vs. $(t-\delta t)^m$ plots (not shown) disclose that $\delta L<0.1Lo$.

On the Johnson-Cutler type plots (which Johnson now tends to disavow (R66), it appears that the δt (or "α" as indicated on the graph, since this is equivalent to a "break point) required to make a straight line is 1, 2, and 5 minutes respectively for TN, TYZ, and TYN. This may be highly inaccurate due to the nature of the simplifying assumptions in making the log-log plot. It would mean that the incubation time (δt) was dependent on the material added to thoria.

Another method, also described in section 1.4, involves the disregard of the inexplicable initial region in order to find out what is occurring in the latter stages. This is easily done through the use of the Johnson-Cutler equation (equation 32) and the assumption that $Lo-\delta L-L = 0$ at $t = \delta t$ (see Appendix D). This means that from a time t_1, when the measured length is L_1 the governing equation would become

$$(L_1-L) = L_1\left\{\frac{K\gamma\delta V}{RTr^n}(t-t_1)\right\}^m$$

This method of non-linear translation is necessary because of the large initial shrinkage of the green compact. When this large initial shrinkage does not closely obey the governing equation (14), then failure to subtract that shrinkage and time effects will cause erroneous conclusions. The obvious reason for this is that the large initial shrinkage will overshadow any subsequent change in length. In figures 4.4, 4.10 and 4.11, the upper sets of curves are the log-log

Johnson-Cutler type plots. In these figures are also the non-linear translated graphs for TN (figure 4.4), TYN (figures 4.5-4.9) and TYZ (figures 4.10-4.11). These are labelled as f(t-α) and appear as the bottom set of those figures that have Johnson-Cutler curves (figures 4.4, 4.10 and 4.11). [See the Appendix D, for a more detailed mathematical explanation of the non-linear translated technique.] On each of these plots, f(t-o) or (t-o) is the basic data and appears as a curved or two straight lines. The translated graphs would show a straight line if only one mechanism were operable. The value of "α" would indicate at what time only one mechanism was operable and the slope would indicate the mechanism. No such one straight line was noted. In addition, if only one mechanism were operable at different temperatures, the slopes of the line when α is large (when initial effects are disregarded) should be the same (see table 4.1).

Table 4.1 - Slopes from Non-Linear Translation Graphs

Fig. #	Mat	Temp.	α	m	$m_{initial}$
4.4	TN	1480	0	.12	
			4	.30	
			8	.50	
4.6	TYN	1200	0	.19	
			2	.25	
			10	.31	1.1
4.7	TYN	1300	0	.08	
			2	.28	
			10	.69	

4.8	TYN	1370	0	.06	
			2	.28	
			10	.43	.77
4.9	TYN	1450	0	.06	
			2	.16	
			10	.47	
4.10	TYZ	1300	0	.20	
			2	.36	
			10	.42	
4.11	TYZ	1370	0	.10	
			2	.16	
			10	.31	

No distinct trend is observable, with the values of the sintering index (m) approaching different values $\sim\frac{1}{2}$ and with an initial slope of about one. The value of the sintering index (m) for $\alpha=2$ seem fairly consistent at ~ 0.27 and those for $\alpha=10$ badly scattered at ~ 0.5. It is unlikely that either should be accepted.

Still another method for correlating and interpreting sintering data is the Johnson kinetic equation (see section 1.3)

$$\frac{L}{Lo} = 1 - \alpha(K\Theta)\frac{d\Theta}{dt} \qquad (17)$$

This equation does not depend on the absolute value of the shrinkage, but only on its slope with respect to time. In this way, errors aren't accumulated as long as the differences

in shrinkage are accurately known. The length vs. time plots for TYN at three different temperatures are given in figures 4.12-4.14. The values of $\left(\frac{d\ell}{dt}\right)$ are given next to each point. To test for either grain boundary or volume diffusion as the sintering mechanism, a plot should be made of length vs. $d\ell/dt$ to the power m_j=-0.48 or m_j=-0.97 respectively. This has been done in figures 4.15-4.17. Neither exponent produces <u>one</u> straight line even approximately, but both yield <u>two</u> well fitted straight lines. This indicates that two mechanisms probably are responsible. The "break points" (α, where there is a change in mechanism) are given in table 4.2.

Table 4.2 Change of Mechanism Points (α)-Johnson Eqn.

Temp.	α grain boundary	α vol. diffusion
1300	4¼	10
1375	6	6½
1450	7	9

These break points should be construed as having only qualitative significance indicating more clearly than the linear plots of $\Delta L/L_o$ vs. time that the initial stage lasts about 5-10 minutes. The nature of the two mechanisms should not be inferred from the linearity of the plots.

At this point, it might be beneficial to summarize the results obtained from the kinetic data by classical methods. The nature of the powders has made a conventional

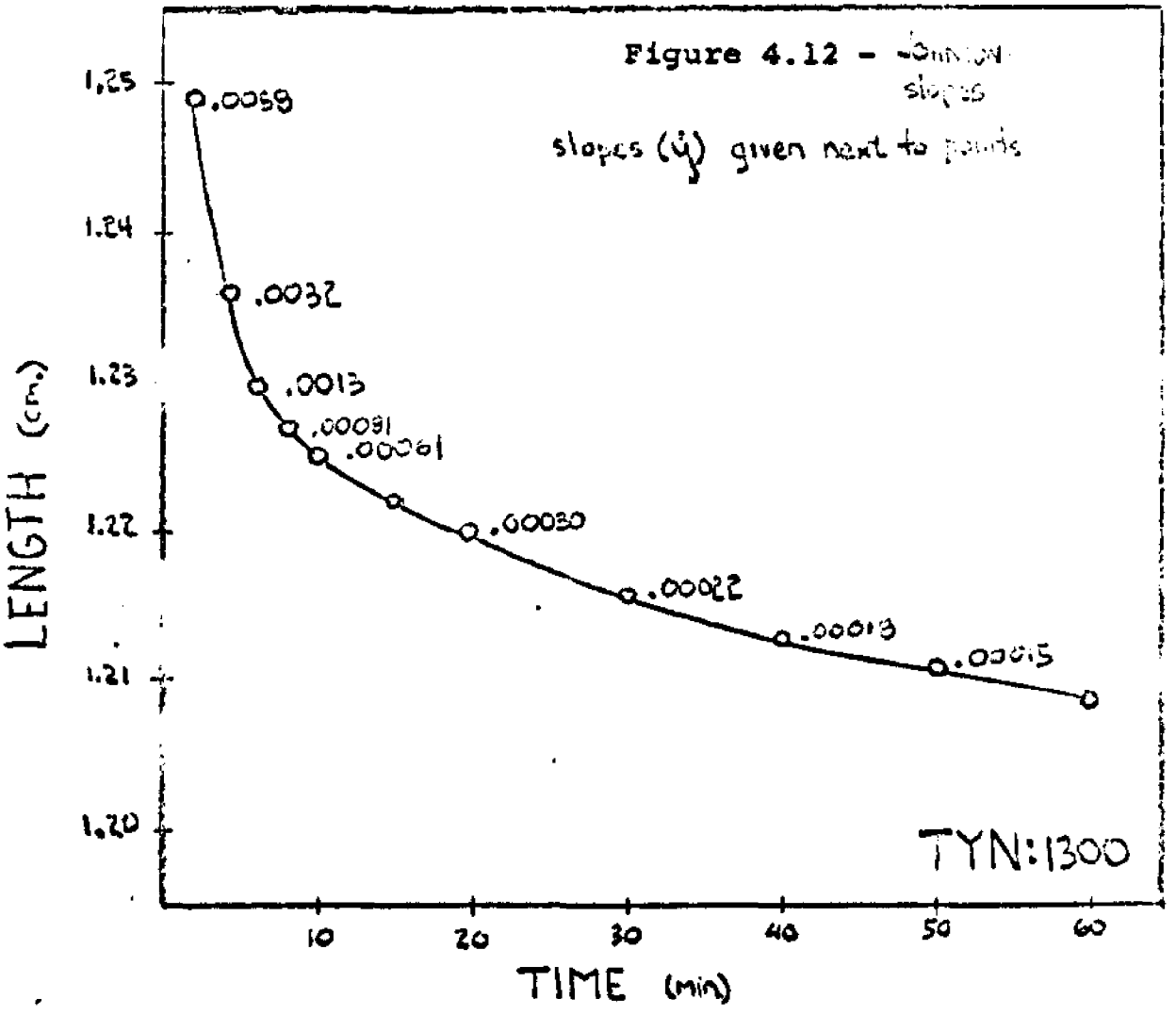
Figure 4.12 – Common slopes
slopes (ẏ) given next to points
LENGTH (cm.)
1.25
1.24
1.23
1.22
1.21
1.20
.0058
.0032
.0013
.00091
.00061
.00030
.00022
.00013
.00015
TYN:1300
10
20
30
40
50
60
TIME (min)

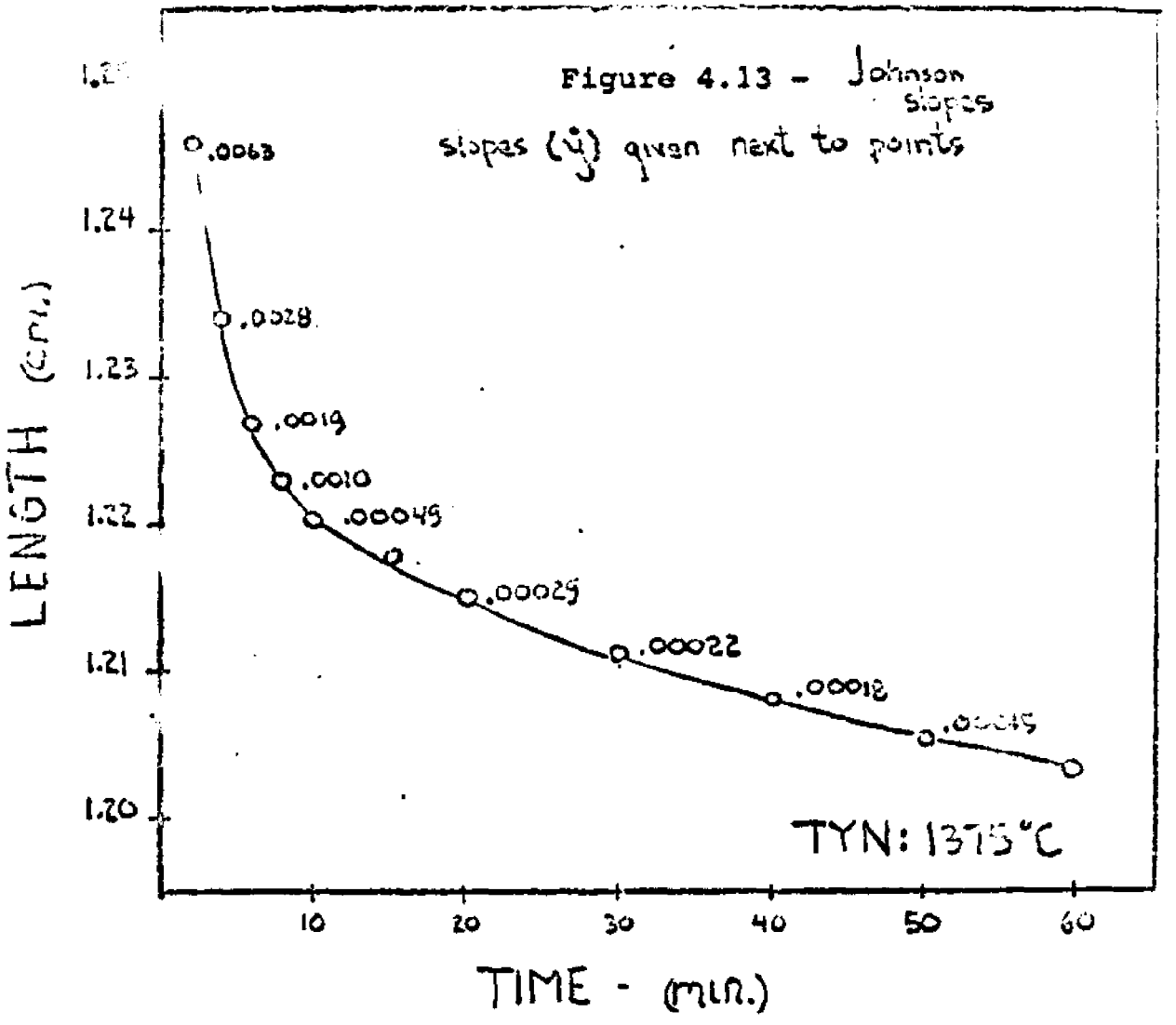
Figure 4.13 - Johnson slopes
slopes ($\dot{\varepsilon}_j$) given next to points
.0063
.0028
.0019
.0010
.00049
.00029
.00022
.00018
TYN: 1375°C
LENGTH (cm.)
1.24
1.23
1.22
1.21
1.20
10
20
30
40
50
60
TIME - (min.)

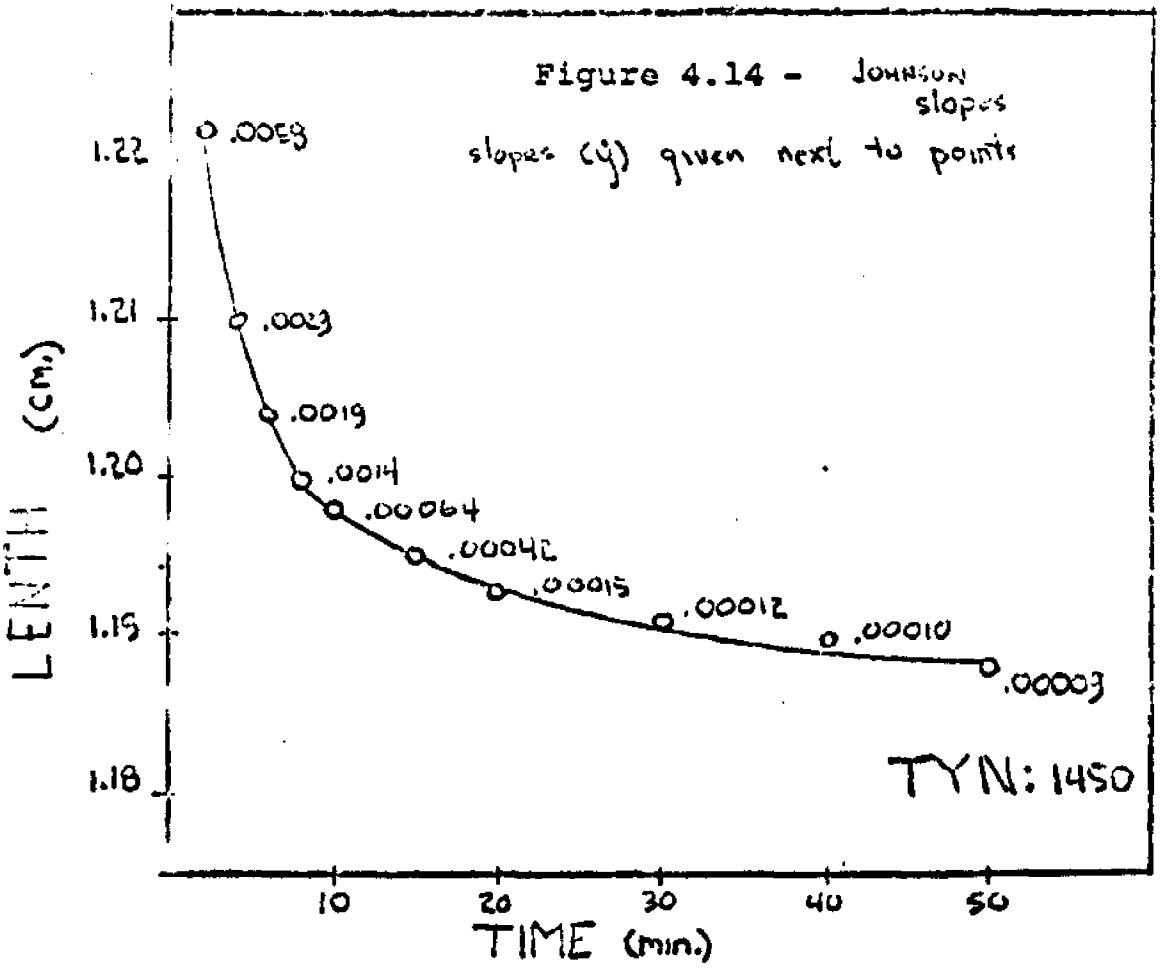
Figure 4.14 - Johnson slopes
slopes (y) given next to points
.0053
.0023
.0019
.0014
.00064
.00042
.00015
.00012
.00010
.00003
TYN: 1450
1.22
1.21
1.20
1.19
1.18
LENGTH (cm.)
10
20
30
40
50
TIME (min.)

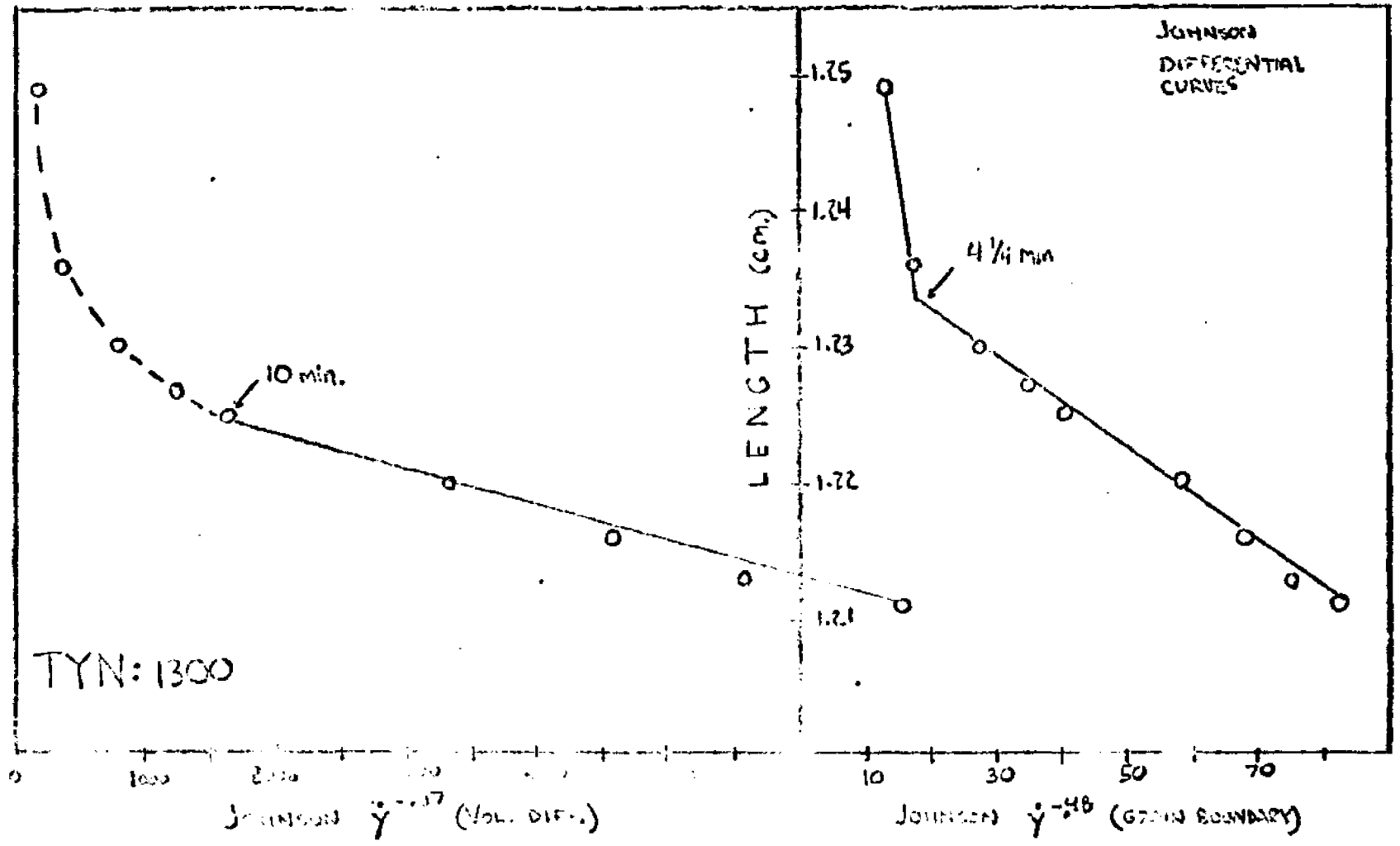

Figure 4.15 - Johnson Differential Equation Curves, TYN, 1300°C

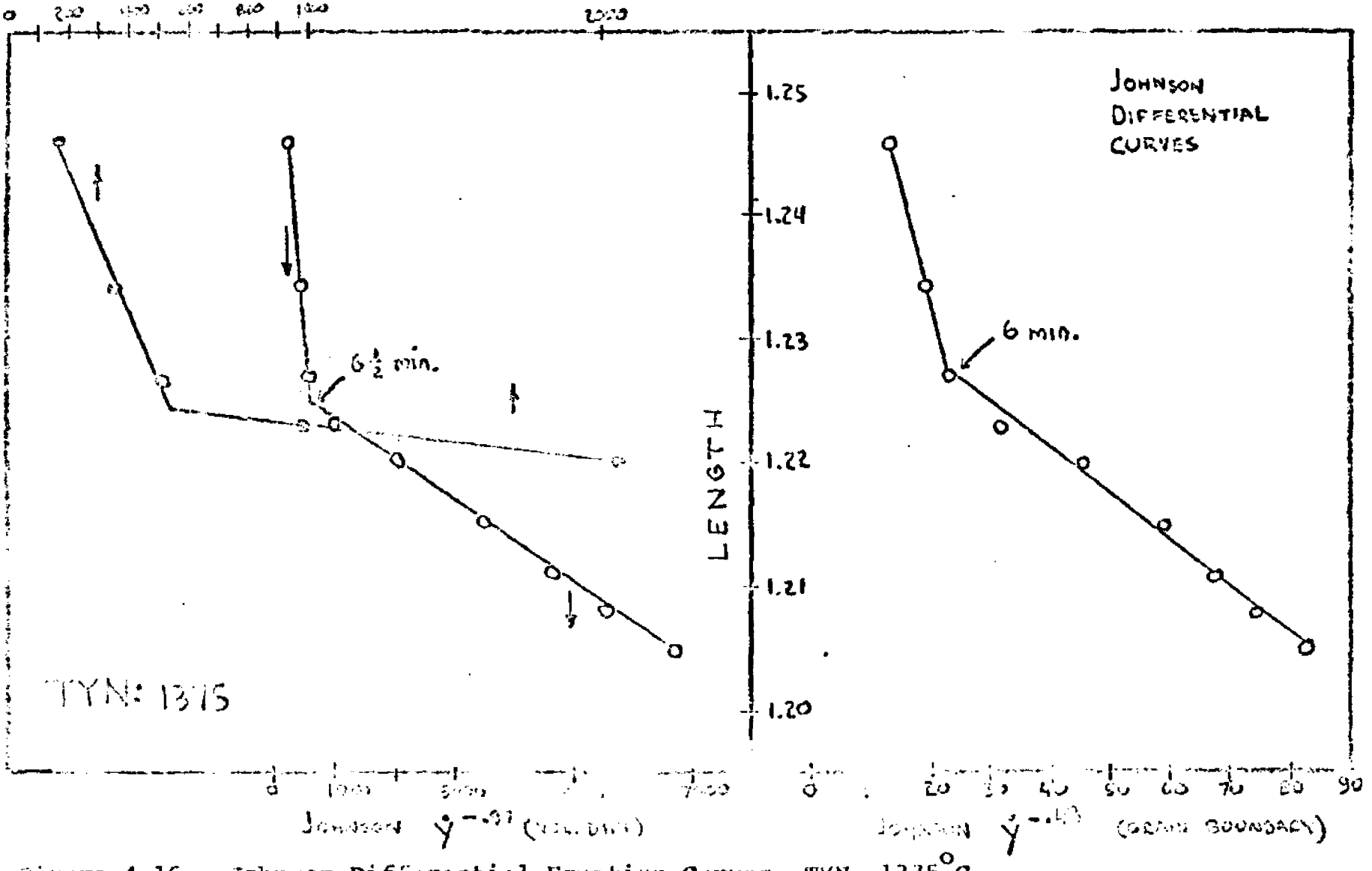

Figure 4.16 - Johnson Differential Equation Curves, TYN, 1375°C

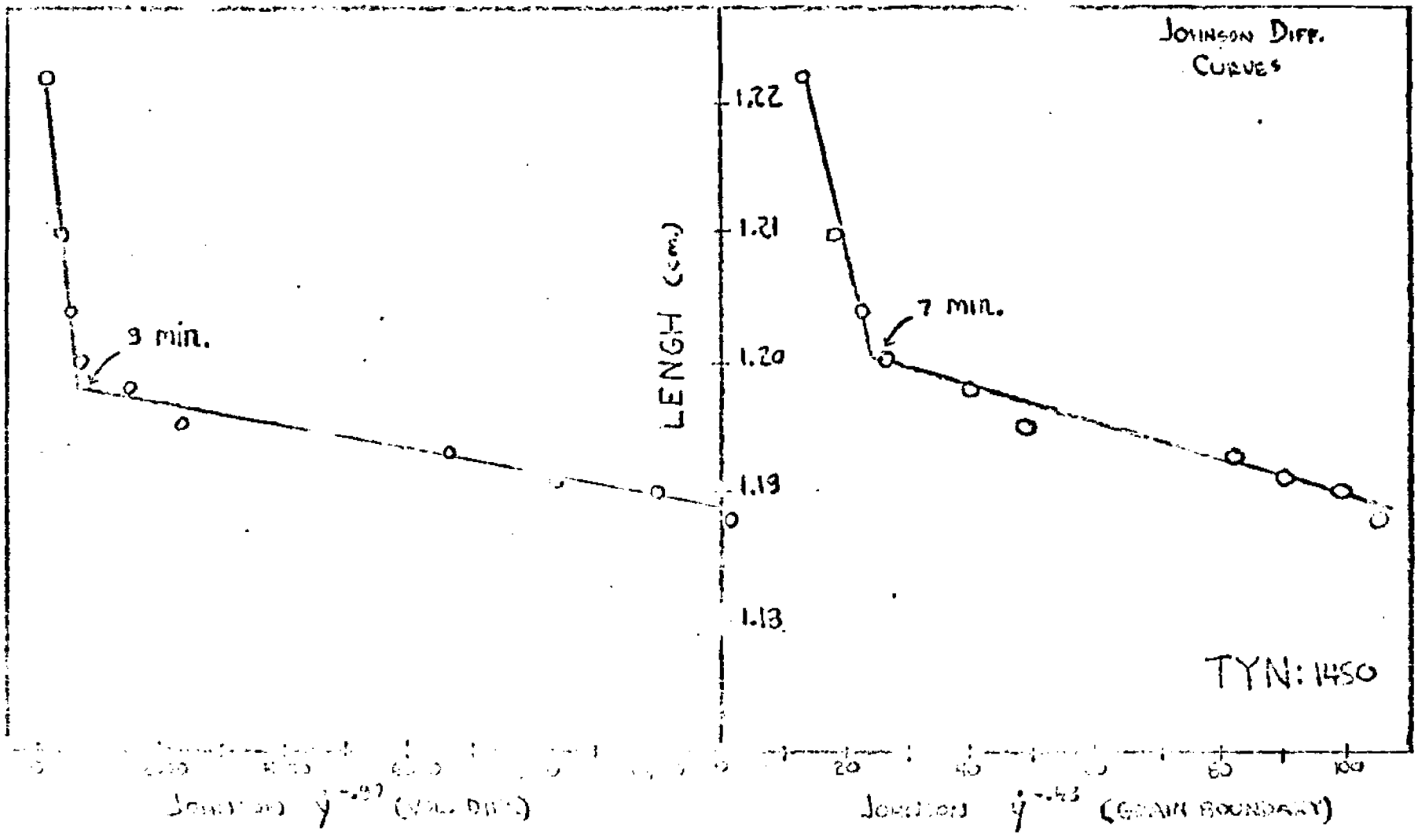

Figure 17 - Johnson Differential Equation Curves, TYN, 1450°C

interpretation of the sintering mechanism for these non-homogeneous, irregular shaped powders impossible. There is probably more than one operative mechanism, and the mechanisms are likely to overlap. However, the repeated evidence of a change in slope of the kinetic and differential curves indicates at least two processes are taking place more or less in succession. The early one leads to a very rapid densification and it is followed by a slower process that more nearly fits the volume diffusion model.

The slopes of the kinetic shrinkage curves on log-log coordinates are initially ~ 1, and later $\sim \frac{1}{2}$. There is apparently a rapid initial rearrangement frequently leading to major densification at less than half the melting point of the material. This strongly suggests the presence of a liquid as described by Kingery (R8). The apparent temperature-dependent end-point could be caused by a sloping liquidus line in a eutectic system that produces increased liquid with increased temperature. This will be discussed later.

4.3 Discontinuous Runs

As previously explained, a series of runs, discontinuous in temperature, was made to determine whether the additive lost its effectiveness after substantial sintering had occurred. The data for these runs were shown in figures 3.17-3.20. These experiments consisted of firing a pellet at one temperature until an end-point (almost complete halt in shrinkage, i.e., the third stage of sintering mentioned in section 4.2) was reached without total densification. The same pellet was

then refired at a higher temperature to observe the new initial effect. A number of control pellets were also refired at the same temperature to determine whether stresses imposed by the rise in temperature or the thermal shock had any effect. No thermal shock or stress effect was noticed.

The graphs show clearly that nickelous oxide additions continued to have a marked effect on the initial behavior for both TYN and TN. This can be seen from the rapid initial increase in shrinkage after the pellet first reached the higher temperature. By contrast, both TY and TYZ showed no rapid initial shrinkage at the new higher temperature, but rather slow rises indicative of a diffusion-controlled mechanism. That the ZnO did not act as an "activator" upon refiring of the pellet is unexpected. Two possible causes come to mind. Either ZnO and NiO activate the sintering of TY by different mechanisms, or, more likely, ZnO is lost via vaporization at these high temperatures. The latter hypothesis was partially verified by weighing a few TYZ pellets fired for 50 minutes at 1500°C. TY pellets were used as controls. It was found that about half of the original ZnO was lost, probably by vaporization to Zn and O_2.

That nickel oxide continues to be "active" after sintering at low temperatures is very significant. Once sintering has occurred for a while, a fairly solid, yet porous network as evidenced by our SEM micrographs, develops. Thoria and yttria with the aid of nickel oxide apparently join to form a bulk solid, yet still remain separate phases, as evidenced by the x-ray pattern for TYN (see fig. 3.20).

The explanation of the behavior of nickel oxide - renewed acceleration of sintering at higher temperatures - is open to conjecture. It may be hypothesized that the nickel oxide is not uniformly distributed in the grains, but tends to concentrate at the boundaries. This NiO-rich band may offer a path for rapid diffusion. If the width of the band increases with temperature, a wider boundary layer through which vacancies can be annihilated is obtained. This explanation is analogous to Burke's (R5) on the annihilation of internal pores of solids. It does not explain the initial rapid shrinkage of TYN (or TY either) on first being heated, when Ni^{++} has not had time to diffuse into the thoria particles.

Another explanation may be based on the stresses that form in the necks between particles. Evidence of this was recently cited by Easterling (R65), Easterling and Tholen (R31) and Young and Cutler (R69). These stresses can cause dislocation movement or Bingham type flow of the material. The susceptibility of the thoria to defect movement or Bingham flow would therefore have to be enhanced by NiO additions. Increasing the temperature would either decrease the critical shear stress, or destroy the ability of the inclusions to stop dislocation movement. This would increase flow and densification. In addition, stresses would be caused by the Kirkendall effect. (A stress induced in a multicomponent inhomogeneous system when both sibstituents have different diffusivities in each other. This causes the less mobile species to go into compression, the more

mobile into tension, and causes pores to form near the interface of the two.) The presence of these pores would also aid in producing a temperature-dependent end-point, since their annihilation would be diffusion controlled. This explanation fails in the initial region of the first run where massive shrinkage occurs before necks are formed, though it is possible that other stresses cause this shrinkage.

Sintering could also be aided by an increase of mobility of the slowest moving species. In thoria, the Th^{+4} diffuses the slowest under our typical operating conditions. The addition of Ni^{++} or Zn^{++} might create Th^{+5} or Th^{+6} ions which are smaller than the Th^{+4} ion and therefore should enhance the diffusivity at the thorium ion. Similar type behavior has been noted for uranium dioxide.

There is another possible explanation, as proposed in section 4.2, i.e., there may be a liquid phase present. However, nickel oxide (m.p. 1990°C) aids the sintering of pure thoria (m.p. 3300°C). Since it is most unlikely that the addition of 2.5 mole percent NiO to ThO_2 lowers its solidus temperature by 2000°C, it is necessary to postulate that any liquid is rich in NiO. That is to say, the addition of ThO_2 to NiO lowers the solidus temperature by about 700°C. This liquid would act initially as a lubricant and supply capillary forces to allow for rearrangement. On refiring at a higher temperature, even more liquid is produced at grain boundaries aiding rearrangement, but perhaps more importantly, filling in pores leading to more densification. However, it is difficult to believe that such

massive shrinkage occurs in such a short time, (the initial few minutes) when so little liquid could be formed. This matter will be discussed in greater detail later.

That the initial rearrangement is so quick tends to indicate that it is caused by a driving force present before heating, possibly stresses. All of these effects, or a combination of them may be operating. Since mathematical models of the first three explanations are not available, analysis of these mechanisms and their relation to the kinetic shrinkage curves cannot be performed.

4.4 Temperature Dependence of the Sintering Rate

The temperature of sintering has a very marked effect on the densities achieved by the materials under investigation. This was briefly discussed in section 3.3 and shown in figure 3.9 for TYN and in 3.10 and 3.11 for TYZ. In order to isolate the effect of temperature, it is customary to graph a term characteristic of the rate on coordinates representative of the governing equation of the phenomena being studied. In this way, it is frequently possible to relate the effect of temperature to the energy required for a process and thereby to obtain a better understanding of the processes involved.

It is, of course, well established that if a process is thermally activated, it follows an Arrhenius rate equation. If the process is controlled by diffusion, the equation for the diffusivity, $\mathcal{D}$, is customarily given by

$$\mathcal{D} = D_o e^{-Q/RT} \qquad (35)$$

where the pre-exponential constant, D_o, is independent of temperature. The activation energy, Q, has a significance that depends upon the actual mechanism of diffusion. Thus, in the case of the diffusion of interstitials at low concentrations, the number of sites available is infinite relative to the number of atoms of the diffusing species, and Q is just the energy required for jumping of a mole of the interstitials. On the other hand, for self-diffusion or substitutional diffusion by a vacancy mechanism, Q is the sum of the energy needed to create vacancies and the energy to allow jumping of the atoms. Thus, the activation energy is a measure of the total energy required for a process. Since it appears in the exponent as Q/T, the effect of temperature on the rate is very strongly affected by its magnitude.

Now if the sintering process is truly controlled by a mechanism linked to diffusion, we have seen that it should be governed by an equation of the form

$$\frac{\Delta L}{Lo} = \left(\frac{K\gamma V}{RTr^n} t\right)^m \qquad (14)$$

Although we have shown that this equation is not obeyed in simple form over the entire range, it is of interest to obtain at least a qualitative idea of the magnitude of Q if the equation were applicable. For this purpose we assume that for small changes in temperature, the interfacial energy, volume and dimensional terms may be considered constant. Therefore, equation (14) reduces to

$$\frac{\Delta L}{L_o} = K_1\left(\frac{\mathcal{O}t}{T}\right)^m \qquad (36)$$

where K_1 is approximately constant.

If one wishes to use this equation to determine the effect of temperature at equal sintering times, this is not easily done, for at constant time

$$\frac{\Delta L}{L_o} = K_2\left(\frac{\mathcal{O}}{T}\right)^m = K_2\left(\frac{D_o e^{-\frac{Q}{RT}}}{T}\right) \qquad (37)$$

taking logs of both sides yields

$$\ln \frac{\Delta L}{L_o} = K_3 - m\left[\frac{Q}{RT} + \ln T\right] \qquad (38)$$

Therefore a plot of $\ln\frac{\Delta L}{L_o}$ vs. $\frac{1}{T}$ should not yield a straight line unless $\ln T$ were negligible by comparison with Q/RT. This is not the case for reasonable values of temperature. As can be shown, only approximate straight lines result when an Arrhenius type plot is used (see Appendix E).

It is possible, nevertheless, to derive an approximate value of the activation energy. Referring back to equation (36) for equal percentage shrinkage at different temperatures and times

$$\left(\frac{\mathcal{O}_1 t_1}{T_1}\right)^m = \left(\frac{\mathcal{O}_2 t_2}{T_2}\right)^m \qquad (39)$$

so that

$$\frac{\mathcal{O}_1}{\mathcal{O}_2} = \frac{T_1 t_2}{T_2 t_1} = \frac{e^{-Q/RT_1}}{e^{-Q_2/RT_2}} \qquad (40)$$

Therefore, if the mechanisms are the same at both temperatures ($Q_1 = Q_2$)

$$\ln \left\{\frac{T_1 t_2}{T_2 t_1}\right\} = \frac{Q}{R}\left(\frac{1}{T_2} - \frac{1}{T_1}\right) \qquad (41)$$

This equation is not easy to apply because the shrinkage chosen for comparison should involve times that are not too short, lest the errors of the initial period become involved. Yet, since the shrinkage rate falls to very small values at later times, comparable shrinkages can be obtained only at relatively short times. The results are likely to be crude. However, since the results are expected to be only qualitative the following comparisons have been made for TYN (table 4.3 and TYZ (table 4.4), where the activation energy is given in kcals/mole.

Table 4.3 Activation Energies, TYN

Temperature Pair (°C)	times, t_1, t_2 (min)	$\frac{\Delta L}{L_o}$ (%)	Q (kcal/mole)
1200 - 1300	18, 2.1	8	103
1300 - 1375	4.5, 3.9	9	13
	17, 9.2	10	46
	87, 40	11	57
1300 - 1450	17, 2.1	10	79
	87, 4.8	11	108
1300 - 1530	87, 1.8	11	103
1375 - 1450	9.2, 2.1	10	115
	40, 4.8	11	164
1375 - 1530	40, 1.8	11	127

1450 - 1530	4.8, 1.8	11	80
	17.5, 3.7	12	124
		AVG =	92.8

Table 4.4 Activation Energies, TYZ

Temperature Pair (°C)	times (min) t_1, t_2	$\frac{\Delta L}{Lo}$(%)	Q(Kcal/mole)
1225 - 1300	4.8, 2.1	5	55
1300 - 1370	5.0, 2.5	7	54
	9.6, 3.4	8	80
1300 - 1440	9.6, 1.2	8	84
1370 - 1440	3.4, 1.2	8	87
	5.5, 2.5	9	67
		AVG =	71.2

It will be observed that apart from the 1300, 1375°C combination which yielded low results, the activation energies for TYN fall in a range from about 80 to 160 kcal/mole. Using all the data, the average is 93 kcal/mole. The TYZ values are generally lower, averaging about 71 kcal/mole. These values are not very far from the measured activation energies for diffusion of the slower moving cation in UO_2 (81-105 kcal/mole) and in ThO_2 (59 kcal/mole) (R71, R72). They are also in reasonable agreement with the estimate of about 100 kcal/mole made from an inspection of the SEM micrographs (see Section 3.5, Plates 3 and 4).

If these values have validity, their significance lies in the indication that a solid state diffusional process appears to be involved, for they are too high for

diffusion in a liquid. This matter will be discussed in more detail in Section 5.

The previous calculations were made for the purpose of acquiring an approximate energy for the overall sintering process rather than to evaluate the effect of temperature on the densification rate at short times. As the tables show, these calculations were made over a very considerable range of times of sintering [from 1.8 to 87 minutes]. It was also shown that if equation (14) did represent the shrinkage, it was not easily possible to show the effect of temperature on the densification achieved after selected times. Yet the effect of temperature on densification in the initial period is of major interest. Just how much densification is achieved after about 2 minutes at different temperatures? To answer this type of question, the shrinkages achieved after selected lengths of time have been plotted on linear coordinates vs. temperature as shown in figure 4.18. Astonishingly enough, the relationship obtained (except for long times at high temperatures) is a family of nearly parallel straight lines. This indicates that at constant sintering times, the governing equation is of the form:

$$\frac{\Delta L}{Lo} = K_4 T + K_5 \qquad (42)$$

No evidence of any such governing equation for sintering has ever previously been found. It seems to call for a mechanism where a temperature difference is the driving

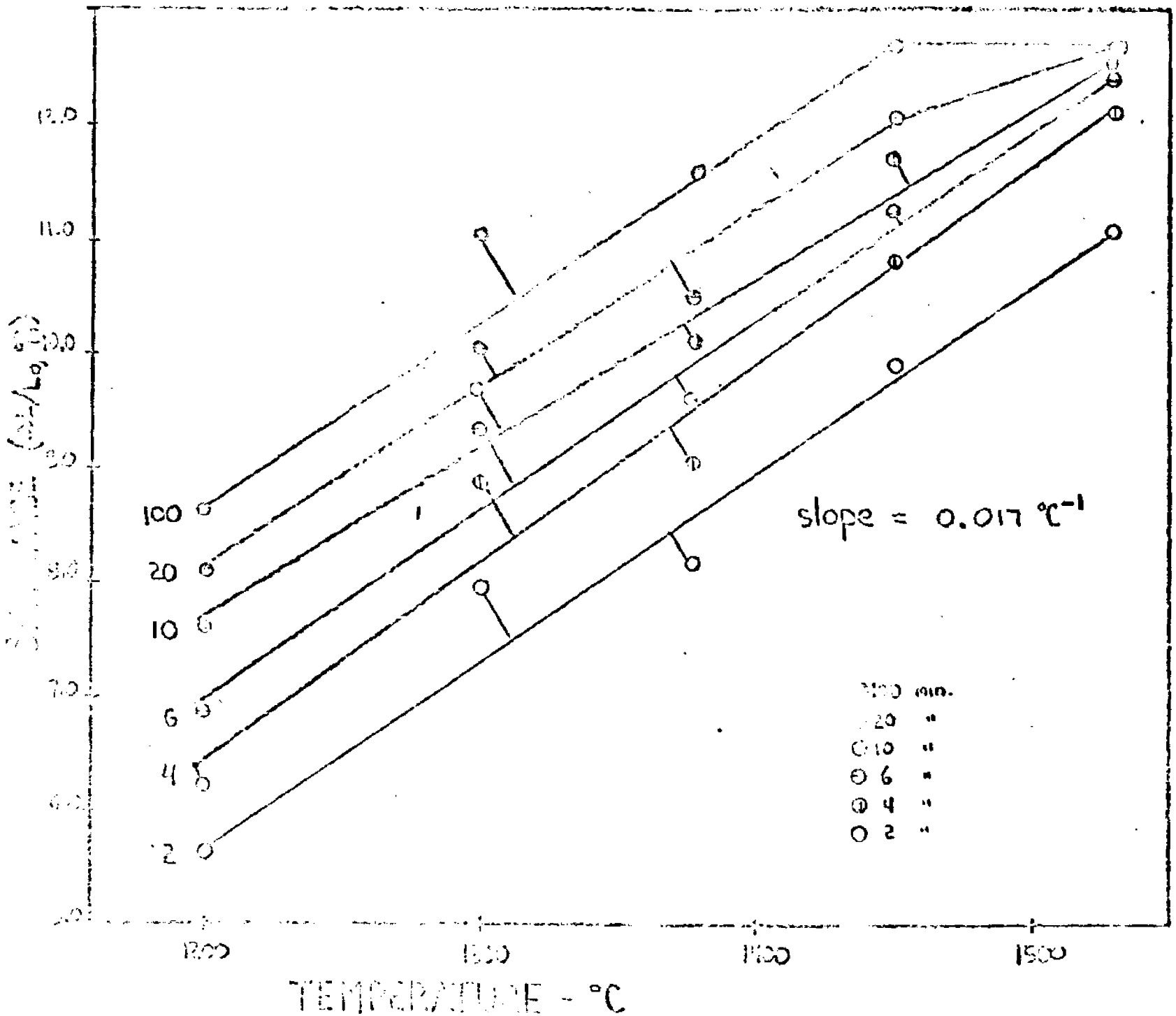

Figure 4.18 - Shrinkage vs. Temperature (Linear), TCN

force. Possible mechanisms of this kind include temperature-induced stresses produced by insertion into the hot zone, or control of densification by the presence of a liquid whose amount is a direct function of temperature. These will be discussed in greater detail in Section 5.

How significant are the shrinkage data at longer times? Any shrinkage plot would have as the major contributor to ΔL the initial sintering where a majority of the shrinkage occurs. To correct for this possible error, a table was prepared by subtracting the 2 minute readings from the 10 minute readings, and the 10 from the 30. These results for TYN are given in table 4.5.

Table 4.5 TYN ΔL's During Different Time Intervals

Temp (^{o}C) →	1100	1170	1230	1300	1380	1440
2-10 min.	.017	.025	.030	.025	.024	.029
10-30 min.	.012	.010	.013	.013	.013	.009

Obviously, the shrinkage is determined almost entirely by the events of the first few minutes. In other words, the behavior is dependent on the extent of the initial rearrangement. The shrinkage and densification that occur within the first couple of minutes is therefore of overwhelming importance, since the subsequent behavior of TYN is similar at all temperatures. The results of table 4.5 could have been deduced from the parallel lines in figure 4.21.

5. Suggested Mechanisms

5.1 Introduction

The previous chapters first described the theoretical means with which to determine mechanisms of sintering of powder compacts. They then gave our experimental results and some brief comments on possible mechanisms to explain the phenomena.

It has been shown that small additions of nickelous oxide (NiO) and zinc oxide (ZnO) are good sintering aids for the densification of thoria-yttria at temperatures near 1500°C. It has also been demonstrated that none of the simple, conventional sintering mechanisms is applicable to this complex situation in which ThO_2 is in the form of flat plates, not monosized, and more than one component is present.

The most striking feature of the kinetic shrinkage curves is the existence of successive stages with possible overlap between them. There are clearly two or three regions; (1) an initial very rapid shrinkage rate (2) a slower shrinkage region where volume diffusion is probably occurring, and (3) a final slow densification region where little or no shrinkage occurs. The presence of these regions have been deduced from the nature of the kinetic shrinkage curves, the observed "break points" in Johnson, Johnson-Cutler and Kuczynski models, and visual observation of rearrangement and densification on the SEM. There is an apparent temperature dependent end point

of density. This is evidenced by the ability to approximately superimpose the kinetic curves after the initial 2 minute reading has been subtracted. The first region, where the major densification occurs, is of major interest and will be discussed more fully. The second and third regions are fairly easily envisioned and contribute little to the unusual shrinkage and densification kinetics of the material investigation.

The very rapid densification so soon after reaching the sintering temperature implies a rearrangement of the powder particles without any substantial amount of diffusion. It is difficult to visualize a cause other than the formation of a liquid phase or the relief of pre-existing stresses. Both of these will be examined in greater detail in the following sections.

5.2 Liquid Theory

The simplest hypothesis that would explain the early and rapid rearrangement would involve the formation of a liquid phase at the sintering temperature. One might visualize a rather low density array of thoria plates which are suddenly in the presence of a liquid that wets them completely. Strong capillary forces compel a rearrangement that will yield the minimum interfacial area. At the same time, the liquid permits easier sliding of the particles over each other, thereby facilitating the rearrangement which leads to a much higher density. Indeed, after reviewing our results, this explanation has been offered by

Dr. J.E. Burke (R64), manager of the Ceramics Branch of General Electric's research laboratory. Dr. Burke is a recognized authority on the sintering of ceramics. Following the initial rapid shrinkage, the presence of the liquid would also facilitate diffusion in the second stage by providing paths of easy diffusion (R8).

It is essential, then, to examine the arguments and evidence pro and con the liquid phase mechanism. Unfortunately, the phase diagrams for ThO_2-NiO and Y_2O_3-NiC are unknown. Although yttria is essential for the creation of the solid electrolyte, its presence adds a further complexity. Therefore, studies on thoria-nickel oxide binary compositions were conducted specifically to improve the understanding of the sintering process.

There can be no doubt that nickel oxide and zinc oxide are aids for the sintering of pure thoria. The isothermal shrinkage curves of figure 3.8 show the effect of NiO plainly even at the test temperature of 1370°C. So do the SEM micrographs in Plates 5 and 6 (1370°C) and more evidently in Plates 7 and 8 (1530°C). The effect is clearly obvious at 1370°C on the SEM photos of unpressed powders shown in Plate 2. It is made dramatically clear by the macro photos of unpressed powders heated for 10 hours at 1370°C, which are shown on the same plate. It is worth emphasizing that in the last instance, not only were no cold-pressing stresses applied, but the specimens were heated slowly to the sintering temperature in a massive furnace. Hence thermal

stresses were minimal. This tends to strengthen belief in the existence of a liquid.

Although the ThO_2-NiO constitution diagram is unknown, it is fruitful to examine the possible forms. Only simple types without compound formation will be described. [Compounds often have melting points higher than one of the components, and the existence of a compound will not alter the basic argument.] A liquid is presumed to exist at 1370°C, and since the melting points of NiO and ThO_2 are about 1990°C and 3300°C respectively, diagrams of the ideal solution, Figure 5.1a or of the simple peritectic type shown in Figure 5.1b are ruled out. Although a diagram of the form of Figure 5.1c might be feasible, it is not as advantageous for liquid formation as the eutectic type to be discussed below.

Eutectic diagrams of the form shown in 5.1d and 5.1e can produce liquids at relatively low temperatures. Obviously, form 5.1e would yield the larger amount of liquid for any given addition of the second component. Let us then assume that the diagram is of form 5.1e shown in assumed realistic detail and drawn to scale in Figure 5.2. A eutectic temperature of 1300°C has been assumed, even though kinetic shrinkage results at 1200°C indicate that the same shrinkage phenomena occur at both temperatures.

Now, visualize ThO_2 plates coated uniformly with 2.5 mole % fine NiO powder, When a temperature of 1370°C is attained, if the NiO moves with extreme rapidity so that

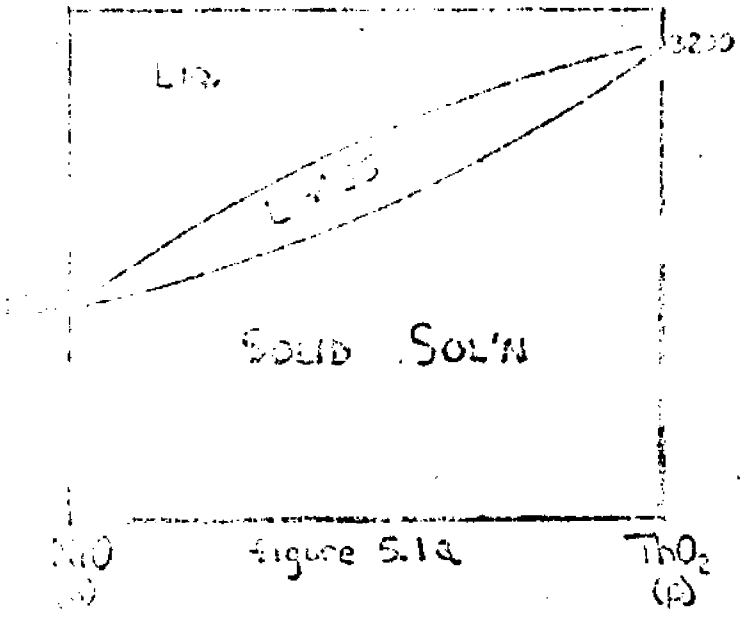

figure 5.1a

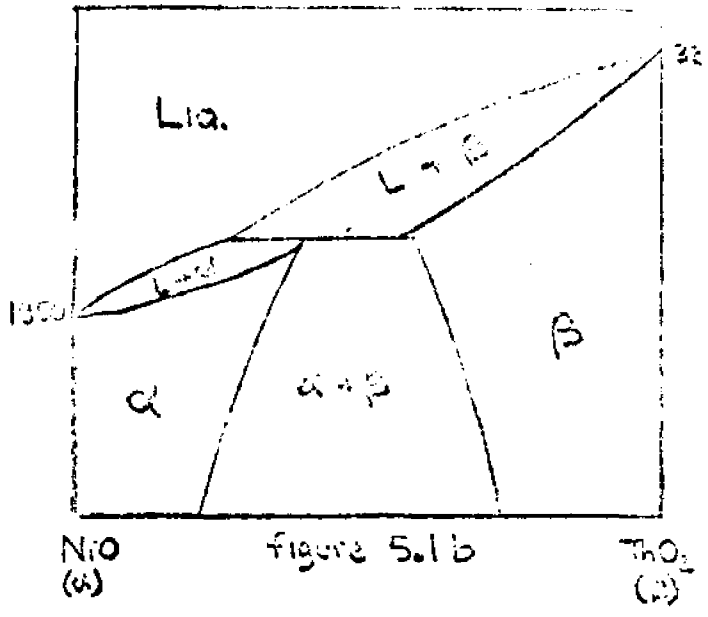

figure 5.1b

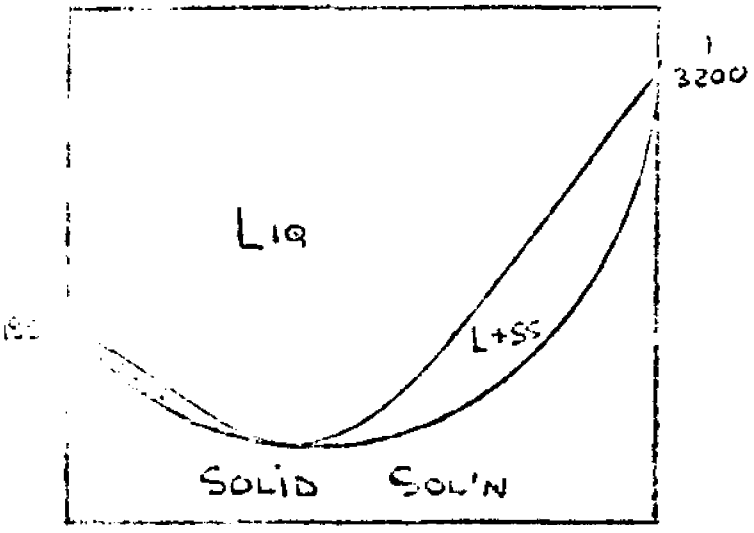

figure 5.1c

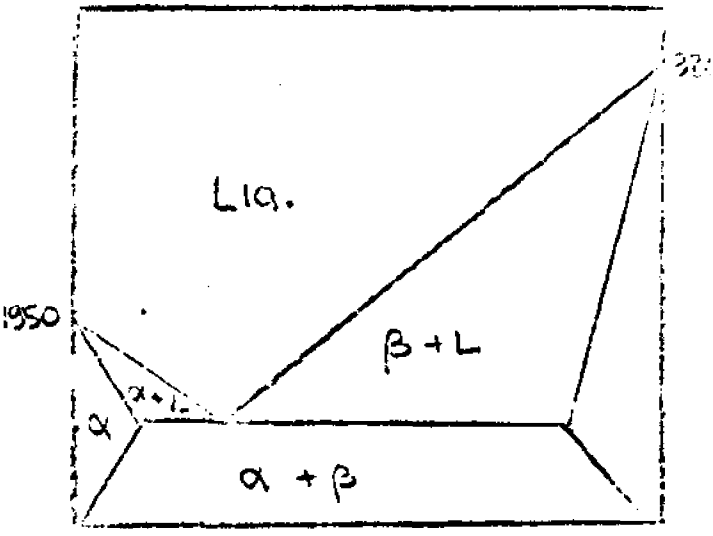

figure 5.1d

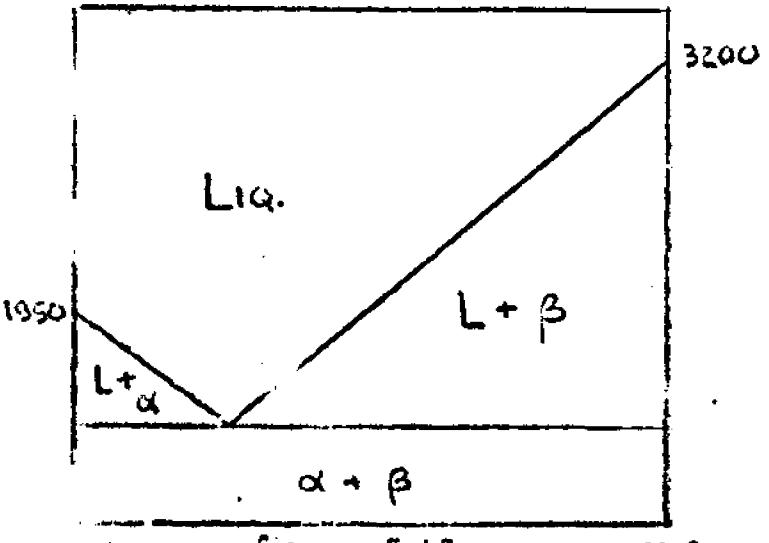

figure 5.1e

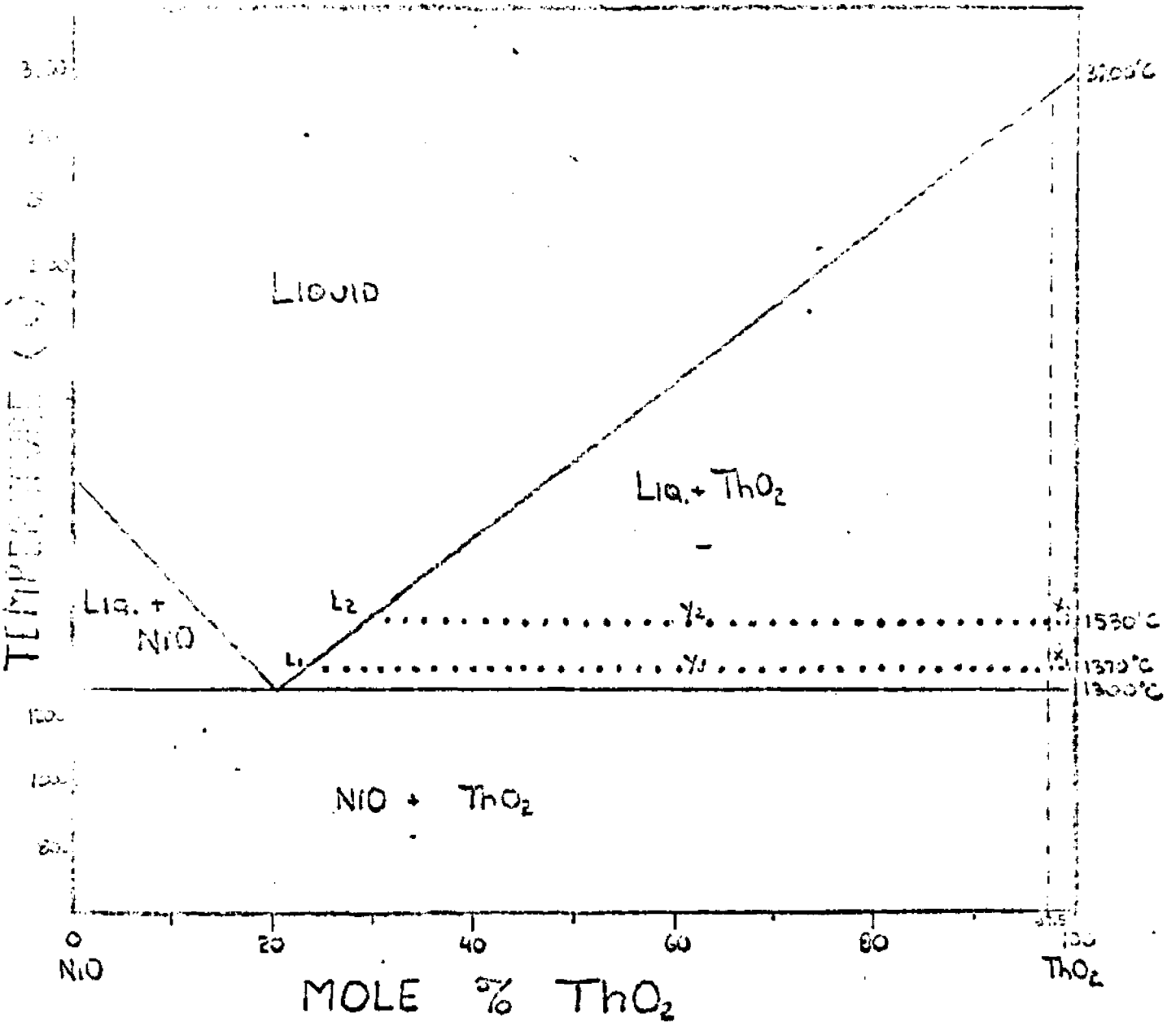

FIG. 5.2 -. ASSUMED EUTECTIC DIAGRAM, NiO-ThO_2

equilibrium is reached in a few seconds, we would have an overall composition of 97.5% ThO_2. The liquid would have composition L_1, (see Figure 5.2) and the ratio of the liquid to solid would be x/y. In the figure as shown, this might mean about 3.0 mole % liquid. At 1530°C, the percentage of thoria in the liquid increases to L_2 and the amount of liquid might be about 4.0 mole %. This would explain the nature of the discontinuous runs, where an increase in temperature will cause more liquid and therefore more densification immediately.

The explanation just given possesses a strong asset. It will be recalled that in the first shrinkage stage, the extent of densification is linear with temperature (see Figure 4.21). This explanation yields a percentage of liquid which increases linearly with temperature and it is easy to believe that the amount of densification increases with the amount of liquid. Unfortunately, this explanation does not account for the experimental fact demonstrated in Figures 3.4 and 3.5. If this explanation is correct, addition of more than 2.5 mole % NiO should produce more liquid at 1370°C and, therefore, greater densification. The experimental data show that beyond about 1 mole percent NiO, no increase in densification is observed. Kingery (R8) showed that a plateau in the densification with amount of liquid was not noticed until 35% liquid. In addition, the activation energy of 90 kcal/mole for TYN is very high if liquid diffusion were controlling.

Furthermore, if an equilibrium liquid is formed, it should continue to exist until full densification is achieved. Thus, it becomes difficult to account for the greatly diminished shrinkage rate after a few minutes and long before full densification has occurred. (Other objections to the liquid phase mechanism will be cited later.)

It is, of course, unlikely that equilibrium is achieved by the diffusion of NiO into the ThO_2 plates in a few seconds. It is far more likely that a non-equilibrium transient condition is ultimately replaced by an approach to equilibrium. Thus, ThO_2 may dissolve in the fine NiO powder, reducing the melting point and forming a liquid rich in NiO. Since only the NiO on the surface of the thoria could see the thoria and create a eutectic, additions are only effective up to a monolayer of particles. Beyond that, no effect would be observed. This could explain the effect of additive demonstrated in Figures 3.4 and 3.5.

If the relationship shown in Figure 5.2 were correct, something less than 20% ThO_2 would convert the NiO phase to 100% liquid at 1370°C. Again, this would be about 3 mole percent of the total material present. Raising the temperature would mean that less ThO_2 would be needed and that the range of thoria contents over which a liquid existed would become much larger.

As time progressed at the elevated temperature, the system would approach equilibrium at 97.5% ThO_2 as previously described. As already noted, the simple

eutectic diagram of Figure 5.2 would imply the existence of a liquid even at equilibrium. However, this need not be the case if there is appreciable solid solubility on the thoria side. Then the diagram might have the form shown in Figure 5.3. Now, a liquid phase would be produced by the addition of ThO_2 to NiO and some liquid would persist until equilibrium were approached. At composition S mole % ThO_2, the material would be entirely solid.

The liquid phase explanation appears to be somewhat strengthened by the appearance of some of the SEM micrographs. In some cases, the sintering powders appear liquid. See for example Plate 6, numbers 29 and 37, or Plate 8, number 33. However, SEM micrographs of the sintering of pure metallic nickel powder well below its melting point show remarkably close resemblance to these (see Figures 5.4-5.8). These micrographs were taken by Juusela et al. (R55).

Any explanation based on the formation of a liquid phase runs afoul of experiment. As previously described, a series of compositions across the entire ThO_2-NiO phase diagram were formed into pellets and heated for long times at 1370°C (TYN was also tested). Not only was no melting found in any of them, but all retained the flash produced on pressing as well as their sharp pellet edges. A pellet containing 50 wt % (78 mole %) NiO was heated to 1530°C for 6 hours with no sign of melting. A pellet containing 80 wt % NiO (93 mole percent) was heated to melting at one edge

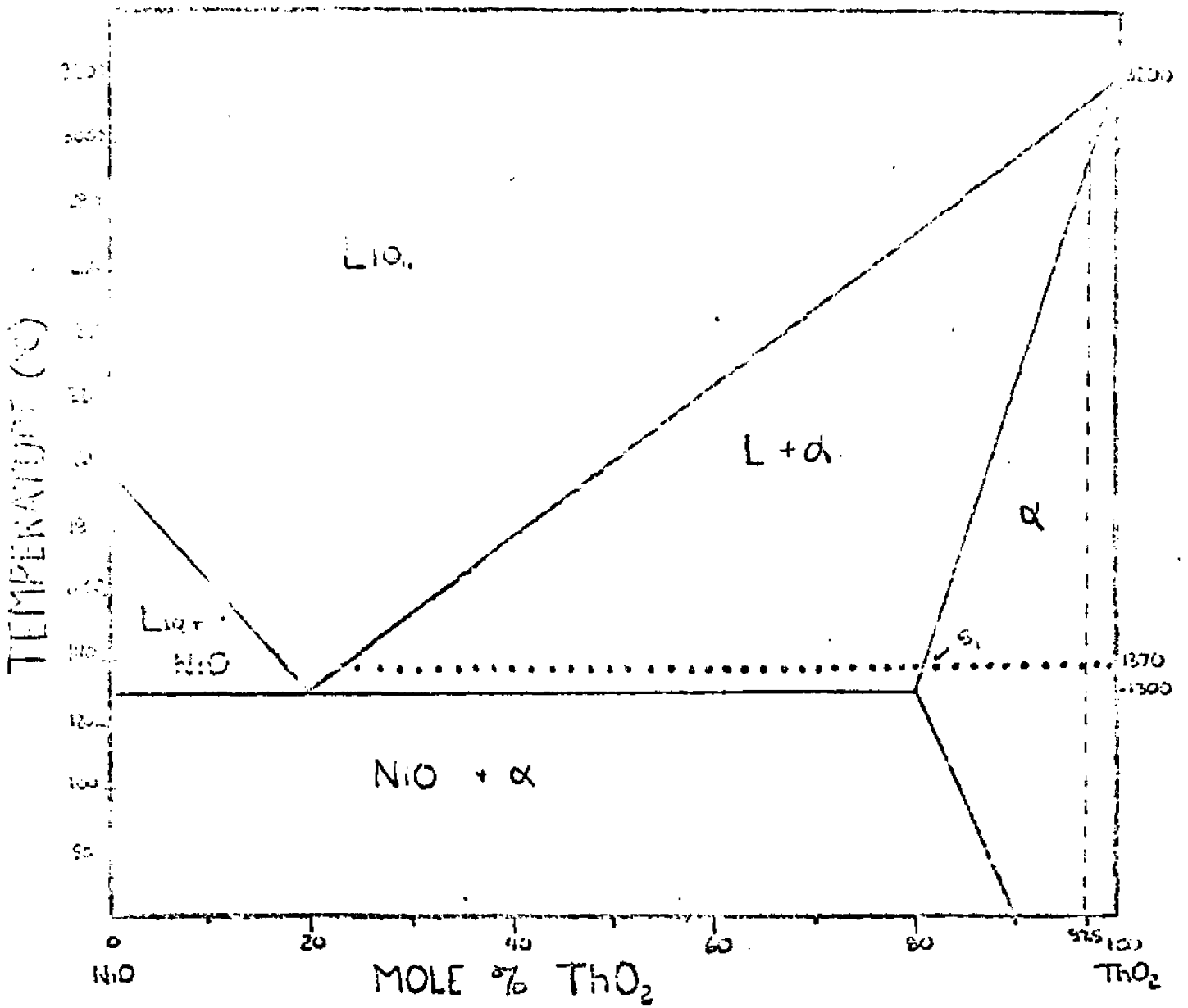

FIG. 5.3 - ASSUMED EUTECTIC - WITH SOLID SOLUBILITY, NiO-ThO_2

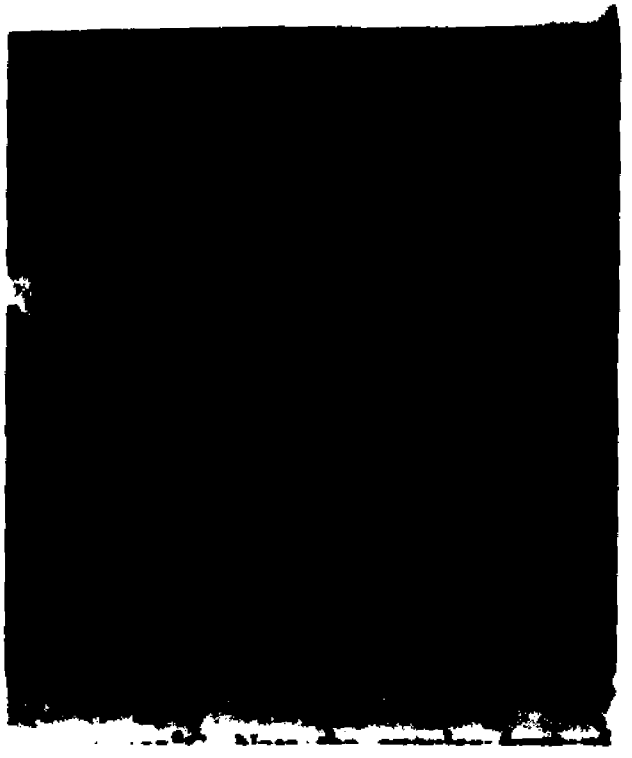

Fig. 5.4 - Ni, 450°C, 20,000x

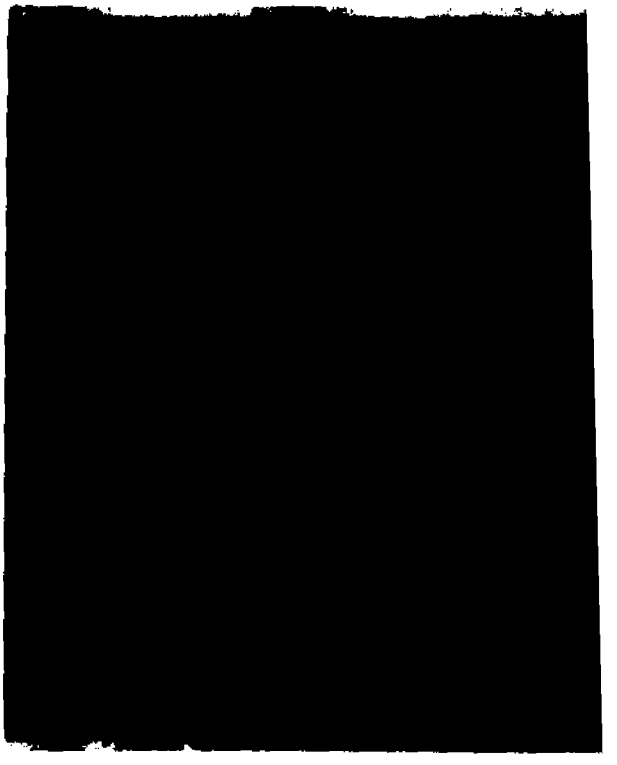

Fig. 5.5 - Ni, 1000°C, 2 hrs
6000x

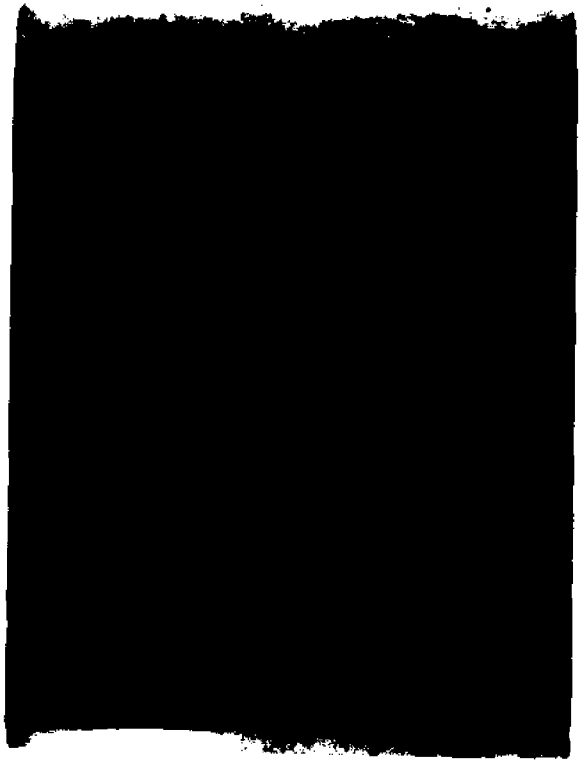

Fig. 5.6 - Ni, 1000°C, 16 hrs

2000x

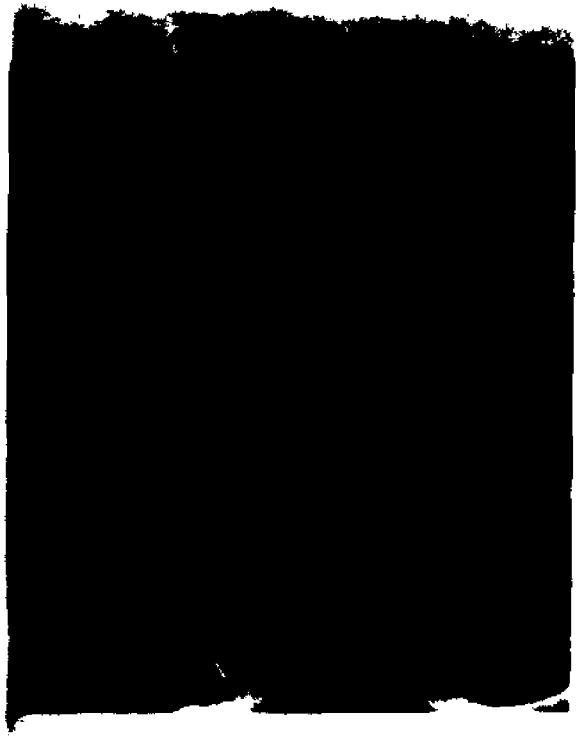

Fig. 5.7 - Ni, 1000°C, 72 hrs

2000x

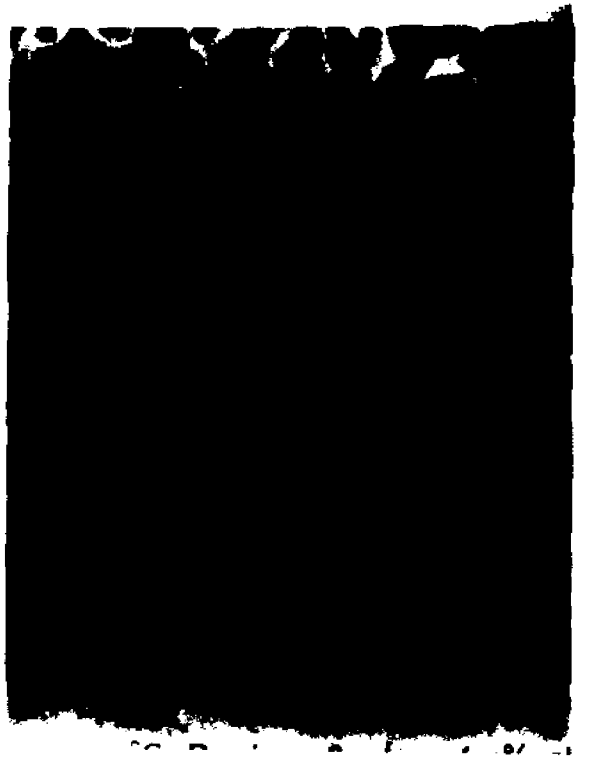

Fig. 5.8 - Ni, 1000°C, 1 hr

2000x

in an oxy-gas flame and the temperature measured with an optical pyrometer was found to be 1650-1725°C at the point of incipient melting. The test was calibrated using 1399°C standard eutectic pellets.

In summary, then, while a rearrangement based upon the formation of a liquid phase is attractive, the experimental evidence leads to considerable doubt. Detailed exploration of the ThO_2-NiO system at high temperatures will be needed.

5.3 Solid State Mechanisms

The determination of the temperature of formation of a liquid phase in the ThO_2-NiO system is of crucial importance. For if a liquid is not formed in the sintering range, then an unexpected solid state phenomenon is responsible for the initial rapid rearrangement. Possible phenomena include:

a. Stress Actuated Rearrangement Stresses may be present in the compacts because of grinding or because of temperature differences. In addition, stresses may be introduced by inequalities in diffusion or by the sintering mechanism itself. The observed linearity between temperature and early shrinkage may be the result of thermal stresses. However, as we have observed, even when both pressing stress and thermal stress are absent, shrinkage does occur in the presence of small amounts of NiO and ZnO while it does not occur in their absence, except for very slight shrinkage of TY.

The stresses formed during sintering try to broaden the neck region and therefore minimize total surface area. If a small particle is in contact with larger one, the overall effect might be to aid in the spreading of the smaller particles over the surface of the larger. If this were occurring on both sides of the smaller particle, rearrangement would indeed occur. In addition, if the stresses formed at the necks are large enough, the material might flow like a Bingham solid, greatly aiding the initial rearrangement by supplying a transient liquid. Whether such behavior is possible in the short length of time that the initial rearrangement occurs is doubtful. Such a mechansim would explain the effect of additives, since additions in excess of a monolayer of particles would not aid and might be detrimental to the rearrangement process. The discontinuous runs could be explained on the basis of the annihilation of inclusions that inhibit dislocation movement at higher temperatures, or that a lower stress is necessary to cause Bingham type flow.

The inhomogeneities may cause a rearrangement similar to that hypothesized for neck stresses. If NiO diffuses more quickly into thoria due to the concentration gradients than vice versa, then the NiO may almost totally disappear as a separate phase. In diffusing into the more abundant thoria from two sides, it can bring the two thoria plates it is in contact with into alignment -

causing rearrangement. This explanation would explain why the unstressed TY had shrunk. Temperature-dependent end points could be explained on the basis of Kirkendall pores formed which are relieved by diffusional mechanisms. This hypothesis suffers from the same drawbacks as did stresses in necks. In addition, the high activation energy implies a solid state diffusional process is occurring.

b. Surface Diffusion It may be that the sintering aid diffuses very rapidly over the surface of the thoria platelets. If the attractive forces between NiO-ThO_2 and NiO-NiO are sufficiently great, the tendency to reduce surface energy in the solid state may result in rearrangement of these coated platelets. This would produce a higher density packing of the thoria, even though no center-to-center approach of the bulk material is occurring.

c. Electrical Effects It is possible to create substantial electrical potentials across thin films during the oxidation of metals. If an ion is transported through an oxide film without accompanying transport of an oppositely charged ion, or transport of electrons, high voltages may be established across thin films. This phenomenon has been used to explain oxidation that follows a logarithmic law (see for example K. Hauffe (R49), chapter 3.5).

We may visualize a situation in which Ni^{++} diffuses into ThO_2 without accompanying $O^{=}$ diffusion (or vice versa). The result would be the creation of high voltage gradients

over short distances and a strong coulombic attraction between ThO_2 and the NiO. This might cause rapid early rearrangement and apparent densification, but would not explain the results of the discontinuous runs when the material was fairly well densified and incapable of movement due to coulombic forces.

d. Creation of Defects As previously indicated, the addition of Y_2O_3 to ThO_2 creates $O^{=}$ vacancies because of the lower valence of Y^{+++}. However, electroneutrality may be maintained by other means. For example, if $O^{=}$ were to enter the ThO_2 lattice without the accompanying Ni^{++}, it could be accompanied by the alteration of Th^{+4} to Th^{+6} to maintain electroneutrality. Now the sintering of thoria is undoubtedly controlled by the mobility of the thorium ion, because it is the slowest mover. Since Th^{+6} is a much smaller ion than Th^{+4}, its diffusivity may be much higher and sintering will be hastened. This phenomenon can hardly account for the rapid early shrinkage or the discontinuous runs, but may assist greatly in the later stages.

In conclusion, since we are not convinced that a liquid phase is formed in the ThO_2-NiO or ThO_2-Y_2O_3-NiO systems, the question of early densification needs far more extensive experimental exploration. If the absence of a liquid is confirmed, it will be necessary to conduct work leading to a satisfactory explanation of the behavior in the first period of thoria sintering. It is possible that

an entirely new explanation is needed to explain this behavior. The subsequent regions are explicable on the basis of solid state diffusion, initially enhanced by the increased mobilities caused by vacancies, then hindered by the residual pores in the solid matrix.

6. Recommended Research

6.1 Areas of Future Investigation

The following is a list of areas of further investigation to both elucidate the mechanisms of sintering in our thoria-yttria-additive compacts, and to produce a fabricated oxygen sensor employing a solid ceramic electrolyte:

1) Methods of fabricating a totally encapsulated electrode with an electrolyte for use as a probe have to be more fully developed. Possible methods include the plating of Ni or Fe on Pt wire, partially oxidizing it, then isostatically pressing the electrolyte around it.
2) An equilibrium study of the thoria-nickelous oxide and thoria-yttria-nickelous oxide systems to detect the temperatures of initial liquid formation. It would also be helpful to find the liquidus temperatures in the entire system. This work will require techniques for sample preparation in excess of 2000°C.
3) If liquid is formed only above the sintering temperature then the nature of the solid state reaction that causes sintering will need to be studied. This should involve tests of the various hypotheses beginning with the most promising.
4) A more complete study of the thoria-yttria-zinc oxide sintering. This is of interest because the additive, ZnO, which might induce electronic conduction, is volatile at the firing temperature. It may therefore be feasible to remove the sintering aid from the final product.

5) The electronic and anionic domains of the thoria-yttria-additive electrolytes, that is, the ionic transport numbers as a function of both temperature and oxygen partial pressure. This is to determine the usable range of the electrolyte.
6) Methods of coprecipitation to yield finer particles or to more evenly distribute the substituents, including thoria-yttria or thoria-yttria-additives as hydroxides or oxalates. This will help determine the sintering mechanism by varying the particle radius (allowing for Herring analysis) and the additive distribution. It may also substantially reduce the required sintering temperature.
7) The effect of particle size distributions and irregular particle shapes on sintering.

APPENDIX A Derivation of a Typical Kuczynski Equation

Mass transfer between spheres is governed by Fick's Law:

$$\frac{dV}{dt} = A\frac{\Delta C}{x}D_v \qquad (a)$$

assuming the following geometrical relationships defining x and y (as shown in Figure 1.3)

$y = x^2/2r \quad \left[x = \sqrt{2\Phi}\, r \text{, where } \Phi \equiv \Delta L/L_o = y/r\right]$

$$V = \pi x^2 y = 2\pi r y^2 = 2\pi r^3 \Phi^2 \qquad (b)$$

$$\frac{dV}{dt} = 2\pi r^3 \frac{d(\Phi)^2}{dt} \qquad (c)$$

$$A = 2\pi y x \qquad (d)$$

$$\rho = y = r\Phi \qquad (e)$$

$$\Delta C = \frac{2\gamma C_o \bar{V}}{RT}\frac{1}{\rho} = \frac{2\gamma C_o \bar{V}}{RT}\frac{1}{\Phi r} \qquad (f)$$

$$D_v = \mathcal{D}/C_o \qquad (g)$$

Plugging into equation (a):

$$2\pi r^3 \frac{d(\Phi)^2}{dt} = \left(2\sqrt{2}\,\pi\Phi^{3/2}r^2\right)\left(\frac{2\gamma C_o \bar{V}}{RT\Phi r}\right)\left(\frac{\mathcal{D}}{C_o}\right)\Big/ r\sqrt{2\Phi} \qquad (h)$$

rearranging yields:

$$\frac{d(\Phi)^2}{dt} = \frac{2\gamma \bar{V}\mathcal{D}}{RT\, r^3} \qquad (i)$$

and on integration:

$$\Phi^2 = \left(\frac{\Delta L}{L}\right)^2 = \frac{2\gamma V \vartheta}{RT r^3} t \qquad (j)$$

APPENDIX B Derivation of the Kuczynski Model for Sintering with a Liquid Present - after Kingery (R8)

As before:

$$\frac{dV}{dt} = D_v A \frac{\Delta C}{x} \qquad (a)$$

$$\Delta C = \frac{2\gamma \bar{V} C_o}{RT} \frac{1}{\Phi r} \qquad (b)$$

The volume is again a cylinder between the necks, and

$$\frac{dV}{dt} = \frac{d(r^3\Phi^2)}{dt} = \pi r^3 \frac{d(\Phi)^2}{dt} \qquad (c)$$

The area is a cylindrical band between the two spheres

$$A = 2\pi\delta x = 2\pi\delta(\sqrt{2}\Phi^{1/2}r) = \sqrt{8}\pi\delta r\Phi^{1/2} \qquad (d)$$

with

$$x = \sqrt{2ry} = \sqrt{2}\, r\Phi^{1/2} \qquad (e)$$

and

$$D_v = \mathcal{D}/C_o \qquad (f)$$

then substitution into equation (a) yields:

$$2\pi r^3\Phi \frac{d\Phi}{dt} = \frac{\left(\frac{\mathcal{D}}{C_o}\right)\left(\sqrt{8}\pi\delta r\Phi^{1/2}\right)\left(\frac{2\gamma\bar{V}C_o}{RT\Phi r}\right)}{\sqrt{2}\, r\Phi^{1/2}} \qquad (g)$$

which simplifies to:

$$\bar{\Phi}^2 r^4 d\bar{\Phi} = \frac{2\delta\vartheta\gamma\bar{V}}{RT} dt \qquad (h)$$

yielding:

$$\bar{\Phi}^3 \equiv \left(\frac{\Delta L}{L_o}\right)^3 = \left(\frac{6\delta\vartheta\gamma\nabla}{RT r^4} t\right) \qquad (i)$$

APPENDIX C Derivation of the Shrinkage Equation for Tetrakaidecahedrons, after Coble (R43)

The shrinkage due to the sintering of tetrakaidecahedron after Coble is described below.

Assume that after sintering has occurred for a while, the particle can be described by a tekrakaidecahedron (see Figure below).

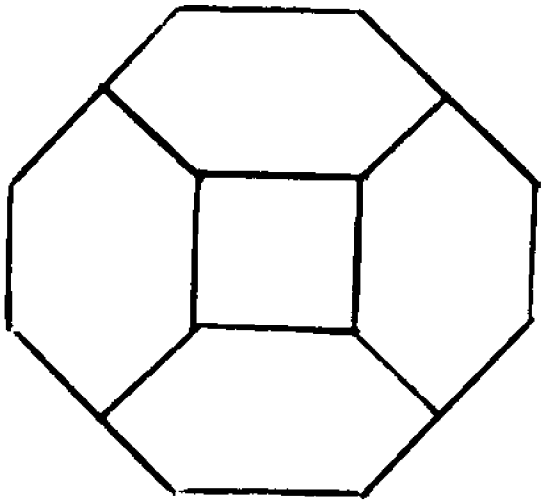

The volume of this polyhedron which has 36 edges and 24 corners, is $8\sqrt{2}\,\ell^3$ where ℓ is the length of the new edge. Consider that at first the pore is a continuous cylinder of radius r distributed along the edges, then, it will have the volume $\frac{1}{3}$ $(36\,\ell\pi r^2)$, then its porosity (P_c) is the volume of pore of volume of polyhedron since this Kelvin polyhedron fully fills three spaces.

$$P_c = 1.06\,\frac{r^2}{\ell^2} \qquad \text{(a)}$$

If bulk diffusion is the mechanism, then the flux per unit length is

$$J/l = 4\pi D_v V \Delta C \quad (cm^3/sec\ cm) \tag{b}$$

where

V = Vacancy volume

ΔC = Vacancy concentration difference

D_v = Vacancy diffusion coefficient

l = Length = pore diameter = $2r$

$$J/2r = 4\pi D_v V \Delta C \tag{c}$$

This flux distributes itself to 2 grains per each of the 14 faces, then

$$\frac{dV}{dt} = \frac{14}{2} J = 7(8\pi D_v V \Delta C r) \tag{d}$$

plugging in ΔC from equation 4 gives

$$\frac{dV}{dt} = \left(\frac{112\pi D \gamma V}{RT}\right) \tag{e}$$

But

$$\int dV = P_c = 12\pi \ell r^2 \Big|_{r_o}^{r} \tag{f}$$

so that

$$r^2 \Big]_r^o \approx -10 \frac{DV\gamma}{\ell RT} t \Big]_t^{t_f} \tag{g}$$

where t_f is the time when the pore vanishes, so:

$$P_c \sim \frac{r^2}{\ell^2} \sim \frac{10D\delta V}{\ell^3 \cdot T}(t_f - t) \sim \left(\frac{\Delta L}{L}\right)^2 \qquad (h)$$

$$\frac{\Delta L}{L} = \frac{10D\delta V}{\ell^3 RT}(t_f - t)^{\frac{1}{2}} \qquad (i)$$

which roughly coincides to Coble's model for bulk diffusion with spheres.

Similarly, Coble gave the case of Boundary Diffusion controlling with cylindrical pores

$$\frac{dV}{dt} = J = 4\pi D_v W \left[\frac{\delta VC_o}{RTr}\right] \qquad (j)$$

where W is the boundary width for this case

$$\frac{r^2}{\ell^2} = 2\frac{DW\delta V}{\ell^4 RT} t^{2/3} \qquad (k)$$

$$\frac{\Delta L}{L_o} = 2\frac{DW\delta V}{\ell^4 RT} t^{1/3} \qquad (l)$$

which corresponds to Kingery's boundary diffusion model with spheres.

For the case of closed pores, where the pores appear at the tips of the polyhedron, Coble gave

$$\frac{r^2}{\ell^2} = \frac{6\pi}{\sqrt{2}} \frac{D\delta V}{\ell^3 RT} (t_f - t) \qquad (m)$$

$$\frac{\Delta L}{L} = \left(\frac{6\pi}{\sqrt{2}} \frac{D\delta V}{\ell^3 RT} (t_f - t)\right)^{\frac{1}{2}} \qquad (n)$$

which corresponds to Coble's model again.

It would definitely appear that use of sophisticated shapes do not add to the general form of the equation.

Appendix D - A Note on the Non-Linear Translated Method

The non-linear translated method is so named because the use of equation (34)

$$(L_1-L) = L_1 \left\{K^1(t-t_1)\right\}^m \tag{34}$$

is not linear to the governing equation, 14. This is easily shown.

The general form of the governing equation is

$$y = kt^m \tag{d-1}$$

At time t_1, the relationship would be

$$y_1 = kt_1^m \tag{d-2}$$

Subtracting (d-1) from (d-2) yields

$$y_1 - y = k(t_1^m - t^m) \tag{d-3}$$

or, since $y = (Lo-L)/Lo$

$$L_1-L = Lo\left\{K(t^m-t_1^m)\right\} \tag{d-4}$$

Equation (d-4) differs from equation 34 in the exponent m. The difference between Lo and L_1 as a coefficient is less than 10% for our compacts and can be neglected. Equation (34) holds then only when $t>>t_1$, or when y_1 and t_1 are picked when one single mechanism <u>starts</u> to be controlling.

This method differs from the Johnson-Cutler method only in the assumption that the assumed t_1 and L_1 do not have to be mathematically derived, but are the observed data points. Values of t_1 and L_1 should be picked such that the break point

is eliminated, but taking cognizance of the physical significance of the value of t_1. This method is good for cathetometer measurements when the initial effects are large and take a relatively long time to manifest themselves.

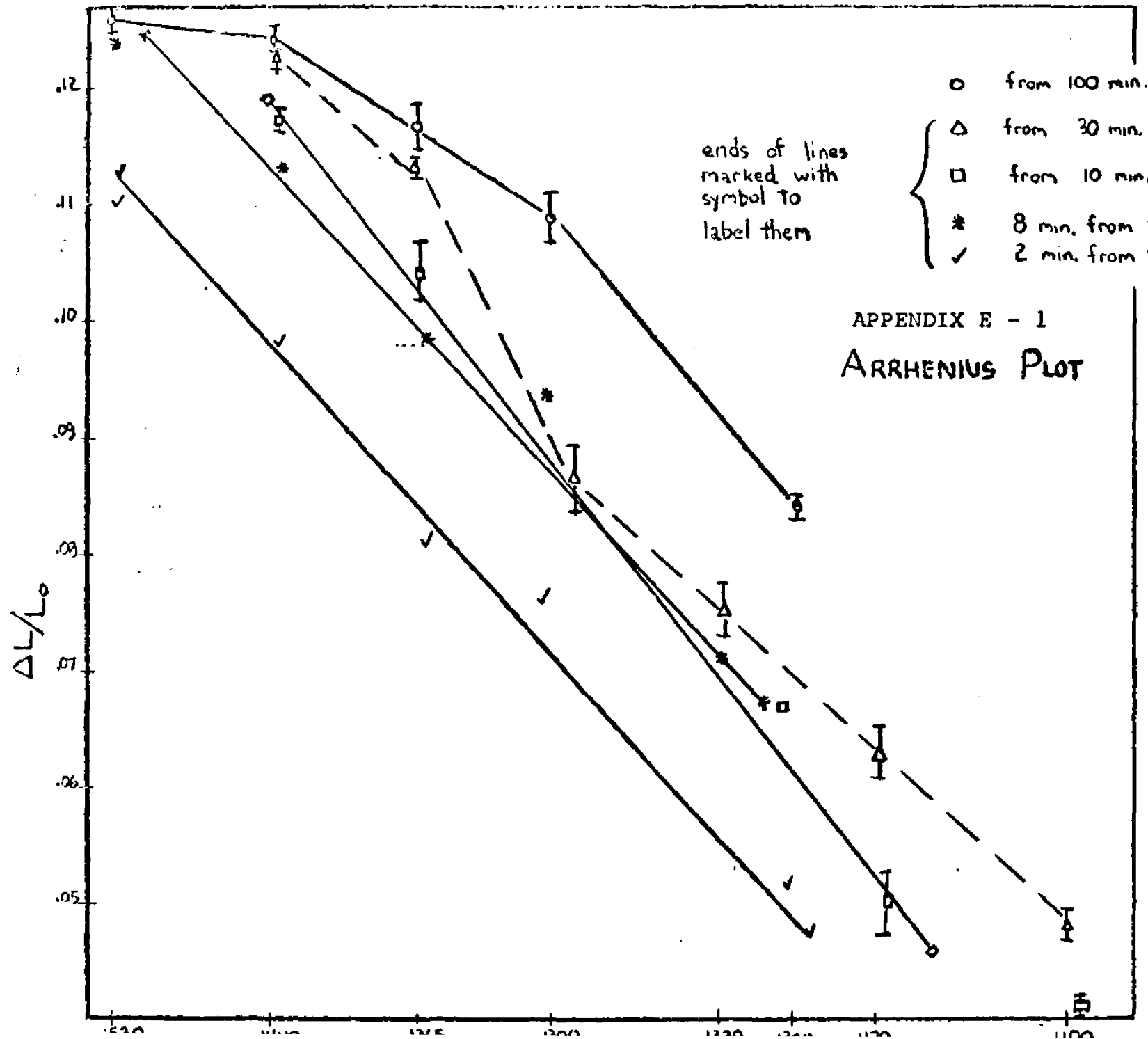

APPENDIX E - 1

ARRHENIUS PLOT

References

1. S. Levine, Thermodynamic Properties of Refractory Metal Silicides by EMF Methods, Ph.D. Thesis, CUNY, 1968.

2. C. Wagner, "The Theory of the Tarnishing Process", Z. Phys. Chem., abst., B21, 25 (1933).

3. C.E. Wicks and F.E. Block, "Thermodynamic Properties of 65 Elements, Their Oxides....", U.S.B.M. Bull. 605 (1963).

4. J.E. Burke, "Sintering and Microstructure Control", G.E. Rpt. # 68-C-368, November 1968.

5. J.E. Burke, "Role of Grain Boundaries in Sintering", J. Am. Ceram. Soc., 40, 80 (1957).

6. R.L. Coble, "Initial Sintering of Alumina and Hematite", J. Am. Ceram. Soc., 41, 55 (1958).

7. D.L. Johnson and I.B. Cutler, "Diffusion Sintering I: Initial Stage Sintering Models and Their Application to Shrinkage of Powder Compacts", J. Am. Ceram. Soc., 46, 541 (1960).

8. W.D. Kingery, "Densification During Sintering in the Presence of a Liquid Phase: I Theory", J. Appl. Phys., 30, 301 (1959).

9. W.D. Kingery and M. Berg, "Study of the Initial Stages of Sintering Solids by Viscous Flow, Evaporation-Condensation and Self Diffusion", J. Appl. Phys., 26, 1205 (1955).

10. D.L. Johnson, "Powder Compact Studies of Initial Sintering", Chapter 18 from Mat. Science Res. Vol. IV, ed. by J. Gray and V.P. Frechette, Plenum Press, New York (1969).

11. J.G.R. Rockland, "The Determination of the Mechanism of Sintering", Acta Met., 15, 277 (1967).

12. K.W. Lay and R.E. Carter, "Time and Length Corrections in the Analysis of the Initial Stages of Diffusion Controlled Sintering", J. Am. Ceram. Soc., 52, 189 (1969).

References (cont.)

13. F. Thummler and W. Thomma, "The Sintering Process", Met. Rev. # 115, 69 (1967).

14. C.A. Arenberg, H.H. Rice and J.J. Handwerk, "Thoria Ceramics", Am. Ceram. Soc. Bull., 36, 302 (1957).

15. T.P. Hoar and J.M. Butler, "Influence of Oxide on the Pressing and Sintering of Cu Compacts", J. Inst. Met., 78, 351 (1950).

16. M. Eudier, "The Sintering Mechanism of Pure Metals, Including Activated Sintering", Met. Abstr., 22, 788 (1955).

17. W.D. Jones, abstracted from ref. 18.

18. A.J. Shaler, "Activated Sintering - A Review" from Sintering and Related Phenomena, Kuczynski ed., Gorden and Breach (1965).

19. J.E. Burke, "Grain Boundary Effects in Ceramics", G.E. Rpt. # 62-RL-3048M, June 1962.

20. E.P. Hyatt, C.J. Christensen and I.B. Cutler, "Sintering of Zircon and Zirconia with the Aid of Certain Additive Oxides", Am. Ceram. Soc. Bull., 36, 307 (1957).

21. H.S. Spacil and C.S. Tedmon, Jr., "Electrochemical Dissociation of H_2O Vapor in Solid Oxide Electrolyte Cells II Materials, Fabrication and Properties", J. Electrochem. Soc., 116, 1627 (1969).

22. P.F. Stablein, Jr. and G.C. Kuczynski, "Sintering in Multicomponent Metallic Systems", Acta Met., 11, 1327 (1963).

23. J.S. Hirshhorn, Intro. to Powder Metallurgy, Am. Powder Met. Inst. (1969).

24. J.H. Brophy, H.W. Hayden, and J. Wulff, "The Sintering and Strength of Coated and Co-Reduced Nickel Tungsten Powder", Trans. Met. Soc. AIME, 221, 1225 (1961).

25. C.S. Morgan and L.L. Hall, "The Creep of ThO_2 and ThO_2-CaO Solid Solutions", Proc. Brit. Ceram. Soc., 6, 233 (1966).

References (cont.)

26. C. Herring, "Diffusional Viscosity of a Polycrystalline Solid", J. Appl. Phys., 21, 437 (1950).

27. W.D. Kingery, Introduction to Ceramics, John Wiley & Sons, 578 (1960).

28. E.B. Allison and P. Murray, "A Fundamental Investigation of the Mechanism of Sintering"; Acta Met., 2, 487 (1954).

29. C.S. Morgan and C.S. Yust, "Material Transport During Sintering of Materials with the Fluorite Structure", J. Nucl. Mat., 10, 182 (1966).

30. C.S. Morgan, C.J. McHargue, and C.S. Yust, "Material Transport in Sintering", Proc. Brit. Ceram. Soc. 3, 177 (1965).

31. K.E. Easterling and A.D. Thölén, "The Role of Dislocations in Sintering", Proc. 1970 Int'l P/M Conf., New York (1970).

32. P.T.B. Shaffer, Materials Index, Plenum Press, New York (1964).

33. I.E. Cambell, and E.M. Sherwood, High Temperature Materials and Technology, 2nd Ed., John Wiley & Sons (1967).

34. E.C. Subbaro, P.H. Sutter, and J. Hrizo, "Defect Structure and Electrical Conductivity of ThO_2-Y_2O_3 Solid Solutions", J. Am. Ceram. Soc., 48, 443 (1965).

35. F.S. Pettit and E.J. Felten, "The Oxidation of Ni-2ThO_2 between 900^{o} and 1400^{o}C", J. Electrochem. Soc., 111, 135 (1964).

36. T.H. Etsell and S.N. Flengas, "The Electrical Properties of Solid Oxide Electrolytes", Chem. Revs., 70, 339 (1970).

37. B.C.H. Steele and C.B. Alcock, "Factors Influencing the Performance of Solid Oxide Electrolytes in High Temperature Thermodynamic Measurements", Trans. Met. Soc. AIME, 233, 1359 (1965).

38. C.S. Morgan, "Mechanistic Interpretation of Non-steady State Sintering", Proc. 1970 Int'l P/M Conf., New York (1970).

References (cont.)

39. D.L. Johnson, "Discussion of Time and Length Corrections in the Analysis of the Initial Stages of Diffusion Controlled Sintering", J. Am. Ceram. Soc., 52, 562 (1969).

40. G.C. Kuczynski, "Self-Diffusion in Sintering of Metallic Particles", Trans. AIME, 185, 169 (1949).

41. D.L. Johnson, "Methods of Determing Sintering Mechanisms", Proc. 1970 Int'l P/M Conf., New York (1970).

42. K.W. Lay and R.E. Carter, "Role of the O/U Ratio on the Sintering of UO_2", J. Nucl. Mat., 30, 74 (1969).

43. R.L. Coble, "Sintering Crystalline Solids I Intermediate and Final Stage Diffusion Models; II Experimental Test of Diffusion Models in Powder Compacts", J. Appl. Phys., 32, 787, 793 (1961).

44. G.C. Kuczynski, "Measurement of Self-Diffusion of Silver without Radioactive Tracers", J. Appl. Phys., 21, 632 (1950).

45. J.D. McClelland, "Kinetics of Hot Pressing", from Powder Metallurgy, Leszynski ed., Interscience Pub. (1961).

46. W.D. Kingery and B. François, "The Sintering of Crystalline Oxides - Interactions Between Grain Boundaries and Pores" from Sintering and Related Phenomena, Kuczynski ed., Gordon and Breach (1965).

47. R.L. Coble and J.E. Burke, "Sintering in Ceramics", from Progress in Ceramic Science III, Pergamon Press, 197 (1963).

48. H.E. Brown, "Thermal Properties", in Zinc Oxide Rediscovered, The N.J. Zinc Co., New York, (1957).

49. K. Hauffe, "Defect Phenomena in Nonstoichiometric Ionic Crystals" in Oxidation of Metals, Plenum Press, N.Y. (1965).

50. S.P. Mitoff, "Electrical Device Including Stabilized Zirconia Solid Electrolyte", U.S. Pat. # 3,404,039, Oct. 1, 1968.

References (cont.)

51. S.P. Mitoff, "Process for the Densification of Zirconia", U.S. Pat. # 3,481,780, December 2, 1969.

52. C.S. Morgan, "Activation Energy in Sintering", J. Am. Ceram. Soc., 52, 453 (1969).

53. P.J. Jorgensen and W.G. Schmidt, "Final Stage Sintering of ThO_2", J. Am. Ceram. Soc., 53, 24, (1970).

54. P.J. Jorgensen and R.C. Anderson, "Grain Boundary Segregation and Final Stage Sintering", J. Am. Ceram. Soc., 50, 553 (1967).

55. J. Juusela, T. Rekola, M.H. Tikkanen, and S. Ylasaari, "On the Use of Scanning Electron Microscopy in Powder Metallurgy", Int'l J. of Powder Met., 5(1), 91 (1969).

56. J.E. Baurle, "Electrical Conduction in Thoria and Thoria-Yttria as a Function of Oxygen Pressure", J. Chem. Phys., 45, 4162 (1966).

57. S.C. Carniglia, S.D. Brown, and T.F. Schroeder, "Phase Equilibria and Physical Properties of Oxygen Difficient Zirconia and Thoria", J.Am. Ceram. Soc., 54, 13 (1971).

58. B.C.H. Steele and C.B. Alcock, "Factors Influencing the Performance of Solid Oxide Electrolytes in High Temperature Thermodynamic Measurements", Trans. Met. Soc., AIME, 233, 1359 (1965).

59. C.B. Alcock, and B.C.H. Steele, "Solid Oxide Electrolytes", Thermodynamics Symposium-Vienna 1965, pp. 397-406.

60. W.L. Worrell, "Measurements of the Thermodynamic Stability of the Niobium and Tantalum Oxide Using a High Temperature Galvanic Cell", Thermodynamics Symposium-Vienna 1965, pp. 131-43.

61. J.W. Patterson, E.C. Bogren and R.A. Rapp, "Mixed Conduction in $Zr_{.85}Ca_{.15}O_{1.85}$ and $Th_{.85}Y_{.15}O_{1.925}$ Solid Electrolytes", J. Electrochem. Soc., 114, 752 (1967).

References (cont.)

62. J.R. Johnson and C.E. Curtis, "Note on Sintering of ThO_2", J. Am. Ceram. Soc., 37, 611 (1954).

63. E. Rystewitch, Oxide Ceramics, Academic Press, New York 1960.

64. J.E. Burke, Manager, Ceramic Branch, Pvt. communication, July 1971.

65. K.E. Easterling, "Electron Microscopy Study of Stresses at Contacts Between Sintering Aluminum Particles", Int'l. J. of Powder Metall., 7(2), 29 (1971).

66. D.L. Johnson, Pvt. communication, July 1970.

67. R.L. Coble and T.K. Gupta, "Intermediate Stage Sintering", in Sintering and Related Phenomena, Kuczynski ed., Gordon and Breach (1965).

68. W. Rao and G.S. Tendolkar, "A Note on Sintering of Crystalline Solids", Int'l.J. of Powder Metall., 5(3), 63 (1969).

69. W.S. Young and I.B. Cutler, "Initial Sintering with Constant Rates of Heating", J. Am. Ceram. Soc., 53, 659 (1970).

70. G. Naesser, "Mechanical Activation of Solid Material and its Technical Significance", Int'l. J. of Powder Metall., 6(2), 3 (1970).

71. R.J. Hawkins and C.B. Alcock, "A Study of Cation Diffusion in UO_{2+} and ThO_2 Using α-Ray Spectrometry", J. Nuc. Mat., 26, 112 (1968).

72. C.B. Alcock, "Transport of Ions and Electrons in Ceramic Oxides", Electromotive Force Measurements in High Temperature Systems", Inst. of Mining and Metallurgy, 1968.

VITA

George Philip Halbfinger was born in Brooklyn on June 4, 1946. He attended the New York City public school system and was graduated from Erasmus Hall High School in June, 1963.

He entered The City College in 1963 and received the degree of Bachelor of Engineering (Chemical) in June, 1967. After summer employment at Oak Ridge National Laboratories, he returned to The City College as a doctoral student. During the summer of 1968 he was employed as a process engineer for American Cyanamid. After he received his Master's degree in January, 1969, he started teaching undergraduate chemical engineering and physical metallurgy courses as a part-time lecturer in the chemical engineering department. He continued teaching until 1971.

He is single and currently resides in Brooklyn.